Title

High resolution synoptic sampling and analysis for understanding groundwater-surface water interactions in lowland rivers

Permalink

https://escholarship.org/uc/item/9ts9s65r

Author

Pai, Henry

Publication Date

2015

Peer reviewed|Thesis/dissertation

University of California, Merced

High resolution synoptic sampling and analysis for understanding groundwater-surface water interactions in lowland rivers

A dissertation submitted in partial satisfaction of the requirements
For the degree Doctor of Philosophy

in

Environmental Systems

by

Henry Pai

Committee in charge:

Professor Thomas Harmon, Chair
Professor Qinghua Guo
Professor Joshua Viers
Professor Michael Modest

2015

The Thesis of Henry Pai is approved, and it is acceptable
in quality and form for publication on microfilm and electronically:

Joshua Viers

Qinghua Guo

Michael F. Modest

Thomas C. Harmon, Chair

University of California, Merced

2015

For my family.

Table of Contents

List of Figures

List of Tables

Notation

<u>Abbreviations</u>

CAFO	Concentrated animal feed operation
CV	Coefficient of variation
CRS	Gauging station along Merced River at Cressey
DWR	Department of Water Resources
GAMA	Groundwater Ambient Monitoring and Assessment
GIS	Geographical information systems
GW	Groundwater
HZ	Hyporheic zone
IDW	Inverse distance weighted
LMR	Lower Merced River
MDL	Maximum detection limit
MST	Gauging station along Merced River near Stevinson
NAWQA	National Water-Quality Assessment Program
NO_3	Nitrate
NPSP	Nonpoint-source pollution
OLS	Ordinary least squares
RMSE	Root mean squared error
SC	Specific conductance
SJR	San Joaquin River
SW	Surface water
SWRCB	State Water Resources Control Board
TDS	Total dissolved solids
TMDL	Total maximum daily load
USGS	United States Geological Survey
UV-Vis	Ultraviolet to visible spectrum
WY	Water year
avg3	Averaging 3 closest GW groundwater for parameterization
lin	Ordinary least squares linear regression
sen	Sen's slope estimate
sp_clo	Spatially closest groundwater well parameterization
idw12	Inverse distance weighted using 12 wells with power of 2
t_avg	Average all well samples given period
t_clo	Average within synoptic sampling or choosing closest temporal GW well

<u>Variables</u>

ϕ	Porosity [-]
$\overline{\%Q_g}$	Percent of GW inflow to upstream flow for all synoptic events [-]
ΔQ_s	Difference of surface water flows between two gauging stations [M L^{-1}]
C	Concentration [M L^{-1}]
Q	Volumetric flow [L^3 T^{-1}]
V	Hypothetical volume the GW travels through [L^3]
k	Decay rate [T^{-1}]

kt	Unitless denitrification term
t	Time [T]

<u>Subscripts</u>

d	Downstream
dn	Downstream nitrate
g	Groundwater
gn	Groundwater, nitrate related
*gn*0	Groundwater, nitrate at well or source
s	Surface water
u	Upstream
un	Upstream nitrate

Acknowledgments

Curriculum Vitae

Education

M.S. Environmental Systems, UCM, 2010

B.S. Electrical Engineering, Minor in Philosophy, University of California Los Angeles (UCLA), 2006

Publications

H. Pai, S.R. Villamizar and T.C. Harmon (2015). High Resolution Synoptic Salinity Mapping To Identify Groundwater-Surface Water Discharges in Lowland Rivers. Environmental Science & Technology, 49(8), 4842-4850.

S.R. Villamizar, H. Pai and T.C. Harmon (2014). Transverse spatiotemporal variability of lowland river properties and effects on metabolic rate estimates. Water Resources Research, 50(1), 482-493.

H. Pai (2010). Field Parameterization and Evaluation of 2-D, Finite-Element Modeling of the Merced River-San Joaquin River Confluence. Master's dissertation.

J. Ros, C. Lee, M. Bruce, R. Quan and H. Pai (2006). A Portable and Sustainable Computer Education Project for Developing Countries- Phase I. International Journal for Service Learning in Engineering, 1(1), 27-47.

Abstract

High resolution synoptic sampling and analysis for understanding groundwater-surface water interactions in lowland rivers

by Henry Pai

Doctor of Philosophy in Environmental Systems
University of California, Merced, 2015
Professor Thomas C. Harmon, Chair

Distributed groundwater discharges to the surface water (GW-SW discharge) in river systems remain difficult to measure across spatiotemporal scales yet are an important metric to understand with respect to nonpoint source constituent loading to rivers and downstream aquatic systems. The work focuses on a long reach (~38 river km) along the lower Merced River (LMR) in Central California, a reach in which GW-SS discharges are perennial. Coupled with elevated GW well concentrations for specific conductance (SC) and nitrate (NO_3^-), the loading of these constituents to the river and transport downstream are of particular interest. This study presents a method for high resolution, in situ synoptic sampling for SW SC and nitrate, and applies a simple mass-balance, mixing model to estimate distributed GW-SW discharge on 1-km intervals. SW data collection spanned from 2010-2012 covering a wide range of flows (1.3 to 31.6 m^3 s^{-1}). To assess the distributed GW-SW discharge, we assumed SC to be conservative and attributed changes in SW SC behavior to nonpoint source loading. We addressed model parameterization considerations in terms of spatial resolution discrepancies between the high resolution, synoptic sensor data and relatively sparse available GW well data, and also tested model sensitivity to GW source characteristics (GW sampling screen depth and timeframe). For spatial interpolations requiring a large number of wells (inverse distance weighting method with 12 wells), we found large differences in GW-SW discharge estimates, and attributed this to well data availability issues. Additionally, GW-SW distributed discharge estimates also showed noticeable variability between GW spatial parameterization methods. Cumulative GW-SW discharge estimates agreed reasonably with observed differential flows between two gauging stations. Distributed GW-SW discharge results clearly identify a zone of higher GW-SW discharge related to elevated hydraulic gradient and supported from previous studies. While SW SC expectedly diluted with increased SW flows, GW-SW discharge did not consistently decrease as anticipated, indicating more complex GW-SW interactions requiring further investigation. The SC-based distributed GW-SW discharge estimates were used to parameterize a reactive nitrate loading model using a similar mass-balance method, incorporating a first-order decay term to explain denitrification. We scaled the unitless decay term using local discharge estimates, and we varied the decay term to achieve the best model fit (i.e., lowest RMSE) to observed river nitrate concentrations. When we censored GW nitrate concentrations less than method detection limits, for GW parameterization, the best fit model agreed well with observed SW nitrate concentrations.

The unitless decay term estimated for each synoptic event generally underestimated previous studies along a local GW flowpath, but showed a similar trend with a regional study for different flow regimes (higher nitrate loss for low flows). The methods and analysis presented in this work provide a practical and rapid assessment tool for estimating longitudinal GW-SW discharge and potential reactive constituent loading at resolutions of interest to land management/change studies, aquatic ecosystem sustainability, and maintaining water quality standards for human consumption.

1.   Introduction

1.1.   Motivation

Human impacts on biogeochemical cycles (i.e. carbon, nitrogen, phosphorous, etc.) in the environment can be profound. Byproducts from industrial processes and practices continue to make their way into the natural aquatic systems, under the assumption that dilution will reduce risks to acceptable levels. However, accumulated effects over time and space can combine with poor understanding of physical transport and biochemical interactions leading to unforeseen and costly consequences. Thus, it is a perpetual challenge to understand risks of action or inaction in regard to chemical distributions, residence times, and potential feedbacks within the every-changing environment [1].

In the aquatic environment, we often classify human impacts through point and nonpoint source pollution. An example of point source can be a pipe or canal effluent directly leading to a river or ocean. Often the effluent is treated and diluted to achieve regulatory standards, but still contains some pollutants. Nonpoint sources, such as agricultural fertilizers and fugitive urban runoff, can either flow directly to surface water (SW) systems in a distributed fashion or percolate into groundwater (GW) aquifer systems and eventually emerge in a fresh SW body or ocean coastal margins [2–4]. Mitigation of point source pollution problems is costly but well understood, and mainly involves effective treatment technologies to remove or destroy contaminants prior to discharging it into the environment. Nonpoint source pollution, because of its distributed nature, is more difficult to mitigate because it generally requires changes in land management practices [5,6]. Land use policy changes can have significant impact on people's livelihood and the economy, and can be difficult to enact without strong evidence of both the need and the potential effectiveness of the proposed policy.

A major challenge with nonpoint source pollution is to adequately characterize it over large spatial domains such that the connection between land use and pollution can be clearly assessed. Measurement of water stage and movement (flows) and water quality (concentrations, temperatures) at adequate spatial coverage remain challenges and costs can easily become prohibitive at the watershed scale [7]. In highly engineered SW systems, rivers have been channelized for better flood control and other management considerations. This has resulted in better estimates of water volumetric flow. However, such systems have effectively sacrificed floodplain access, while dams have dampened storm flow intensity and timing. One negative consequence of this human dominated system is that it can make the connections between GW and SW more difficult to delineate, which renders the challenge of understanding and mapping nonpoint source pollution still more challenging. For assessing the GW flow and transport side of the nonpoint source pollution problem, these difficulties are compounded by inadequate spatial coverage in horizontal and vertical domains in most watersheds.

1.2.   General Approach

Better methods to characterize constituent transport and reaction rates will assist in strategies to mitigate negative human impacts on freshwater systems and clarify risks of freshwater degradation. This dissertation focuses on improving our understanding of surface water (SW)-groundwater (GW) interaction longitudinally along a lowland,

human-impacted river system, where GW-SW flow exchange and pollutant loading are both difficult to measure and difficult to scale. We develop a high spatial resolution measurement method for multiple ambient chemical tracers (pollutants) within the river and link SW concentration changes to localized GW-SW exchange by using a steady-state mixing model. The ambient tracers of interest in this work are specific conductance (SC), a proxy for total dissolved solids (or salts) associated with agricultural and industrial processes, and nitrate (NO_3^-), where elevated concentrations can largely be associated with fertilizer use and livestock waste in our setting. We connect measured river (SW) nitrate and salinity concentrations to GW using existing groundwater well data to parameterize our mixing model. Then, we test the model with the two tracers, one conservatively (SC) and the other non-conservatively (NO_3 with a first-order decay rate). The results in our study for the lower Merced River located in the Central Valley, CA are promising, and demonstrate the potential to explicitly delineate nonpoint source pollution as it moves from land surface to the aquifer and is subsequently transported to river systems.

While previous studies have presented techniques for assessing GW-SW exchange, they have often focused on isotope parameterization (requiring sample collection and relatively high laboratory costs) [8] or been limited with spatial resolution [9]. Our method, while dependent on differences in GW and SW concentrations and consistent discharge from GW to SW, exemplifies ease of data collection and potential characterization of GW-SW exchange in a human-impacted watershed. Unfortunately, as is the case with like many watershed characterizations, limitations on available GW GW spatial and temporal data resolution can limit the effectiveness of a study. Despite that potential limitation, we believe using existing wells and associated data can be a practical method to characterizing GW transport to the SW in systems similar to ours. The novel aspects of our work include (i) the ease in data collection, (ii) scale of GW-SW exchange characterization, and (iii) the resolution of transport characterization from aquifer to river as a measurement-analysis package. Such collection and analysis has potential to improve watershed-scale GW-SW exchange model validation, to localize potential GW-SW exchange zones encouraging increased spatial and temporal monitoring, and encourage better practices to prevent chemical transport with often unknown and potentially costly downstream effects.

1.3. Dissertation Overview

The dissertation is organized into 3 major body chapters in the form of submitted journal articles. Presenting in this fashion leads to some redundancy in methods and site description as I analyze the same large datasets from multiple synoptic sampling events, for different purposes. We attempted to tailor the chapters to be more specific in the methods and site description to each scientific objective for the chapters that are described briefly here. To add details not allowed by typical journal limitations, we added supplemental figures along with the journal format figures of each chapter.

Chapter 2 focuses on data collection and aggregation and GW-SW discharge parameterization methods using specific conductance (SC) as a conservative tracer. This chapter differs from Chapter 3 in that it focuses more on justification for SC as an ambient tracer and on parameterization methods that justify the observational resolution

differences between SW (upscaling) and GW (downscaling). These differences are, in effect, a prevailing theme of the methods in this dissertation and until now, to our knowledge, have not been adequately addressed in GW-SW mixing models. As we anticipated, downscaling sparser GW well SC and focusing on more realistic source attributions of the GW (shallow and more recent) caused large variability in model results. This could not be avoided without undertaking a massive GW sampling program, including the installation of numerous riparian zone observation wells.

Chapter 3 analyzes the best model results from the conservative ambient tracer (SC) survey data, and provides further discussion and analyses. The work has been published [10] and the chapter is presented in largely unaltered form. The 1-km distributed model independently identify a previously assessed GW-SW discharge zone and performed reasonably with differential flow estimates between 2 gauging stations along our stretch, excluding comparisons when an unmeasured point source visibly affected SW SC concentrations. While the behavior of SW SC with flow clearly showed dilution with increasing upstream flow, GW-SW discharge did not behave similarly. Without higher temporal resolution for GW wells fluctuations from potential residual bank storage, or nearby GW pumping information, the model can only elucidate so much to complex dynamics between upstream flow, local GW conditions, and other localized heterogeneities. The validation itself, however, is an argument that higher resolution SW data that are increasingly being measured remotely or autonomously can provide reasonable results between GW-SW interactions.

Chapter 4 builds on Chapter 3, but extends to the case of reactive ambient tracer in the form of nitrate (NO_3^-). We present more specific background on nitrate state and measurement methods. We also present a mixing model scaling term for nitrate reduction (as a first-order decay process) with the distributed GW-SW discharge, discussed from previous chapters. In effect Chapters 2 and 3 define the methods surrounding GW discharge (flow) estimates, while Chapter 4 describes reactive transport. If the previous GW-SW discharge model performed poorly, then the transport model would also perform poorly. However, the model showed reasonable results when censoring low concentration nitrate wells, indicating potential hotspot for nitrate reduction, and underestimates nitrate reduction compared with other studies [11,12], with the caveat that decay rate itself can vary by orders of magnitude.

The conclusions chapter summarizes major findings and potential future directions. The combined study of flow and transport at this resolution and scale is of a sort that a few others have undertaken for GW-SW interactions. We present an approach that is relatively easily replicated, relatively cost-effective aside from initial sensor investments, and potentially reproducible across different reaches of large river networks. Future considerations involve collecting higher temporal resolution signatures for ambient tracers of interest (in both SW and GW systems) and GW surface elevation data, in a cost-effective manner. Such data coupled with the high resolution synoptic surveys can bring rich understanding and characterization of GW-SW interaction of river systems and their biogeochemical roles for transport of the interested tracers.

1.4. References

[1] J.L. Montgomery, T. Harmon, C.N. Haas, R. Hooper, N.L. Clesceri, W. Graham, et al., The WATERS Network: An Integrated Environmental Observatory Network for Water Research, Environ. Sci. Technol. 41 (2007) 6642–6647. doi:10.1021/es072618f.

[2] A.E. Fryar, E.J. Wallin, D.L. Brown, Spatial and Temporal Variability in Seepage Between a Contaminated Aquifer and Tributaries to the Ohio River, Ground Water Monitoring & Remediation. 20 (2000) 129–146. doi:10.1111/j.1745-6592.2000.tb00279.x.

[3] T. Pohlert, J.A. Huisman, L. Breuer, H.-G. Frede, Modelling of point and non-point source pollution of nitrate with SWAT in the river Dill, Germany, Adv. Geosci. 5 (2005) 7–12. doi:10.5194/adgeo-5-7-2005.

[4] G. Vazquez-Amabile, B.A. Engel, D.C. Flanagan, Modeling and risk analysis of nonpoint-source pollution caused by atrazine using SWAT, Transactions of the ASABE. 49 (2006) 667–678.

[5] D.R. Mandelker, Controlling Nonpoint Source Water Pollution: Can It Be Done, Chi.-Kent L. Rev. 65 (1989) 479.

[6] Z. Qiu, Comparative Assessment of Stormwater and Nonpoint Source Pollution Best Management Practices in Suburban Watershed Management, Water. 5 (2013) 280–291. doi:10.3390/w5010280.

[7] R. Niraula, L. Kalin, P. Srivastava, C.J. Anderson, Identifying critical source areas of nonpoint source pollution with SWAT and GWLF, Ecological Modelling. 268 (2013) 123–133. doi:10.1016/j.ecolmodel.2013.08.007.

[8] P.G. Cook, S. Lamontagne, D. Berhane, J.F. Clark, Quantifying groundwater discharge to Cockburn River, southeastern Australia, using dissolved gas tracers 222Rn and SF6, Water Resour. Res. 42 (2006) W10411. doi:10.1029/2006WR004921.

[9] S. Jasechko, J.J. Gibson, S. Jean Birks, Y. Yi, Quantifying saline groundwater seepage to surface waters in the Athabasca oil sands region, Applied Geochemistry. 27 (2012) 2068–2076. doi:10.1016/j.apgeochem.2012.06.007.

[10] H. Pai, S.R. Villamizar, T.C. Harmon, High Resolution Synoptic Salinity Mapping To Identify Groundwater–Surface Water Discharges in Lowland Rivers, Environ. Sci. Technol. 49 (2015) 4842–4850. doi:10.1021/es504483q.

[11] C.T. Green, J.K. Böhlke, B.A. Bekins, S.P. Phillips, Mixing effects on apparent reaction rates and isotope fractionation during denitrification in a heterogeneous aquifer, Water Resour. Res. 46 (2010) W08525. doi:10.1029/2009WR008903.

[12] D. Saleh, J. Domagalski, SPARROW Modeling of Nitrogen Sources and Transport in Rivers and Streams of California and Adjacent States, U.S., J Am Water Resour Assoc. (2015). doi:10.1111/1752-1688.12325.

2. Developing a high resolution longitudinal river synoptic sampling method for delineating groundwater discharges in a lowland, gaining river

2.1. Abstract

Linking groundwater-surface water (GW-SW) interactions across spatial scales remains challenging due to spatiotemporally varying processes affecting both GW and SW flow. While river GW-SW exchange is important for water budgeting, there is also increased interest in localized impacts on freshwater ecosystems, such as identification of favorable conditions for habitat restoration and other applications. As in-situ and remotely-sensed water quality data collection methods become more robust, high resolution SW quality data products are becoming more readily available. However, these approaches still lack physically quantitative explanations for observed spatial distributions in flow and water quality. In this work, we develop a method for high frequency water quality data collection and analysis to support GW-SW discharge mapping. We use sample data sets collected along a 38-km river gaining reach of the Lower Merced River (LMR). First, the data are collected synoptically using a kayak with GPS and water quality sensors. Next, the data are temporally assimilated and spatially transformed to a linear river distance. We then explain localized responses in the high resolution SW data (e.g., local changes in the longitudinal gradient of water quality parameters, such as specific conductance, SC, and nitrate concentrations) by discretizing the river line and associating GW discharges to the local water quality changes in every discretization cell. While GW quality data are readily available from multiple agencies, the data are sparse in time and space compared to the collected SW data, and this work considers multiple methods of assigning near-field GW quality data to the river line. The resulting framework is proposed for a reduced-form physical model with options to adjust discretization size, SW piecewise trend estimation methods, and linking GW with spatiotemporal considerations. Overall, this novel protocol developed for collecting and analyzing SW quality data enables the exploration of GW-SW linkages in large scale, lowland rivers with unprecedented spatial resolution.

2.2. Introduction

Rivers integrate watershed processes occurring along natural- and human-influenced pathways. The associated constituent transport within the watershed system eventual impacts downstream water quality with respect to aquatic ecosystems and services they provide [1]. However, challenges arise in accounting for point and nonpoint source water and constituent river fluxes [2–4] and constituent in-stream processes [5,6]. Such fluxes and processes demand multiple spatiotemporally distributed parameters in the framework of calibrating distributed hydrologic or watershed models [7] or even for simplified reduced-form model representation of such systems [8,9]. In this work, we collect high resolution surface water (SW) quality data and propose a parameterization approach for a reduced-form river SW model with particular emphasis on groundwater (GW) quality influences on SW.

Characterizing watershed responses and drivers at disparate spatiotemporal resolutions is an ongoing area of active research. As noted for physically-based, watershed-scale models, the temporal data availability and its poor spatial resolution limit our ability to model integrated GW-SW systems. Hence, such process-based models

require an additional layer of sensitivity and uncertainty analysis if they are to support meaningful applications [10]. Higher resolution temporal and synoptic sampling approaches are needed to support distributed models, as they have demonstrated the capacity to resolve varying spatial SW quality behavior under different flow and environmental conditions [11–14]. These promising outcomes are motivating advances to mobile in-situ multi-sensor platforms [12,13,15].

Relating longitudinal SW quality behavior to GW influences remains a challenge due to the unknown distributed nature of GW-SW exchanges. While GW-SW exchange is driven by hydraulic head gradients between GW and SW, influences affecting actual GW flowpaths to SW occur across different spatial scales, ranging from larger-scale channel curvatures to local bedforms and sediment permeability heterogeneities [16–18]. For sites of known GW recharge pathways, studies associated higher GW constituent concentrations to respective increases in SW concentrations [19,20]. For a site with elevated GW nitrate concentrations and along a losing stream, (when SW discharges to surrounding sediments), a multi-scale experiment examined found minor changes in nitrate over the whole reach, (indicating little GW-SW discharge), but noticeable nitrate increases at likely zones of GW upwelling points [21]. This finding points to the complexity of GW-SW nonpoint source pollutant behavior. When GW and SW tracer concentrations are similar, careful considerations attributing SW increases due to evaporation rather than GW inflow need to be considered [22].

In this work, we focus on the observational and analytical methods for linking high resolution synoptic SW surveys with relatively sparse institutional spatiotemporal GW data to parameterize a discretized, reduced-form model for gaining river reaches, similar to previous studies [20]. We examine several methods of handling differences in spatial scales between SW and GW constituent data with model resolution. We tested combinations of different parameterization schemes for GW and SW characteristics and linked the parameterization schemes to varying GW-SW discharge estimates. To our knowledge, this analysis linking GW-SW interaction using ambient SC conditions and pre-existing wells is novel, and the considerations presented lay out framework for potential further similar analysis of spatial GW-SW exchange.

2.3. Methods and Model Scenarios

We created high resolution longitudinal maps of various water quality sensors from GPS-tagged multi-parameter sensors on a motor-powered kayak platform. The SW data assimilation required time-synchronization between logger clocks and multiple linear piecewise regression methods assisted to effectively account for nonlinear spatial SW behavior. The actual discretization of models incorporating the SW data should dictate spacing for piecewise regressions. Where GW data are sparse in comparison to SW data, considerations of applying distance proximity to both the river location and model cell should be considered. Aggregation of well data to each model segment becomes a potential method of sensitivity in itself. In this work, we considered different GW and SW treatments of specific conductance (SC) when parameterizing a distributed mass-balance model, disregarding potential interactions of SC and potential media between actual wells and SW, hence, the reduced-model description.

2.3.1. Specific Conductance as a Tracer and Measurement

Specific conductance is a common ambient tracer within the environment. For aqueous solutions, the electrical current is measured at a fixed length between a cathode and anode. While metallic conductance is a measure of transport of valence electrons, in aqueous solutions, this is a measure of ion migration. When an electrical potential is applied, the cations migrate toward the cathode and anions migrate towards the anode [23]. For freshwater systems, common dissolved ions are Ca^{2+}, Mg^{2+}, Na^+, K^+, HCO_3^-, CO_3^{2-}, SO_4^{2-}, NO_3^-, and Cl^- [24,25]. The bulk solution measurement of SC is empirically related to the concentration of total dissolved ions, or solids (TDS), by multiplying the conductance by a constant ranging from 0.55-0.75 for most natural waters [26]. While SC is treated conservatively, there is a potential for daily fluctuations [27]. The main advantage for monitoring SC is the simple sensing techniques with low cost, commercially available sensor products. In contrast, measurement of individual ions requires field sample collection and laboratory analysis by ion chromatography [28] or ion selective electrodes that can be prone to interferences [29] and other problems.

In this work, we measured SC using a multi-parameter sonde (Hydrolab MS5) from Hach Environmental. Our sonde is equipped with temperature, depth, dissolved oxygen, and SC sensors. The SC sensor uses 4 electrodes with an open cell to allow water to flow between the electrodes. We calibrated the sensor the day prior to field-sampling using the manufacturer-recommended one-point calibration to a potassium chloride solution. The manufacturer reported SC sensor accuracy is $\pm$ (0.5% of reading + 1 μS cm^{-1}) and incorporates temperature correction constants described in the U.S. Geological Survey Water-Supply Paper 2311, a common standard for freshwater systems [23,30].

2.3.2. Site Groundwater and Surface Water Conditions

Along the lower Merced River (LMR) corridor located in Central Valley, CA, the adjacent geology is dominated by Quaternary alluvium deposits with loamy soil texture, and transitions to predominantly dune sand deposits with sandy loam texture further from the corridor [31]. Regionally, the shallow aquifer is underlain by the Corcoran clay layer ranging from 28 to 85 m below ground surface [32]. We created an interpolated GW surface elevation map and SC surface (Figure 2.1), using California Department of Water Resources (CA DWR) [33] and State Water Resources Control Board (SWRCB) [34] online data, respectively. The interpolated maps were generated using the default inverse-distance weighted method within the ArcGIS software platform. A noticeably elevated water table along the north LMR from river km 23-33 [31] corresponds with a lower percentage of coarse-grain texture at shallower depths [32] as seen in Figure 2.1a. The depth to GW table is shallower north of the LMR, agreeing with total GW pumpage estimates showing heavier extraction south of the Merced River [32]. Though GW inflow into the LMR generally sustains baseflow [35], an identified GW preferential flowpath to the LMR upstream of Highline Canal (river km 26), supported by the described elevated water table, has been the site of numerous field [36,37] and modeling [38,39] studies for GW-SW discharge and nutrient transport. For GW SC, an apparent hotspot for elevated SC concentrations corresponds with lined industrial wastewater retention ponds seen in Figure 2.1b. Surrounding land use along the LMR is dominated by agriculture with some nearby municipalities [31], where crop fertilizer application,

dairy operations, and septic systems can leach nitrates and potentially increase SC [40–42]. GW dissolution of sediment minerals can also naturally affect SC concentrations.
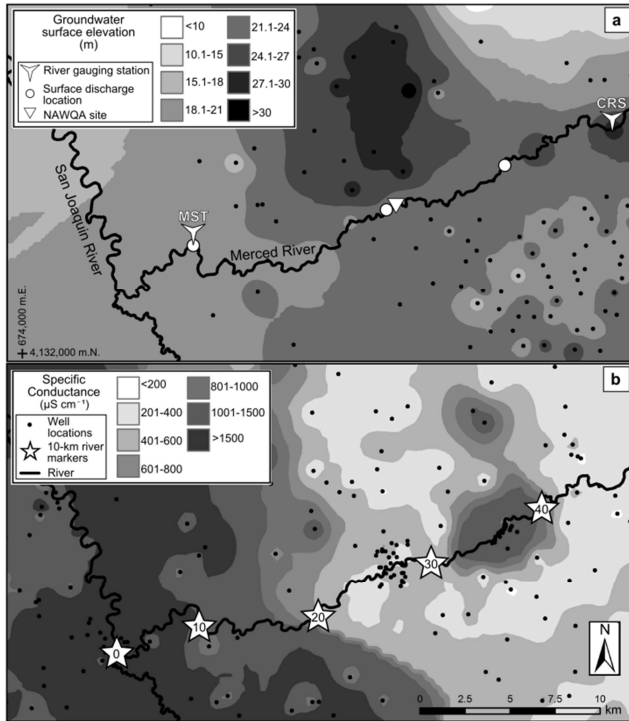
Figure 2.1. Interpolated contours of groundwater surface elevations for Spring 2012 showing regional hydraulic gradient (E to W) with local N-S gradients toward the LMR (a); and groundwater specific conductance (SC) contour map for the same region (GW data aggregated from 1950-present) showing elevated SC levels between river km 40 and 33, and in the lower end of the study ready (downstream of river km 20) (b). (The inverse distance weighting (IDW) method was used for the interpolations and generated in ArcGIS). The figure is reproduced from Pai et al [43] and the original well data are from the CA DWR and GAMA online repositories [34].

The LMR flow is controlled upstream by dams used for flood control, hydroelectricity, and storage for irrigation. Exchequer Dam was originally constructed 1926 with an expansion of capacity in 1976 (New Exchequer Dam). There are two smaller diversion dams (McSwain and Crocker-Huffman) to delivery canals. The Merced River drains to the San Joaquin River and the Sacramento-San Joaquin Delta. The mean annual streamflow for 1941 to 2004 was 19.4 m^3 s^{-1} but varies with precipitation and snowmelt in the Sierra Nevada mountains, where the Merced River originates. Artificial variability was created for the Vernalis Adaptive Management Plan releasing water from New Exechequer Dam to both attract and transport salmon population during October and May [31], respectively. During our study (2010-2012), there was a wet water year (WY2011) leading to increased dam release.

For our study, river km 0 corresponds to the Merced-San Joaquin River confluence and increases upstream with river path distance (see Figure 2.1b). Within our study reach there were 3 visible drainage canals: Livingston Canal (river km 36), Highline Canal (river km 26), and Lower Stevinson Lateral (river km 8). Also, there are

8

two gauging stations, Merced River at Cressey (station ID: CRS) and near Stevinson (MST) seen in Figure 2.1a, measuring SW SC, river stage, and associated flow from rating curves.

2.3.3. Surface Water Sampling and Data Preparation

Synoptic sampling surveys collected SW data SC using the Hydrolab Model MS5 and GPS telemetry (Valeport Midas Surveyor Echo Sounder, 210 MHz, GPS $\pm$ 4 m accuracy). The MS5 was housed within a polyvinyl chloride (PVC) for protection with drilled holes to allow for flow. The SC sensor and PVC were immersed slightly below water surface to prevent snags. A battery-powered trolling motor attached to a tandem kayak transported the sensor payload down a 38-km reach of the LMR. Surveys started early in the morning and took 5 to 7 h to complete. We maintained a path along the thalweg (center) of the river, occasionally having to deviate to avoid woody debris and for battery-exchange stops. We conducted 17 surveys from a period from 3/31/2010 to 3/23/2012 over a range of CRS reported daily flows (1.3 to 150 m^3s^{-1}) managed from upstream dam releases. All sensor platforms collected data at one sample per minute or higher frequency, with the highest collection frequency of 6 samples per second for GPS data.

Assimilating data from different loggers and providing spatial context for river distances requires 3 major steps seen in Figure 2.2. First, geotagging the collected water quality data from the MS5 with a different frequency GPS involved taking the minimum absolute time difference between the water quality sensor and GPS, using a Python (2.7) script. Then, we estimated river distance from spatial coordinates that were extracted from a traced thalweg line in Google Earth. Using an R-script spatial statistics package called *spatstat* [44], we mapped the water quality tracer point data to the closest location on the thalweg line, and then calculated the river distance from confluence of the mapped, or projected, data. Major filtering conditions included in this study were necessary due to inadvertent SC spikes (from battery-exchange stops at approximately river km 20 and 26.5 or SW inlets), signal drops (from sensor lifting out of water to avoid potential snags), unknown shifts, and periods of noisy data. Because this study focuses on linking GW sources, collected data downstream of a major SW SC spike at the Lower Stevinson Lateral (river km 8) were filtered. Other potential major SW inputs, Highline Canal (river km 26) and Livingston Canal (river km 36), did not noticeably change SW SC concentrations. We created a buffer excluding data 600 m up- and downstream of the battery exchange stops. Other filters were manually applied.

9
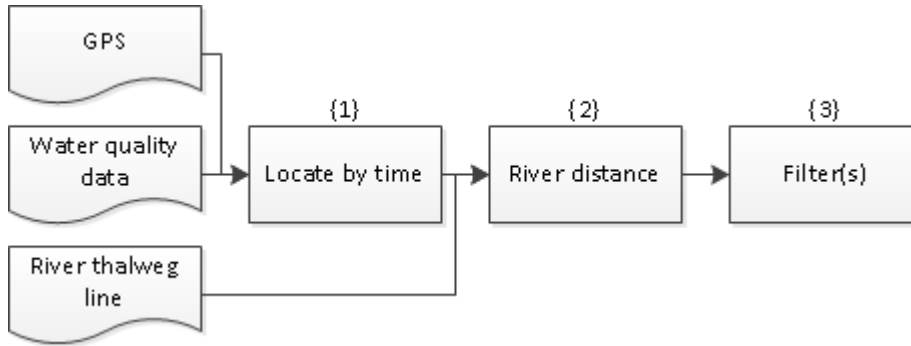
Figure 2.2. Flow diagram of initial SW data preparation which included spatial data assimilation {1}, projecting spatial coordinates to river coordinate system {2}, and probable filtering considerations {3}.

To prepare SW data for potential discretization needed for models or additional longitudinal analysis, we added river distance breakpoints (between user-determined river segments) to longitudinal data and perform user-defined methods of regression within the breakpoints. In this study, we examined the use of three piecewise regression methods. First, we tested the ordinary least squares (OLS) method to estimate linear regressions by minimizing residuals with all observed data within each km discretization independently, (finding the best fit for river km 1, then different then finding the best fit for river km 2, etc.). The OLS method would provide satisfactory fits to the observed SW data, but not necessarily describe GW-SW discharge. We also tested a nonparametric regression method, Sen's slope estimator, taking the median of all uniquely ranked pairwise of slopes [45]. This method would be useful for minimizing potential point source phenomena or other SC spikes that bypassed the filtering protocol. Again, each km discretization would be evaluated independently from one another. Last, we explored using a piecewise linear regression using the R-package, *segmented*, that forces concentration values at the breakpoints to connect smoothly (no data gap or jump). This approach eliminates potential continuities (unrealistic step increases) in the estimates which are likely to occur using the other two methods. The algorithm attempts to minimize residuals given this condition of breakpoint continuity, and is updated with every additional breakpoint [46]. While this method forces connectivity, best fits may be sacrificed for an individual discretization segment.

2.3.4. Groundwater Data Preparation

Due to the sparse (relative to collected SW data) and uneven distribution of GW SC data seen in Figure 2.1b, establishing the groundwater concentration distribution along the river (used to estimate fluxes) was challenging and we examined several approaches. We considered 1-km river segments and tried (1) assigning the concentration of the closest well, (2) the average concentration of the 3 closest wells, and (3) using the interpolated concentration (inverse distance weighting, IDW) from a raster surface developed from the well data (see Figure 2.1b) to link GW with SW data characteristics. We applied a 5-km exclusionary buffer around the river when considering the closest or average of 3 closest wells. One potential weakness for linking the closest GW well to multiple river segments is if the closest well sees dilution effects

from river mixing. A weakness for using IDW interpolation using the 12 closest wells (default ArcGIS setting), was for potentially unrealistic smoothing of GW SC data.

The available GW data were also temporally sparse. For both Merced and Stanislaus counties, 1246 of the 2600 wells with unique names had only one sample from 1950 to 2014. We held GW SC values constant for the duration for the synoptic runs. We averaged SC data from wells that had replicate data (more than two samples on the same day). For wells with multiple time samples (excluding replicates), we considered two approaches for handling the data. The more direct approach involved averaging the whole time period. The other considered samples closest to the synoptic sampling range (3/31/2010 to 3/23/2012). If there were multiple samples within the relevant date range, values were averaged. If there were no samples with date range, the closest samples to the date range were averaged.

Other considerations for preparing GW well data included potential temporal trends and differences with respect to well screen depths. While no noticeable temporal trend was seen in GW SC (Figure 2.3), increasing trends in nitrate concentrations have been documented in the region [40]. We examined periods from 1950 to present (almost all available well SC data) and from 1980 to present, when the confidence intervals for regional nitrate concentration did not consistently increase [40]. The tradeoff for excluding older water quality data was the potential for even fewer wells for linking GW to river segments, as discussed before. With respect to well-screen depth considerations, nitrate concentrations were notably different between shallow and deep wells, below the confining Corcoran clay layer [40]. For available Merced and Stanislaus county SC data from the SWRCB [34], we defined shallow conditions as above the confining layer, as differentiated by sampling responsibilities from different agencies or studies [47]. The shallow conditions (or filter) excluded any datasets from agency or study data that had data only below the confining layer, but included datasets that overlapped both above and below the confining layer. For data from the US Geological Survey National Water Information System (USGS-NWIS), we cross-referenced well depth information [48] and filtered out well depths below 85 m, the deepest range of the clay layer.
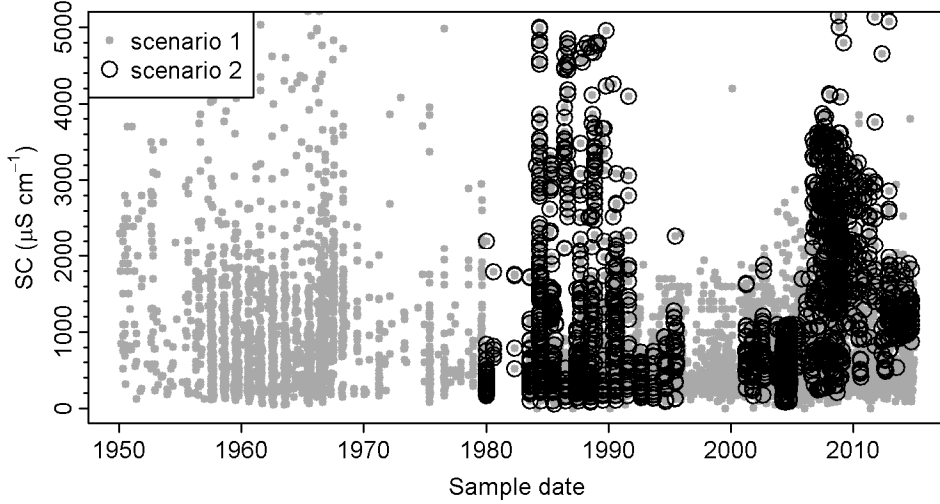
Figure 2.3. Well GW SC values plotted less than 5000 µS cm^{-1} for Merced and Stanislaus counties. The two scenarios, 1950 on and all depths (Scenario 1) and 1980 on and shallow depths (Scenario 2), are highlighted. The data fail to show a clear trend with either scenario. The well data were aggregated from GAMA [34] and USGS-NWIS [48].

2.3.5. Linking GW-SW Discharge and Parameterization Scenarios

We build from previous work taking a simple mass balance approach to link GW discharge, Q_g (m^{3}s^{-1}), to SW [20,22]. To create a distributed GW-SW model, we discretized the mass balance model to take advantage of the high resolution SW-collected data. We apply this model to many potential scenarios involving parameterization preparation for both SW and GW data. To simplify the mass balance flow equation, we assume negligible SW inflow, evaporation outflow, and aggregate GW inflow as a singular input.

$$Q_d = Q_u + Q_g \tag{2.1}$$

where Q_d is downstream flow computed by the model and Q_u is upstream flow initially supplied by the CRS gauging station. The model assumes steady state upstream and groundwater conditions. Additionally, linking potential GW discharge to the SW requires distinct differences in GW and SW tracer concentrations [22] and discussed previously in the site setting. Without noticeable concentration differences, no inference of GW-SW exchange can be inferred. The accompanying tracer mass balance model is:

$$Q_d C_d = Q_u C_u + Q_g C_g \tag{2.2}$$

where downstream and upstream concentrations, C_d and C_u (µS cm^{-1}), are parameterized from collected SW SC data and C_g is parameterized from available GW SC data. A schematic shows the discretized form of Equation (2.2) in Figure 2.4a showing the mass fluxes per segment and likely wells parameterizing the GW-SW flux in a hypothetical river corridor (Figure 2.4b). Substituting Equation (2.1) into (2.2), we arrive at the final GW discharge, Q_g, relationship:

$$Q_g = \frac{Q_u(C_d - C_u)}{C_g - C_d}. \tag{2.3}$$

12
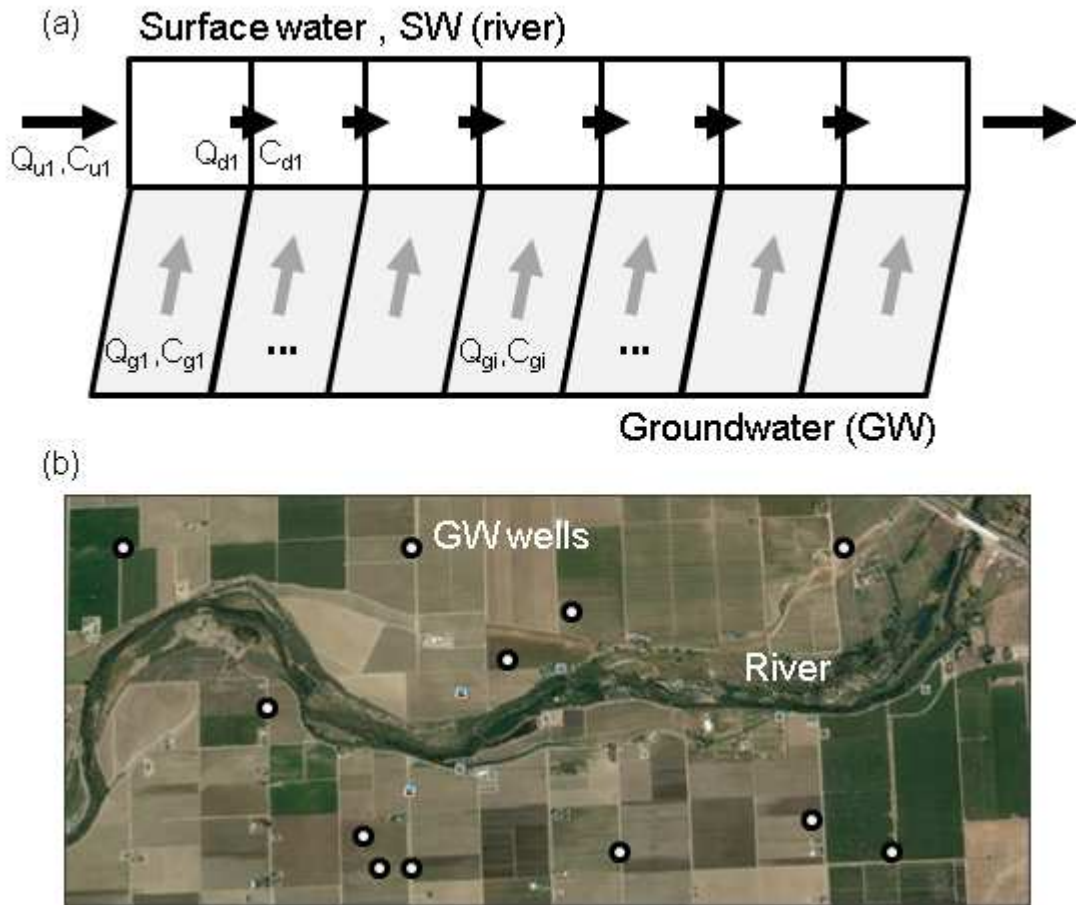
Figure 2.4. Schematic diagram of Equation (2.2) in a discretized form (a) for a river corridor with a hypothetical well distribution (b), parameterizing segment loads ($Q_{gi}C_{gi}$).

Given that the LMR is considered a net gaining reach [35] with higher GW SC than SW SC, we anticipate the model to exhibit positive GW inflow (gaining) from model parameterizations. While computed SW losses are possible (negative Q_g) due to negative SW SC gradients, we attribute negative Q_g to unaccounted sources of low SC. Because negative Q_g is not associated with SW loss, we set Q_g to zero when computed. Additionally, this reduced-form model simplifies potential localized GW-SW exchange within a given river segment. Potential physical drivers of GW-SW exchange, such as regional hydraulic gradients (Figure 2.1a), local sediment heterogeneities, channel tortuosity, and bed topography [16], are not distinguished within this model.

We tested the model formulation under multiple parameterization schemes. Given the multiple methods of preparing and discretizing SW and GW SC parameters previously presented, we tested all combinations of spatial and temporal parameterizations to examine the variability between schemes. Initially, we focused on SW piecewise trend regressions and GW spatiotemporal projections to the model. We then focused on two scenarios including all GW data from 1950 on and all depths versus from 1980 on and shallow depths. The scenarios are summarized in Table 2.1. As a metric to examine results across multiple flows, we propose taking the average of the

percentages of total reach groundwater inflows with recorded upstream daily flows, $\overline{\%Q_g}$. We expected GW SC parameterization methods would have the largest effect on GW-SW discharge due to the sparse nature of available data, particularly close to the river corridor.

Table 2.1. Multiple methods to treat collected SW and available GW SC data (by different agencies online). Abbreviations for methods are found in parentheses.

SW linear regression methods	GW spatial methods	GW temporal methods	Other GW considerations
Ordinary least squares (lin)	Closest (sp_clo)	Closest (t_clo)	1950 on, all depths (Scenario 1)
Sen's slope (sen)	Average of 3 closest wells (avg3)	Average over period (t_avg)	1980 on, shallow depths (Scenario 2)
Segmented (seg)	IDW of 12 closest wells (idw12)		

2.4.   Results and Discussion

After filtering SW SC irregularities and truncating downstream results of river km 8 due to noticeable SC concentration increase from the Lower Stevinson Lateral, we split the SW SC in 1-km river segments to perform piecewise linear regressions and examine non-linear behavior within larger study reaches. The three SW regression methods discussed in Table 2.1 are depicted as lines for 4 representative flows in Figure 2.5. For the most part, the SW regression methods agree well with each other. Potential deviations consistently occur at the battery exchange stop locations (river km ~20 and 26.5), where filtering removed data 600 m buffer up- and downstream (1.2 km total) of those locations. The missing data potentially weakened regressed slope estimates at the stops. Unexplained SW SC spikes (11/22/2011) that withstood our filtering protocol and other abrupt changes in SW SC at lower flows created noticeable deviation between regression methods. Flows greater 31.6 m^3 s^{-1} (4 of the 17 synoptic sampling runs) exhibited little noticeable SW SC change are not included in further analysis. The end points for the piecewise linearly regressed lines parameterized C_u and C_d for each 1-km river segment.   The ordinary least squares and Sen's linear regression estimates potentially create unrealistic SW SC discontinuities between the river segments, while the segmented piecewise slope estimate enforces connectivity, a more realistic scenario.
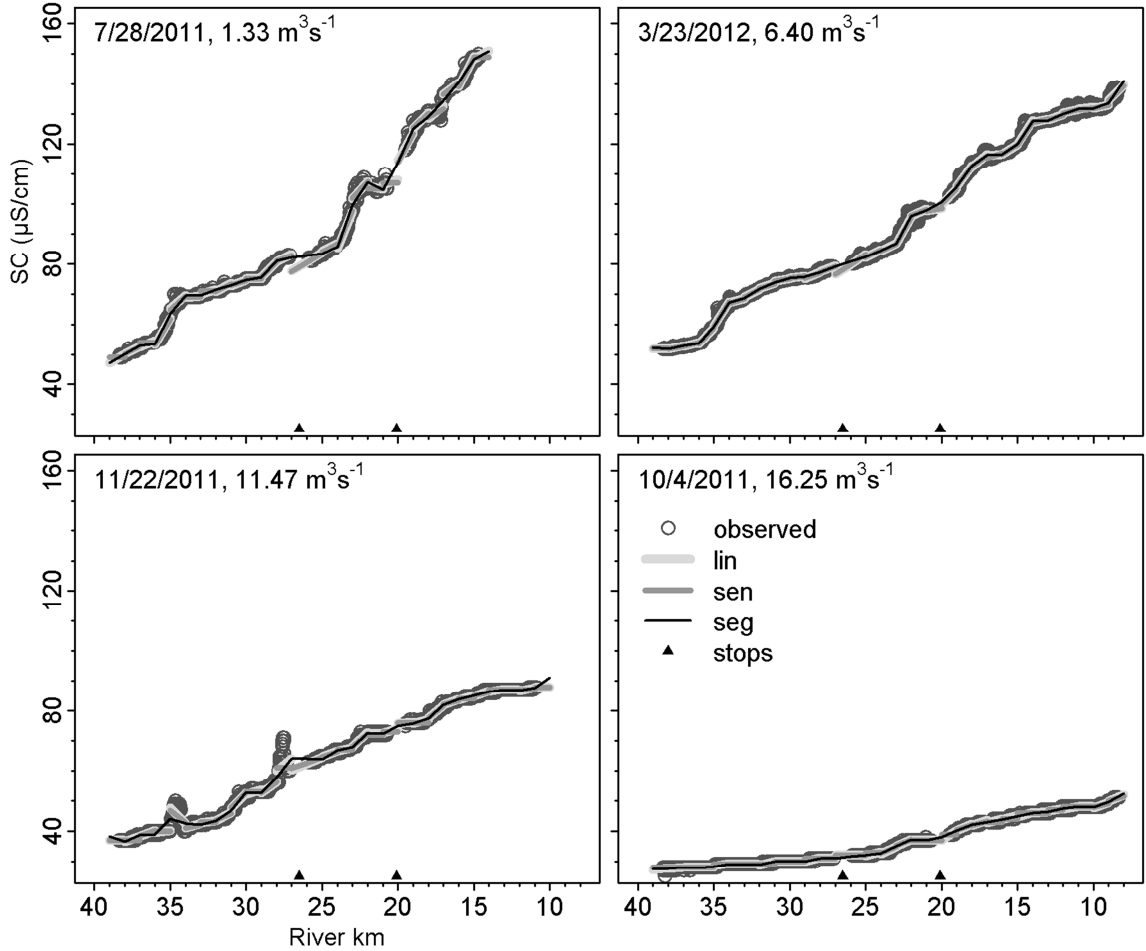
Figure 2.5. Four representative flows with different piecewise trend methods (lines) plotted over the observed SW SC (circles) with observed filtered SC at battery exchange locations (triangles).

For GW SC parameterization to model river segments, we examined 3 spatial methods with the 2 aforementioned scenarios considering well data period and depth, summarized in Table 2.1. Figure 2.6 depicts 2 of the spatial methods (sp_clo and avg3) along the LMR (river km 0 to 40 shown) for the 2 scenarios, (1950 on and all well depths in Figure 2.6a; 1980 on and shallow depths in Figure 2.6b). The well density for Scenario 2 drastically decreased and unique well assignments to the distributed model would likely be greatly affected by this approach. The wells used for IDW spacing were not included in Figure 2.6 as the 12 closest wells would likely encompass a large fraction of all the wells depicted, especially for Scenario 2. We analyzed both scenarios for further sensitivity analysis.
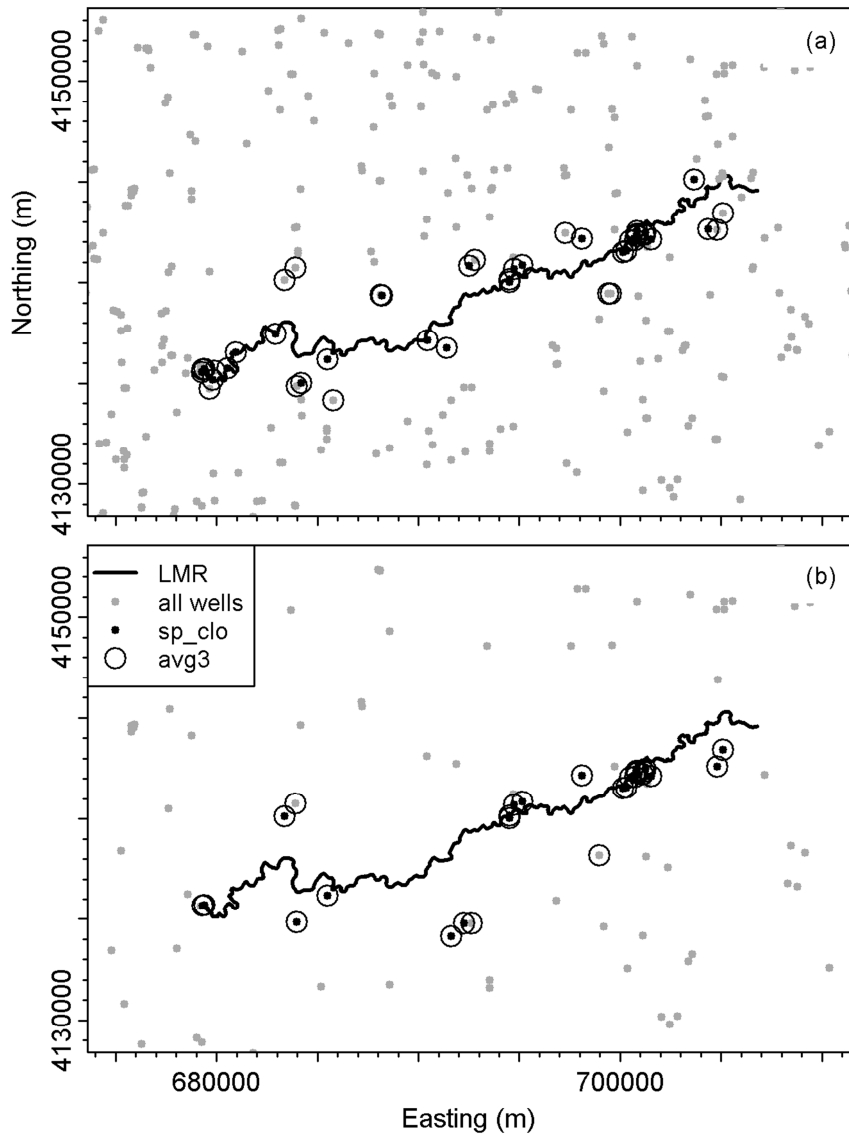
Figure 2.6. Available GW SC well locations for available data for (a) Scenario 1 and (b) Scenario 2, described previously in Table 2.1. Black dots and circles indicate wells used to parameterize GW-SW discharge model.

For all synoptic sampling runs of interest, we examined how the different SW and GW parameterization schemes affect $\overline{\%Q_g}$, the averaged percentages of cumulative GW-SW discharge estimates to respective daily upstream flows for all sampling events (Figure 2.7). For Scenario 2, the interpolated IDW GW parameterization scheme (idw12) estimates an unusually large percentage of GW inflow. This is likely due the interpolation scheme including wells further from the river than Scenario 1 resulting in less accurate representation of localized SC concentrations. Imposing spatial constraints on IDW or lowering number of considered wells would likely be a good consideration. Viewing the sp_clo GW parameterizations, the well data reduction seen in scenario 2 also increased $\overline{\%Q_g}$ from Scenario 1. These increases suggest that low concentration SC wells, likely due to hyporheic mixing, were included in Scenario 2 while other nearby

wells were excluded. The avg3 GW parameterization exhibited the least variation between the scenarios.
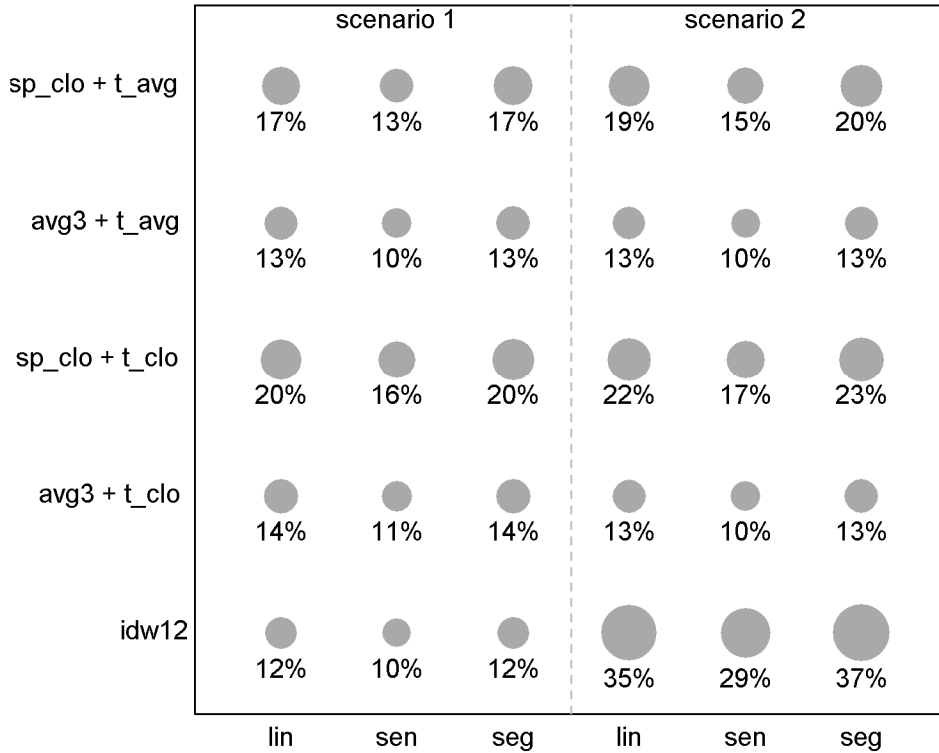
Figure 2.7. Sensitivity plot examining the average percentage of GW inflow to upstream daily flow, $\overline{\%Q_g}$, for all synoptic sampling runs. The SW trend methods (x-axis), combination of GW spatiotemporal assignment methods (y-axis), and 2 scenarios (all described in Table 2.1) are shown. The average GW percentage inflows are labeled below each circle whose radius is proportional to the percentage.

The considerations between GW spatial parameterizations (sp_clo, avg3, and idw12) and temporal schemes (t_avg and t_clo) also exhibited noticeable patterns in $\overline{\%Q_g}$. When considering the closest temporal GW SC parameterization (t_clo), $\overline{\%Q_g}$ values are larger than or equal to period-averaged parameterization (t_avg), with higher percentage differences estimated when coupled with sp_close parameterization than with avg3. This suggests that spatially close wells near the LMR during our sampling period likely saw a decrease in well SC relative to the averaged periods (1950 on for Scenario 1; 1980 on for Scenario 2). A likely cause is an increase in upstream dam releases during the wet water year (WY2011) forcing subsequent GW-SW flux changes (from gaining to losing) and mixing of lower concentration SW SC with nearby sampled wells. Such phenomenon agree with previous studies along the LMR [49,50,36]. From a long term perspective, gradual decrease in GW surface elevation from increased well extractions could also cause directional flux changes or decreased GW-SW discharge leading to similar mixing effects described above. Spatially, the closest well parameterization (sp_clo) consistently estimated higher $\overline{\%Q_g}$, with exception to the Scenario 2, idw12 case described previously. Again, the high GW to upstream flow percentage is likely due to low GW well SC concentration with associated GW-SW mixing and spatially sparse

wells, associating multiple segment parameterizations of C_g with the low well SC concentration(s).

By comparison, SW regression parameterization methods caused less $\overline{\%Q_g}$ variation. Sen's slope estimation method did consistently underestimate $\overline{\%Q_g}$ compared to ordinary least square and segmented piecewise linear regression methods. Given thorough filtering methods, we believe that the median slope selection method (sen) would likely underestimate segment slopes that general upward trends as seen in the observed LMR SC concentrations. For instance on the synoptic sampling run on 7/28/2011 (Figure 2.5), such nonlinear river segment behavior is noticeable for river km 17 and 36, and likely to occur for several segments at low flow conditions, when whole reach slopes are larger. Overall, the SW parameterization methods had less impact than GW parameterization methods. We expected this as GW SC parameterization methods focused on downscaling sparser well measurements to the denser 1-km river.

To view local sensitivities between spatial GW parameterization methods for all sampling events, we created individual sample plots (Figure 2.8) for distributed GW-SW discharge while holding temporal methods constant (i.e., sp_clo + t_clo; avg3 + t_clo; idw12). The GW SC concentrations, C_g, for every river segment are located in the final plot and assumed to be invariant over all the sampling runs. The greatest range of spatially assigned C_g values (500-1500 µS cm^{-1}) between parametrization methods clearly occurs along downstream segments from river km 8-18, where higher GW SC wells near the San Joaquin River likely elevate the interpolated scheme (idw12) concentrations (C_g). Likewise, this decreases estimated GW-SW discharge inferred from Equation (2.3) and likely contributes to the lower estimated $\overline{\%Q_g}$ for the idw12 case relative to sp_clo and avg3 cases. For some sample dates (8/9/2010, 8/11/2011, 3/31/2010), downstream distributed discharges (river km 8-10) show large differences between parameterization schemes. This is likely due to the higher local SW SC slopes specific to those sampling dates and seen in supporting Figure 2.9. Another large spike in local Q_g occurs on 11/22/2011 that is unseen for other sampling dates. The estimated anomaly is also due to SW behavior, specifically the unfiltered SW SC spike seen in Figure 2.5. For Scenario 1, additional sensitivity analysis for GW temporal methods (Figure 2.10) and SW regression selection methods (Figure 2.11) generally showed less effect on distributed GW-SW discharge estimates.
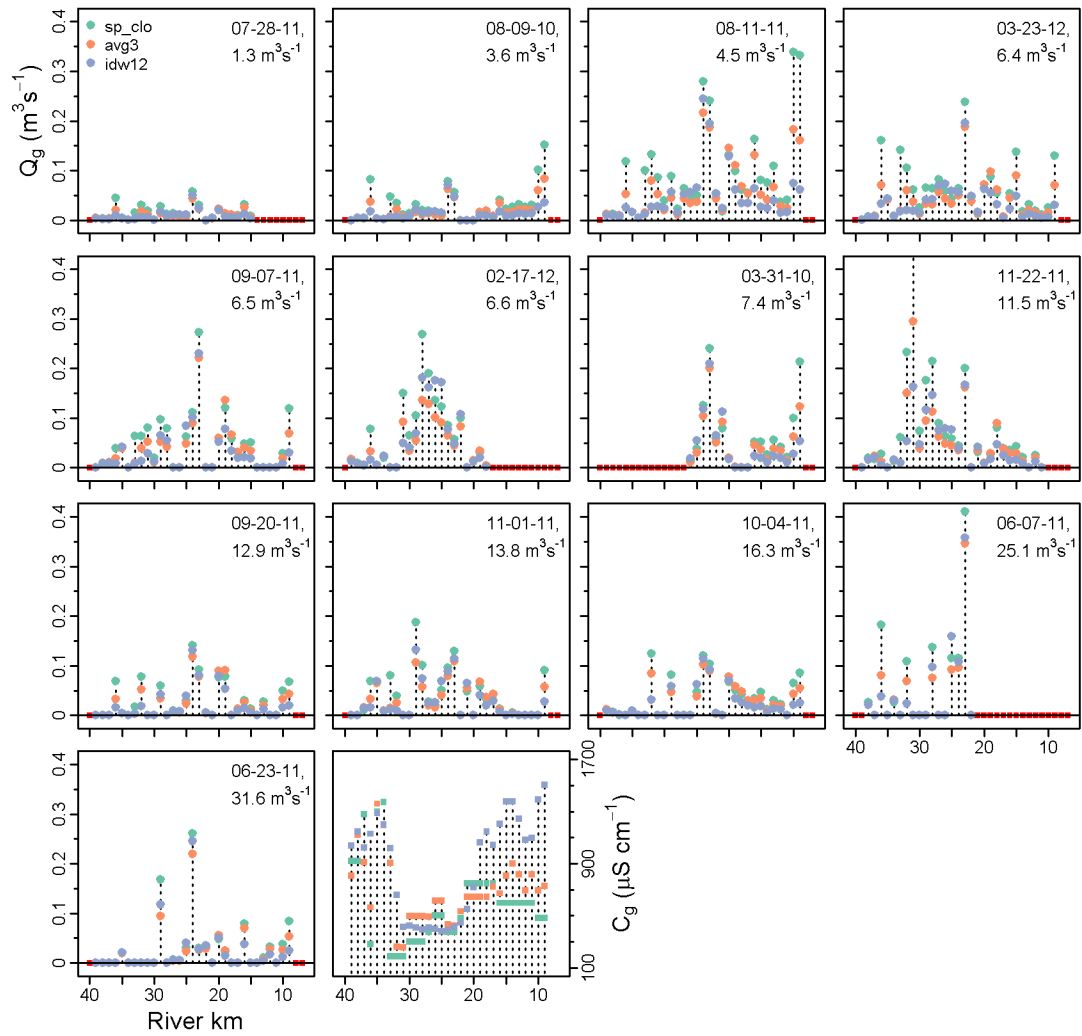
Figure 2.8. Discretized sensitivity plots for the 3 methods of spatial GW parameterization methods, while not varying other parameterizations (Scenario 1, lin SW parameterization, t_clo GW temporal parameterization). The vertical dashed lines connecting the dots delineate data at every river km. Red squares denote locations without data. The last plot shows the different GW SC values, C_g, assigned to 1-km segments that were used for all synoptic sample runs.
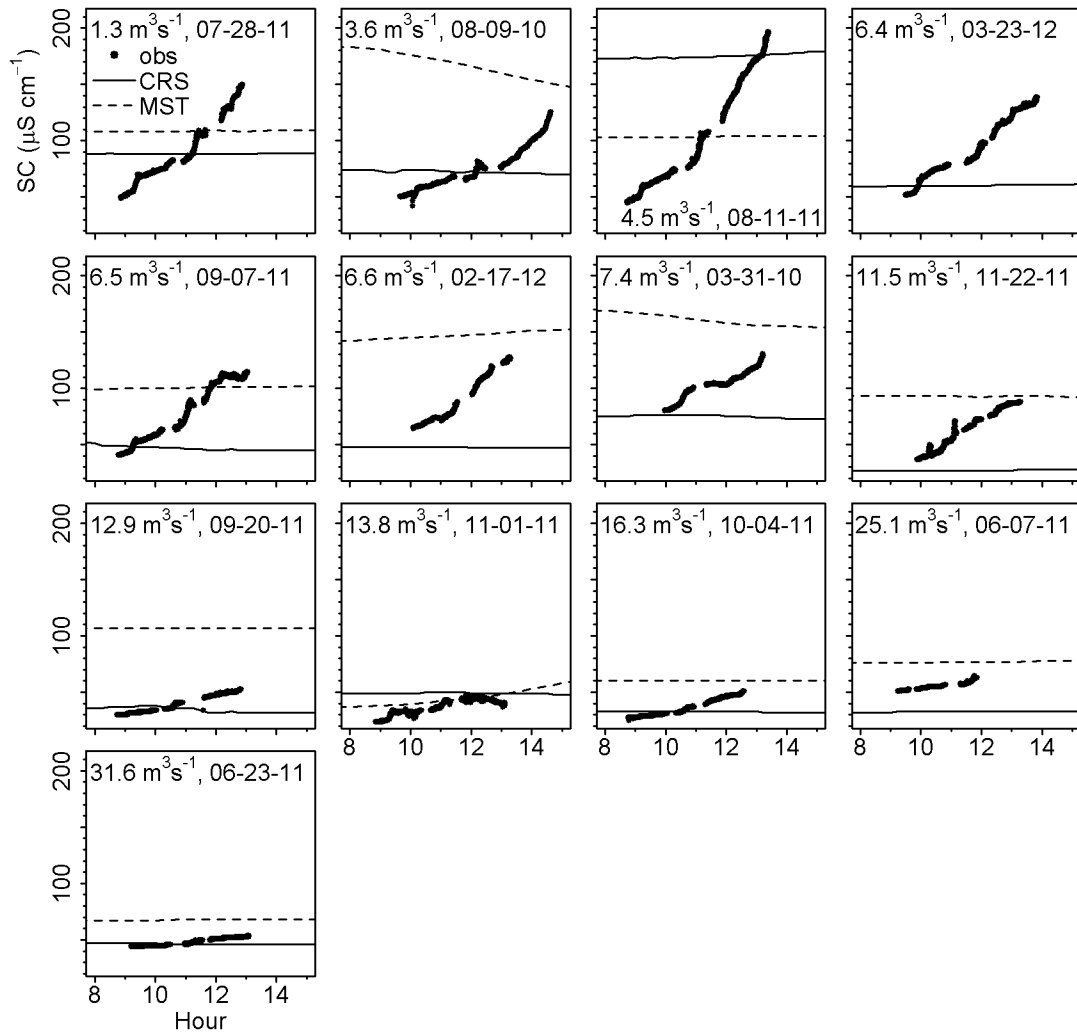
Figure 2.9. Plot of all SC for the observed synoptic sampling and gauging stations (CRS and MST) with time. CRS exhibited small fluctuations supporting steady state upstream conditions. However, MST shows noticeable trends for some of the sampling sessions. MST was missing data for 3/23/2012.
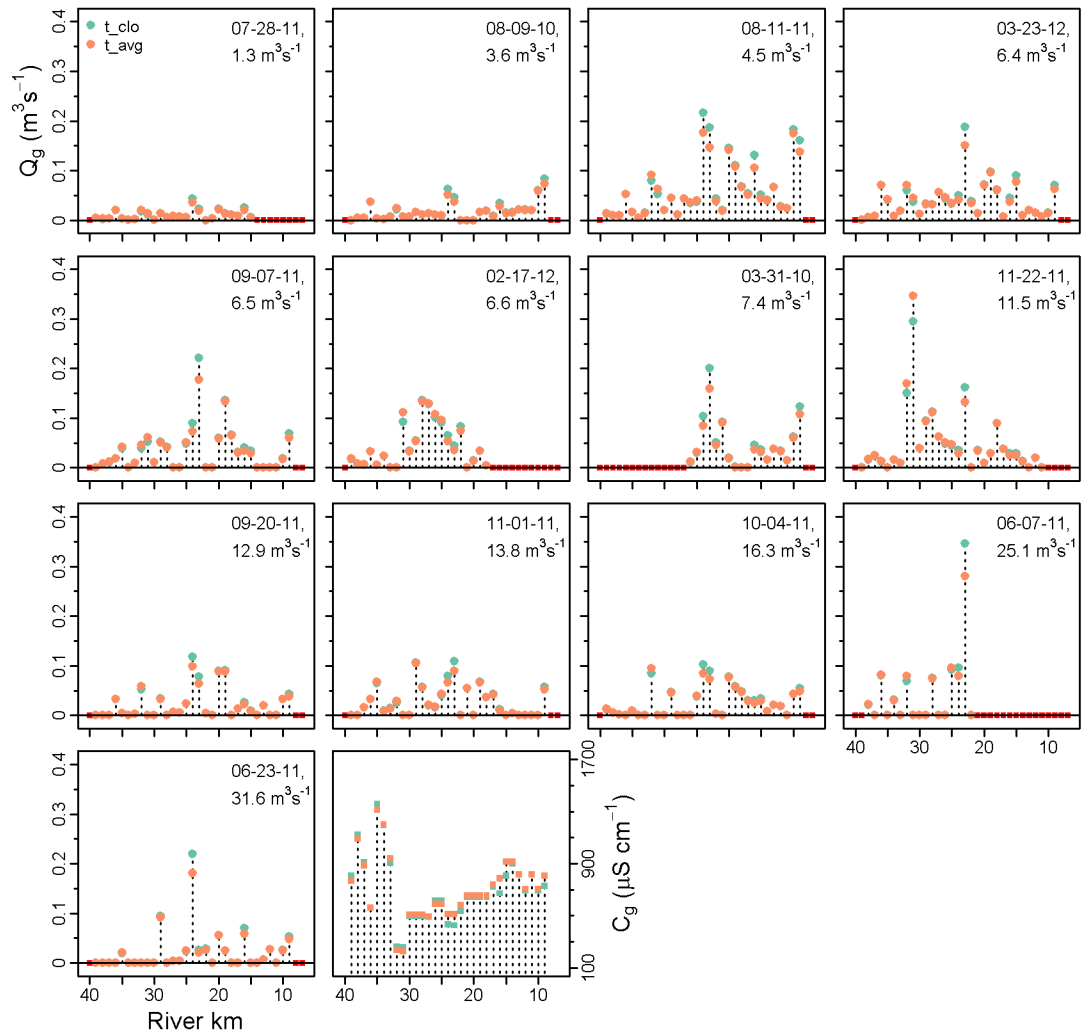
Figure 2.10. Discretized sensitivity plots for the 2 methods of temporal GW parameterization methods, while not varying other parameterizations (Scenario 1, lin SW parameterization, avg3 GW spatial parameterization). The vertical dashed lines connecting the dots delineate data at every river km. Red squares denote locations without data. The last plot shows the different GW SC values, C_g, assigned to 1-km segments that were used for all synoptic sample runs.

21
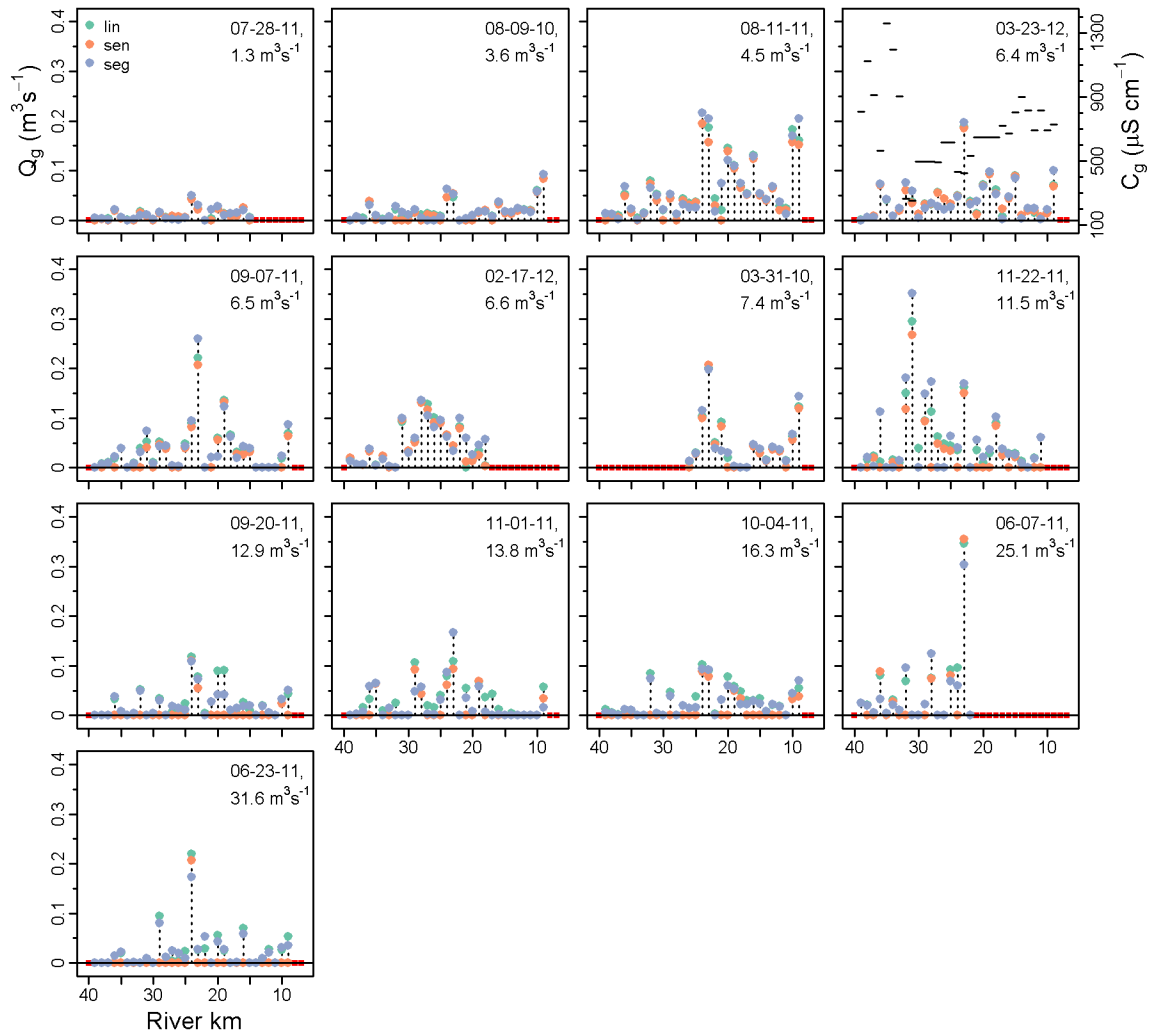
Figure 2.11. Discretized sensitivity plots for the 3 methods of SW piecewise regression election methods, while not varying other parameterizations (Scenario 1, avg3 GW spatial parameterization, t_clo GW temporal parameterization). The vertical dashed lines connecting the dots delineate data at every river km. Red squares denote locations without data. The top right plot shows the different GW SC values, C_g, as black horizontal lines, assigned to 1-km segments that were used for all synoptic sample runs.

2.4.1. Summary and Considerations

The results of this work present both collection methodology and analysis of high resolution SW quality data along a lowland river of known GW discharge to the SW and significant differences between GW and SW ambient SC concentrations, (i.e., elevated GW SC). Attributing longitudinal and localized SW SC changes to GW inputs required spatial and temporal methods to parameterize a distributed mass-balance model. Greater influence is seen when applying different methods to downscale the sparser GW data set (in both space and time). The key findings are that defining attributes of the well source data and associated filtering (Scenario 1 versus Scenario 2) and that well spatial parameterization methods (sp_clo, avg3, and idw12) created the largest variabilities in both cumulative (Figure 2.7) and distributed GW-SW discharge estimates (Figure 2.8).

Such sensitivities to GW SC assignment encourage further research in methods to measure GW well concentrations at higher resolutions than currently available. While similar studies have often installed piezometers [51], there are practical limitations of installation and property access. Less invasive methods such as electromagnetic and resistivity array systems towed behind boats generate local depth maps of SC and could provide further justification GW SC spatial assignment we used in our study [52]. Finally, increased used of more advanced geostatistics for GW quality spatial interpolations could also be applied for further sensitivity analyses [53,54].

Applying this method and analysis to other gaining rivers should consider steady state assumptions, mixing characteristics for model discretization schemes, and differences in GW and SW SC concentrations. While we assumed our system to be steady for SW SC and flow, the idealization simplifies minor temporal variations (see supporting Figures 2.8 and 2.11 for station SC concentrations and flows respectively). The figures depict relatively steady upstream conditions at the gauging station, CRS, but slight temporal trends at the downstream station, MST. A likely unsteady case for 11/11/2011 (Figure 2.9) shows increasing flow (Figure 2.12) corresponding with increasing SC concentration with time (less SW dilution). This case could potentially elevated GW-SW discharges from the abrupt decrease in SW flows and residual bank storage. Discretization of our system also assumed well-mixed conditions likely to be true for our river dimensions. While vertical mixing generally occurs quickly in river systems, higher flow conditions causing stage and associate river width increases will have to account for longer lengths to attain full lateral mixing for discretization purposes [55]. Finally, the low differences between ambient tracer (SC) concentrations between the GW and SW would render this analysis ineffective and would likely not see the SW concentration gradients we observed in this work.

Overall, this work provides a framework for synoptic sampling and analysis considerations to estimate GW-SW discharge. The resulting distributed estimates from 1-km to multi-km scales provide a potential tool for assessing nonpoint source impacts of interest to maintaining general watershed sustainability. This is of particular interest in human-impacted watersheds, where nonpoint source loading from the GW can affect potential SW quality and ecosystems. Coupled with land-use change information and better spatial and temporal GW well data, these synoptic analyses would provide a better picture of human watershed impacts leading to better-informed land management practices.
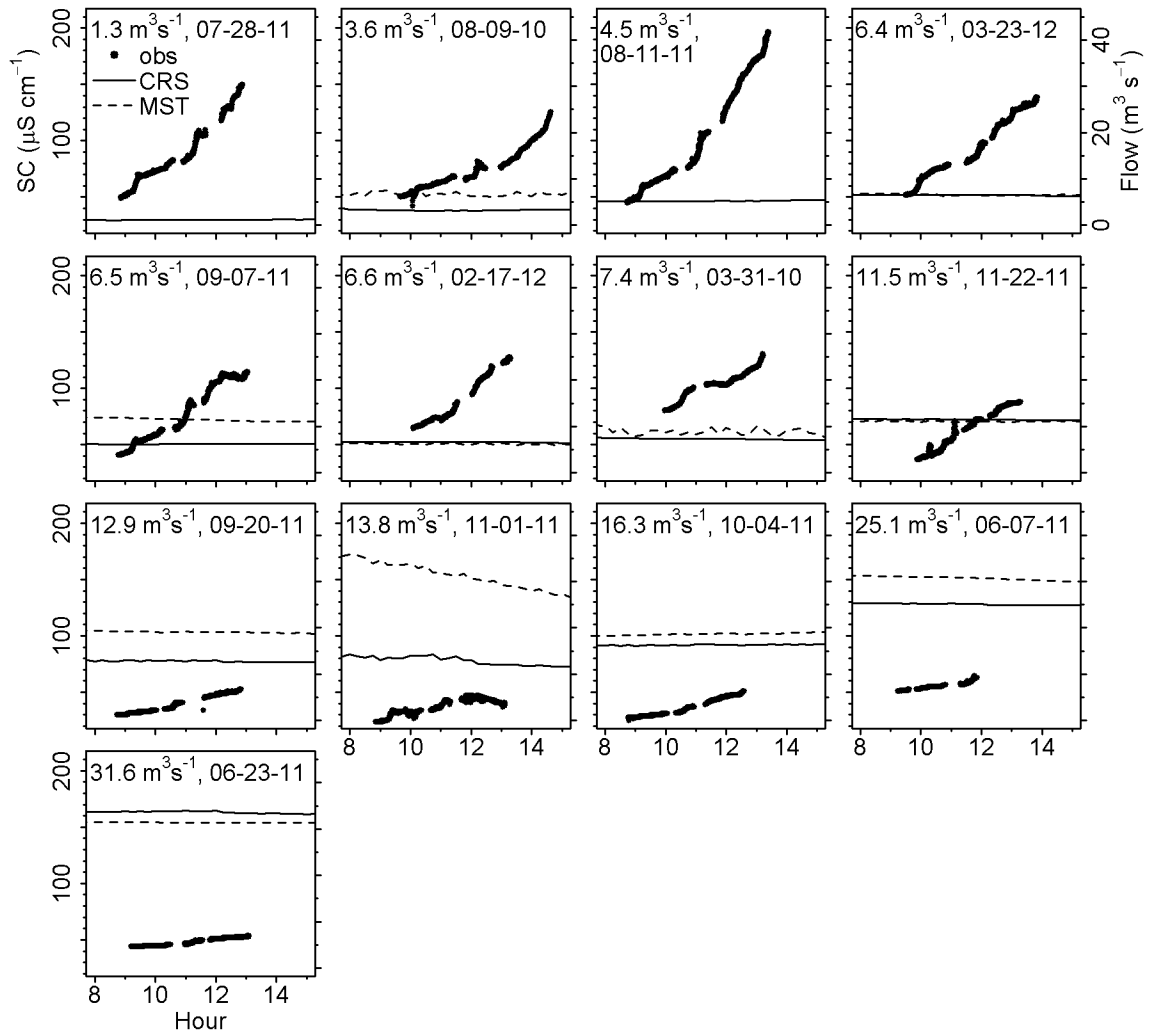
Figure 2.12. Plot of observed SC and flow at the gauging stations (CRS and MST). For the most part steady conditions were observed with exception to 11/1/2011. MST was missing flow data on 7/28/2011 and 8/11/2011.

2.5. References

[1] C.J. Vörösmarty, P.B. McIntyre, M.O. Gessner, D. Dudgeon, A. Prusevich, P. Green, et al., Global threats to human water security and river biodiversity, Nature. 467 (2010) 555–561. doi:10.1038/nature09440.

[2] E. Kalbus, F. Reinstorf, M. Schirmer, Measuring methods for groundwater - surface water interactions: a review, Hydrology and Earth System Sciences. 10 (2006) 873–887.

[3] J. Dehotin, P. Breil, I. Braud, A. de Lavenne, M. Lagouy, B. Sarrazin, Detecting surface runoff location in a small catchment using distributed and simple observation method, Journal of Hydrology. 525 (2015) 113–129. doi:10.1016/j.jhydrol.2015.02.051.

[4] S.S. Kaushal, P.M. Groffman, L.E. Band, E.M. Elliott, C.A. Shields, C. Kendall, Tracking Nonpoint Source Nitrogen Pollution in Human-Impacted Watersheds, Environ. Sci. Technol. 45 (2011) 8225–8232. doi:10.1021/es200779e.

[5] S.H. Ensign, M.W. Doyle, Nutrient spiraling in streams and river networks, J. Geophys. Res. 111 (2006) G04009. doi:10.1029/2005JG000114.

[6] A.J. Ranalli, D.L. Macalady, The importance of the riparian zone and in-stream processes in nitrate attenuation in undisturbed and agricultural watersheds – A review of the scientific literature, Journal of Hydrology. 389 (2010) 406–415. doi:10.1016/j.jhydrol.2010.05.045.

[7] Q.D. Lam, B. Schmalz, N. Fohrer, Modelling point and diffuse source pollution of nitrate in a rural lowland catchment using the SWAT model, Agricultural Water Management. 97 (2010) 317–325. doi:10.1016/j.agwat.2009.10.004.

[8] D. Yates, J. Sieber, D. Purkey, A. Huber-Lee, WEAP21—A Demand-, Priority-, and Preference-Driven Water Planning Model, Water International. 30 (2005) 487–500. doi:10.1080/02508060508691893.

[9] K. Beven, Towards an alternative blueprint for a physically based digitally simulated hydrologic response modelling system, Hydrol. Process. 16 (2002) 189–206. doi:10.1002/hyp.343.

[10] J. Dehotin, I. Braud, Which spatial discretization for distributed hydrological models? Proposition of a methodology and illustration for medium to large-scale catchments, Hydrol. Earth Syst. Sci. 12 (2008) 769–796. doi:10.5194/hess-12-769-2008.

[11] C.L. Dent, N.B. Grimm, Spatial heterogeneity of stream water nutrient concentrations over successional time, Ecology. 80 (1999) 2283–2298. doi:10.1890/0012-9658(1999)080[2283:SHOSWN]2.0.CO;2.

[12] S.R. Villamizar, H. Pai, C.A. Butler, T.C. Harmon, Transverse spatiotemporal variability of lowland river properties and effects on metabolic rate estimates, Water Resour. Res. 50 (2014) 482–493. doi:10.1002/2013WR014245.

[13] J.T. Crawford, L.C. Loken, N.J. Casson, C. Smith, A.G. Stone, L.A. Winslow, High-Speed Limnology: Using Advanced Sensors to Investigate Spatial Variability in Biogeochemistry and Hydrology, Environ. Sci. Technol. 49 (2015) 442–450. doi:10.1021/es504773x.

[14] G.M. Sivirichi, S.S. Kaushal, P.M. Mayer, C. Welty, K.T. Belt, T.A. Newcomer, et al., Longitudinal variability in streamwater chemistry and carbon and nitrogen

fluxes in restored and degraded urban stream networks, J Environ Monit. 13 (2011) 288–303. doi:10.1039/c0em00055h.

[15] A. Tinka, M. Rafiee, A.M. Bayen, Floating Sensor Networks for River Studies, IEEE Systems Journal. 7 (2013) 36–49. doi:10.1109/JSYST.2012.2204914.

[16] T.C. Winter, J.W. Harvey, O.L. Franke, W.M. Alley, Ground Water And Surface Water A Single Resource, Denver, Co, 1998. http://pubs.usgs.gov/circ/circ1139/#pdf.

[17] A.E. Fryar, E.J. Wallin, D.L. Brown, Spatial and Temporal Variability in Seepage Between a Contaminated Aquifer and Tributaries to the Ohio River, Ground Water Monitoring & Remediation. 20 (2000) 129–146. doi:10.1111/j.1745-6592.2000.tb00279.x.

[18] D.P. Genereux, S. Leahy, H. Mitasova, C.D. Kennedy, D.R. Corbett, Spatial and temporal variability of streambed hydraulic conductivity in West Bear Creek, North Carolina, USA, Journal of Hydrology. 358 (2008) 332–353. doi:10.1016/j.jhydrol.2008.06.017.

[19] A.H. Haria, P. Shand, C. Soulsby, S. Noorduijn, Spatial delineation of groundwater–surface water interactions through intensive in-stream profiling, Hydrol. Process. 27 (2013) 628–634. doi:10.1002/hyp.9551.

[20] S. Jasechko, J.J. Gibson, S. Jean Birks, Y. Yi, Quantifying saline groundwater seepage to surface waters in the Athabasca oil sands region, Applied Geochemistry. 27 (2012) 2068–2076. doi:10.1016/j.apgeochem.2012.06.007.

[21] C.L. Dent, Nancy B. Grimm, S.G. Fisher, Multiscale effects of surface–subsurface exchange on stream water nutrient concentrations, Journal of the North American Benthological Society. 20 (2001) 162–181. doi:10.2307/1468313.

[22] P.G. Cook, Estimating groundwater discharge to rivers from river chemistry surveys, Hydrol. Process. 27 (2013) 3694–3707. doi:10.1002/hyp.9493.

[23] R.L. Miller, W.L. Bradford, N.E. Peters, Specific conductance; theoretical considerations and application to analytical quality control, U.S. G.P.O., 1988. http://pubs.er.usgs.gov/publication/wsp2311.

[24] M.H. Cox, G.W. Su, J. Constantz, Heat, Chloride, and Specific Conductance as Ground Water Tracers near Streams, Ground Water. 45 (2007) 187–195. doi:10.1111/j.1745-6584.2006.00276.x.

[25] R.B. McCleskey, D.K. Nordstrom, J.N. Ryan, Comparison of electrical conductivity calculation methods for natural waters, Limnol. Oceanogr. Methods. 10 (2012) 952–967. doi:10.4319/lom.2012.10.952.

[26] J.D. Hem, Study and Interpretation of the Chemical Characteristics of Natural Water, 3rd ed., U.S. Geological Survey, 1985. http://pubs.usgs.gov/wsp/wsp2254/.

[27] G. Bertrand, D. Siergieiev, P. Ala-Aho, P.M. Rossi, Environmental tracers and indicators bringing together groundwater, surface water and groundwater-dependent ecosystems: importance of scale in choosing relevant tools, Environ Earth Sci. 72 (2013) 813–827. doi:10.1007/s12665-013-3005-8.

[28] T.I. Brinton, R.C. Antweiler, H.E. Taylor, Method for the determination of dissolved chloride, nitrate, and sulfate in natural water using ion chromatography, U.S. Geological Survey ;, 1996. http://pubs.er.usgs.gov/publication/ofr95426A.

[29] R. De Marco, G. Clarke, B. Pejcic, Ion-Selective Electrode Potentiometry in Environmental Analysis, Electroanalysis. 19 (2007) 1987–2001. doi:10.1002/elan.200703916.

[30] Hach Environmental, Hydrolab DS5X, DS5, and MS5 Water Quality Multiprobes: User Manual, 2006.

[31] J.A.M. Gronberg, C.R. Kratzer, Environmental Setting of the Lower Merced River Basin, USGS, 2006.

[32] K.R. Burow, J.L. Shelton, J.A. Hevesi, G.S. Weissmann, Hydrogeologic Characterization of the Modesto Area, San Joaquin Valley, California, 2004.

[33] California Deparment of Water Resources (CA DWR) Contour Data Report, (n.d.). http://www.water.ca.gov/waterdatalibrary/groundwater/contour/.

[34] State Water Resources Control Board (CA SWRCB) Groundwater Ambient Monitoring and Assessment, (n.d.). http://geotracker.waterboards.ca.gov/gama/.

[35] C.C. Faunt, Groundwater Availability of the Central Valley Aquifer, California, U.S. Geological Survey, 2009. http://pubs.usgs.gov/pp/1766/.

[36] J.L. Domagalski, S.P. Phillips, E.R. Bayless, C. Zamora, C. Kendall, R.A.W. Jr, et al., Influences of the unsaturated, saturated, and riparian zones on the transport of nitrate near the Merced River, California, USA, Hydrogeol J. 16 (2008) 675–690. doi:10.1007/s10040-007-0266-x.

[37] C. Zamora, Estimating Water Fluxes Across the Sediment–Water Interface in the Lower Merced River, California, USGS, 2007.

[38] S.P. Phillips, C.T. Green, K.R. Burow, J.L. Shelton, D.L. Rewis, Simulation of Multiscale Ground-Water Flow in Part of the Northeastern San Joaquin Valley, California, U.S. Geological Survey, 2007. http://pubs.usgs.gov/sir/2007/5009/.

[39] C.T. Green, J.K. Böhlke, B.A. Bekins, S.P. Phillips, Mixing effects on apparent reaction rates and isotope fractionation during denitrification in a heterogeneous aquifer, Water Resour. Res. 46 (2010) W08525. doi:10.1029/2009WR008903.

[40] K.R. Burow, B.C. Jurgens, K. Belitz, N.M. Dubrovsky, Assessment of regional change in nitrate concentrations in groundwater in the Central Valley, California, USA, 1950s–2000s, Environ Earth Sci. 69 (2012) 2609–2621. doi:10.1007/s12665-012-2082-4.

[41] K.R. Burow, J.L. Shelton, N.M. Dubrovsky, Occurrence of nitrate and pesticides in ground water beneath three agricultural land-use settings in the eastern San Joaquin Valley, California, 1993-1995, U.S. Geological Survey ; Information Services [distributor], 1998. http://pubs.er.usgs.gov/publication/wri974284.

[42] M.L. van der Schans, T. Harter, A. Leijnse, M.C. Mathews, R.D. Meyer, Characterizing sources of nitrate leaching from an irrigated dairy farm in Merced County, California, Journal of Contaminant Hydrology. 110 (2009) 9–21. doi:10.1016/j.jconhyd.2009.06.002.

[43] H. Pai, S.R. Villamizar, T.C. Harmon, High Resolution Synoptic Salinity Mapping To Identify Groundwater–Surface Water Discharges in Lowland Rivers, Environ. Sci. Technol. 49 (2015) 4842–4850. doi:10.1021/es504483q.

[44] A. Baddeley, R. Turner, spatstat: An R Package for Analyzing Spatial Point Patterns, Journal of Statistical Software. 12 (2005) 1–42.

[45] R.O. Gilbert, Statistical Methods for Environmental Pollution Monitoring, John Wiley and Sons, 1987.

[46] V.M.R. Muggeo, segmented: an R Package to Fit Regression Models with Broken-Line Relationships, R News. 8 (2008) 20–25.

[47] GAMA – Groundwater Ambient Monitoring & Assessment Program, (n.d.). http://www.waterboards.ca.gov/gama/geotracker_gama.shtml.

[48] US Geological Survey (USGS)- National Water Information System: Web Interface, (n.d.). http://waterdata.usgs.gov/nwis.

[49] H.I. Essaid, C.M. Zamora, K.A. McCarthy, J.R. Vogel, J.T. Wilson, Using heat to characterize streambed water flux variability in four stream reaches, J. Environ. Qual. 37 (2008) 1010–1023. doi:10.2134/jeq2006.0448.

[50] L.J. Puckett, C. Zamora, H. Essaid, J.T. Wilson, H.M. Johnson, M.J. Brayton, et al., Transport and Fate of Nitrate at the Ground-Water/Surface-Water Interface, Journal of Environment Quality. 37 (2008) 1034. doi:10.2134/jeq2006.0550.

[51] P.G. Cook, S. Lamontagne, D. Berhane, J.F. Clark, Quantifying groundwater discharge to Cockburn River, southeastern Australia, using dissolved gas tracers 222Rn and SF6, Water Resour. Res. 42 (2006) W10411. doi:10.1029/2006WR004921.

[52] M. Hatch, T. Munday, G. Heinson, A comparative study of in-river geophysical techniques to define variations in riverbed salt load and aid managing river salinization, GEOPHYSICS. 75 (2010) WA135–WA147. doi:10.1190/1.3475706.

[53] A. Bárdossy, J. Li, Geostatistical interpolation using copulas, Water Resour. Res. 44 (2008) W07412. doi:10.1029/2007WR006115.

[54] B. Nas, A. Berktay, Groundwater quality mapping in urban groundwater using GIS, Environ Monit Assess. 160 (2008) 215–227. doi:10.1007/s10661-008-0689-4.

[55] S.A. Socolofsky, G.H. Jirka, Special topics in mixing and transport processes in the environment, Engineering—lectures, Fifth Ed., Coastal and Ocean Engineering Division, Texas A&M University. (2005).

3. High resolution synoptic salinity mapping to identify groundwater-surface water discharges in lowland rivers

3.1. Abstract

Quantifying distributed lateral groundwater contributions to surface water (GW-SW discharges) is a key aspect of tracking nonpoint-source pollution (NPSP) within a watershed. In this study, we characterized distributed GW-SW discharges and associated salt loading using elevated GW specific conductance (SC) as a tracer along a 38 km reach of the Lower Merced River in Central California. High resolution longitudinal surveys for multiple flows (1.3-150 $m^3 s^{-1}$) revealed river SC gradients that mainly decreased with increasing flow, suggesting a dilution effect and/or reduced GW-SW discharges due to hydraulic gradient reductions. However, exceptions occurred (gradients increasing with increasing flow), pointing to complex spatiotemporal influences on GW-SW dynamics. The surveys revealed detailed variability in salinity gradients, from which we estimated distributed GW-SW discharge and salt loading using a simple mixing model. Modeled cumulative GW discharges for two surveys unaffected by ungauged SW discharges were comparable in magnitude to differential gauging-based discharge estimates and prior GW-SW studies along the same river reach. Ungauged lateral inlets and sparse GW data limited the study, and argue for enhancing monitoring efforts. Our approach provides a rapid and economical method for characterizing NPSP for gaining rivers in the context of integrated watershed modeling and management.

3.2. Introduction

Spatiotemporal variability of groundwater discharges to surface water (GW-SW discharges) can contribute significantly to the dynamics of natural and anthropogenic chemical loading along a river. Effective and economical characterization of these discharges is needed to support distributed watershed modeling and the development of best management practices [1–3]. For example, subsurface contamination (nonpoint-source pollution, NPSP) in the form of nitrate and other salts, organic matter and pesticides is widespread in intensively agricultural watersheds [4–6]. A better understanding of distributed GW-SW discharges would support policy-making with regard to the spatial and temporal connections between land use and the water quality in such watersheds [7,8]. In this work, we explore high resolution synoptic salinity (specific conductance) sensing as a means for rapidly delineating longitudinal changes in a river controlled by groundwater discharges over scales of interest to decision-makers.

There has been significant research on groundwater discharges (in the presence and absence of chemical loads) over a variety of spatial scales [9–11]. Point scale measurement techniques include gradient-flux based approaches that employ direct seepage measurements [8,12] as well as head differential measurements, transient heat [8,9,13–15] and chemical tracer monitoring [7,16,17]. At sub-reach and smaller spatial scales, these approaches have revealed complex spatiotemporal variability in both the magnitude and direction of GW-SW fluxes. The variability is generally attributed to permeability variability in the river bed and adjacent groundwater media, with

temperature-viscosity effects also playing a role [7,8,18]. Given these observations, scaling up these approaches to the watershed scale would likely be a labor intensive proposition.

Characterization of distributed GW-SW discharges over large scales is often focused on baseflow contributions or chemical loading from watershed management units. Differential gauging together with water quality sampling can be used to estimate gain/loss and associated pollutant loading over a reach, providing it constitutes a significant fraction of the streamflow (~10% or more [19,20]). However, this approach is relatively labor intensive for ungauged reaches. Tracer dilution tests and end member mixing of ambient tracers, including isotopes, are also useful approaches for understanding the contributions of groundwater and the sources of pollution in rivers [19,20], but may require expensive analytical efforts. Lastly, distributed temperature sensing (DTS) [14,20–23] and remote sensing (e.g., thermal infrared imaging) approaches [24–26] have seen increasing use in delineating GW-SW exchanges.

This work focuses on synoptic in-stream sampling campaigns for assessing distributed groundwater discharges and salt loads. Manual geochemical sampling campaigns of this type have been used to identify and map discharge zones along rivers [27–30]. In this work we use a rapid, high resolution synoptic in-stream sensing to create a detailed segment-by-segment estimate of salt loading over a wide range of flow conditions. We tested this approach on a regulated river in an agriculturally dominated watershed, examining nonuniform salinity gradients over a wide range of flow and stage and over several seasons.

3.3. Sampling and Analysis

We developed specific conductance (SC) profiles as a proxy for salinity in a series of 1 day synoptic sampling campaigns along a lowland river reach, using a GPS-synchronized SC sensor mounted on a kayak. With a moving trend analysis, we identified river segments significantly gaining in SC and repeated the profiling campaign over a range of flow rates to identify longitudinal trends in salt loading. Using aggregated historical groundwater salinity data, we parameterized a distributed mixing model and developed estimates for the longitudinal distribution of salt load over the range of river conditions.

3.3.1. Study Setting

We tested our synoptic sampling approach on a 38 km reach of the Lower Merced River (LMR) in Central California's San Joaquin Valley. The Valley's steppe biome is characterized by cool, moist winters and hot, dry summers. The average annual precipitation (32 cm) contributes negligibly to surface flow. Instead, flow is dependent on precipitation and snowpack in the upper watershed and regulated by a series of reservoirs. Reservoir operations are closely coupled to water year type on the LMR, and our study period included a wet year (WY2011) between two below-average years (WYs 2010 and 2012). In wet years, flood releases result in flows spanning 2 orders of magnitude (1.3 to 150 m^3 s^{-1}), while in drier years the range is less extensive (1.3 to 20 m^3 s^{-1}). Land use along the LMR is dominated by agriculture, some municipal land uses (2 towns totaling about 17,000 in population), and relatively narrow natural riparian buffers.

Regional geology is dominated by quaternary deposits with dune sand occupying the upstream section and transitioning to alluvial deposits downstream [31]. We interpolated available data from the California Department of Water Resources (CA DWR) [32] and State Water Resources Control Board (SWRCB) [33] for groundwater elevation and SC levels, respectively, to approximate the regional piezometric surface (Figure 3.1a) and SC contours (Figure 3.1b). The piezometric surface exhibits a pattern consistent with the geology of the region and the pumping rates associated with the area's agricultural and urban land uses. The water mound appearing on the northeastern area of the river reach (Figure 3.1 and Figure 3.2) coincides with a lens of finer sediment (Corcoran clay) located at depth ~50 m between approximately river km 23-33 [34]. From there, the piezometric surfaces show regional groundwater movement toward both the Merced and San Joaquin Rivers. The larger pumping rates of the south side and the northeast portion of our study reach are evidenced by the lower groundwater elevations in those regions [34]. Characterizing groundwater SC levels was more challenging due to the scarcity of recent observations. Available data suggested that salinity levels have not changed markedly over the past several decades (Figure 3.3). We therefore aggregated historical data (1950 to present) to create a salinity map for the region (Figure 3.1b). The map shows that salinity increases down the watershed, with the exception of a localized upstream region of higher SC from river km 33-40, adjacent to a set of lined industrial wastewater retention ponds.

The study reach presents the characteristics of a baseflow-dominated system (channel slope between 5×10^{-5} and 5×10^{-4}, sinuosity ratio of 1.75, river penetration greater than 20%, and width to depth ratios at bankfull conditions less than 60) [35]. Previous work on GW-SW interactions along the middle segments of the study reach (USGS National Water-Quality Assessment (NAWQA) Program) demonstrated that, while LMR baseflow conditions are sustained by GW discharges, local transitions from net gaining to losing conditions occurred as stage surpassed a threshold [8,16,36,37]. These researchers measured point-scale specific discharge, (volumetric GW-SW discharge divided by the seepage meter area), to the river ranging from -1.1×10^{-7} to 5.9×10^{-7} m s^{-1} for stages associated with flow rates less than about 8 m^3 s^{-1} [8]. This range corresponds to volumetric discharges of -0.003 to 0.015 m^3 s^{-1} per river km, assuming a wetted perimeter of 25 m. Groundwater modeling results for water-year 2000 along the Lower Merced River estimated a total volumetric discharge of 0.20 m^3 s^{-1} for an 8-km segment within our study reach (roughly river km 23-31) [38].
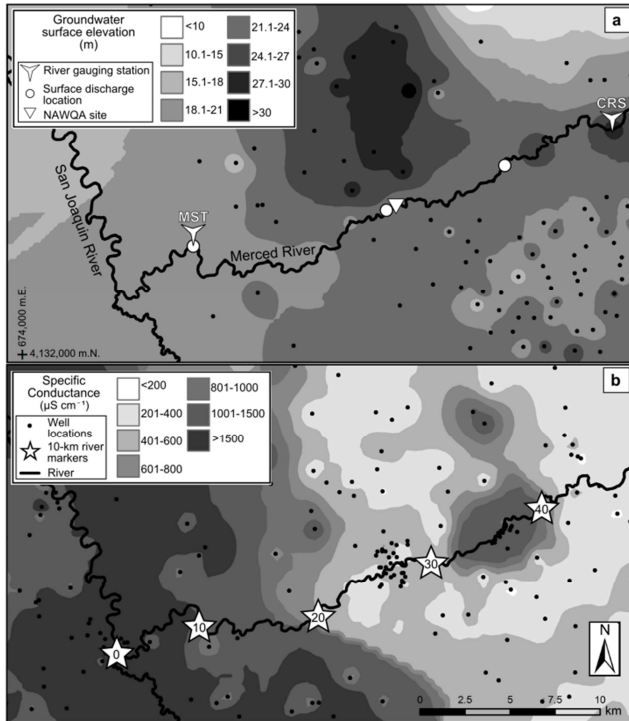
Figure 3.1. Interpolated contours of groundwater surface elevations for Spring 2012 (for other periods see Figure 3.2) showing regional hydraulic gradient (E to W) with local N-S gradients toward the LMR (a); and groundwater specific conductance (SC) contour map for the same region (GW data aggregated from 1950-present) showing elevated SC levels between river km 40 and 33, and in the lower end of the study ready (downstream of river km 20) (b). (The inverse distance weighting (IDW) method was used for the interpolations). The contours were generated from data availably online from the CA DWR [32] and the GAMA program [33].
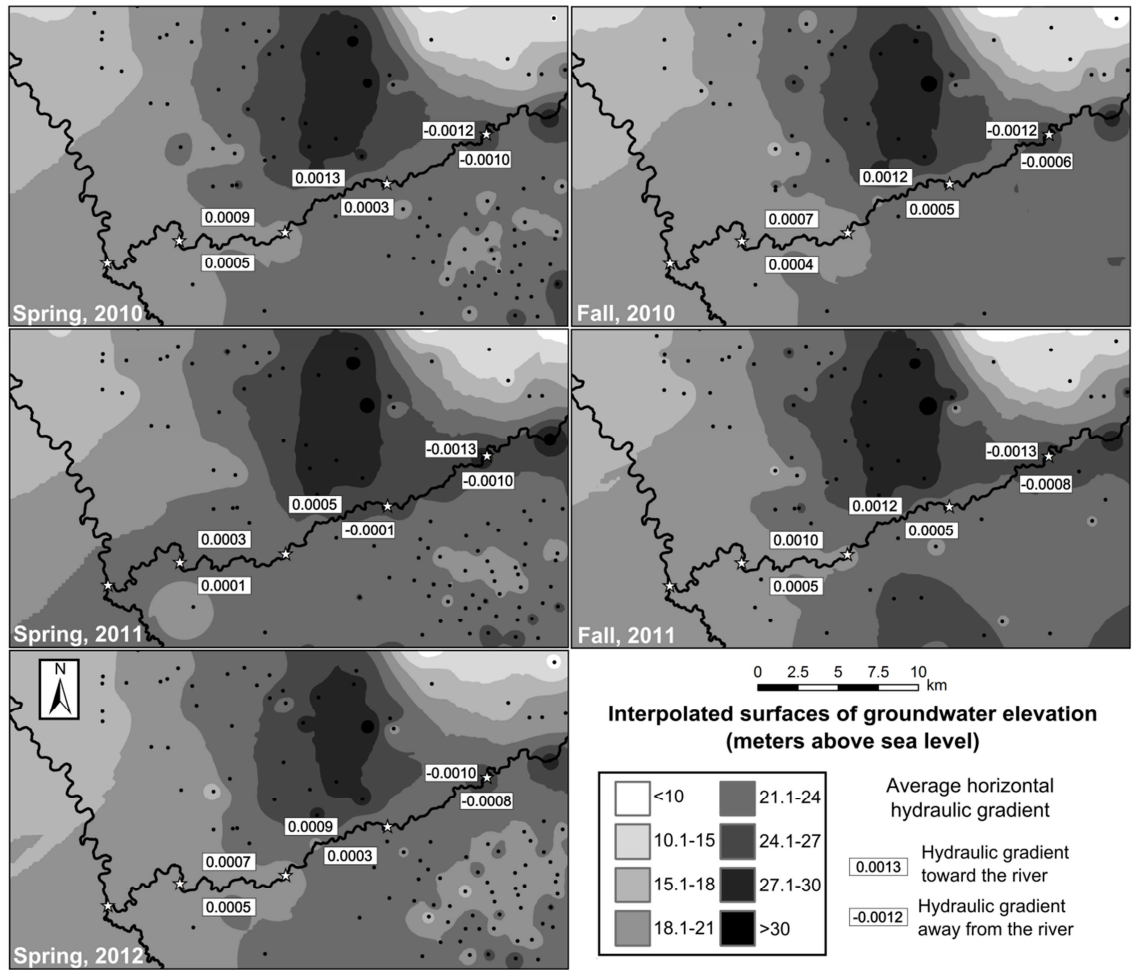
Figure 3.2. Interpolated groundwater surface elevation using the inverse distance weighting (IDW) method for the well data collected by the Stanislaus and Merced Counties during the 2010-2012 period. By assuming connection between the groundwater and surface water, we calculated an average horizontal hydraulic gradient for upper, middle, and lower areas of the study site using the groundwater surface elevation of wells (within an approximate 5 km buffer) and the estimated river stage at the point of interest. The data presented are from the CA DWR [32].
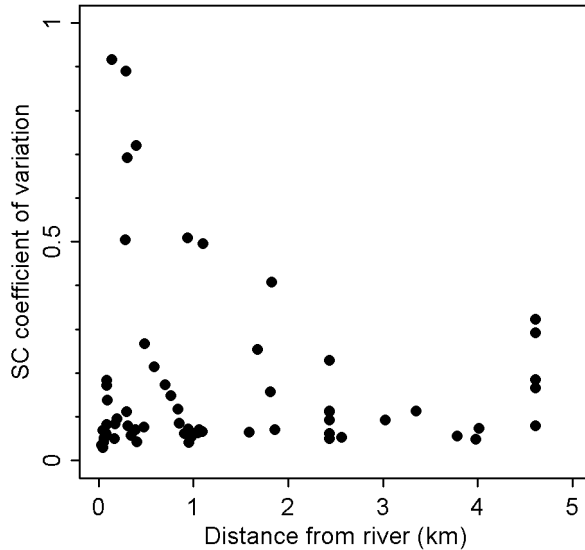
Figure 3.3. Salinity coefficient of variation (CV) for all wells within a 5 km buffer along the river. Only wells having 5 or more observations are shown (64 unique wells total). 54 of the 64 (84%) of the wells had a CV of less than 0.3.

3.3.2. Synoptic Sampling

We tested the synoptic data against CA DWR data (sub-hourly to hourly river stage, flow, and SC levels) from two gauging stations, Merced River at Cressey (station ID: CRS) and near Stevinson (MST), located near the upper and lower limits of the surveyed reach, respectively. We assessed the longitudinal SC gradient 17 times over a range of seasons and flow rates. River conditions included spring flood control/pre-irrigation, summer irrigation, and fall post-irrigation flows (Figure 3.4). Flow conditions were assumed as stable for most of the sampling events, although there were stage changes for some of the higher flow events (the maximum change was 3.7 cm on 11/1/11 at a flow of 13.8 m^3 s^{-1} occurring about 1 day after a significant reduction in reservoir releases, and was during the late stages of a flow recession event). Other observed stage changes during surveys were less than 1.2 cm for flows below 13 m^3 s^{-1}, and 0.9 to 2.4 cm for the four highest flows. These stage changes are discussed further below in the context of the transient flow behavior during surveys.

Surveys employed a tandem kayak equipped with time-synchronized multi-parameter water quality sensors (Hydrolab Model MS5), GPS telemetry (Valeport Midas Surveyor Echo Sounder, 210 MHz, GPS ± 4 m accuracy) for tracing the survey path, and a battery-powered trolling motor. Lagrangian sampling would have required approximately 15 h (an average travel time for the reach estimated from CRS and MST hydrograph peaks) due to low velocity in the lower half of the reach (< 0.5 m/s). The motorized kayak traveled faster than the river water velocity, with surveys requiring 5 to 7 h depending on the flow conditions. All surveys were started in the morning and finished by mid-to-late afternoon. We assumed that the distributed salinity inputs were steady during each survey and therefore insensitive to travel velocity. We maintained a course along the thalweg, and stopped at river km 20 and 26.5 for battery exchanges. SC measurements near stoppage points exhibited high variability due to slow flows, vegetation and bed disturbances during landing.
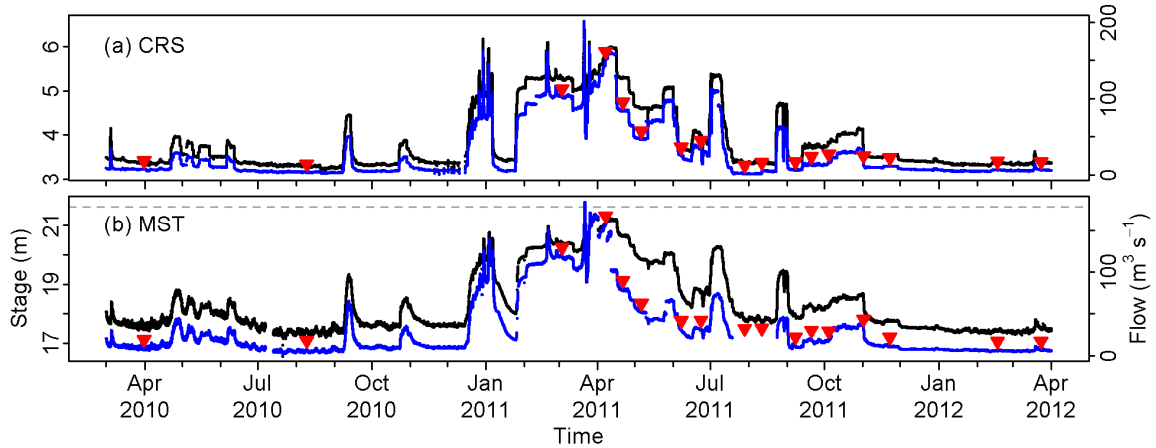
Figure 3.4. Flow (blue line) and stage (black) at (a) upstream (CRS) and (b) downstream (MST) gauging stations on the LMR study reach, where red pointers denote synoptic sampling events. Vertical and horizontal data gaps are due to rating curve adjustments and missing data, respectively. The dashed grey line is reported flood stage for MST (not available for CRS).
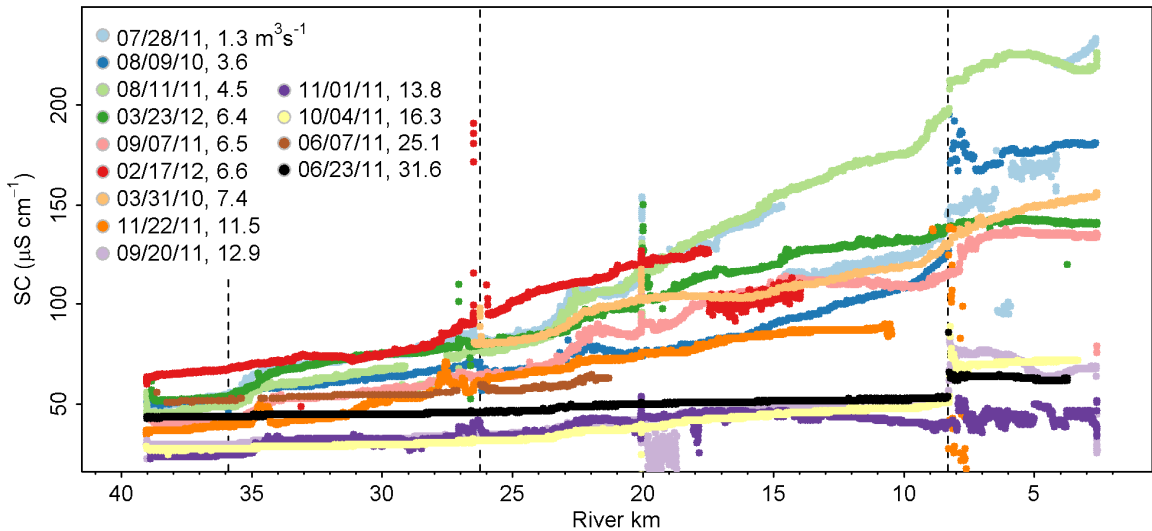
Figure 3.5. Unfiltered specific conductivity values with the sampling dates and daily upstream flow values denoted in the legend. The dashed vertical lines indicate the major SW inlets. The last inlet (Lower Stevinson Lateral around river km 8) showed significant disturbance to SC values on multiple runs and data downstream from the inlet were filtered (i.e., analysis was stopped at river km 8). Two additional spikes around river km 20 and 26 were from transition locations where the kayak required battery replacement causing sediment disturbance and corresponding SC spikes. To filter the spikes, a 600 m buffer both upstream and downstream of the transition locations was applied. Finally, we manually filtered SC data when the sensor values exhibited high variance (e.g., 9/20/11, river km 20 to 18) due to known investigator error (sensor out of water) and sensor cleaning, and for two unexplained shifts (2/17/11 for river km 18 to 14 and 7/28/11 at river km 14 and beyond).

We filtered observations within 600 m upstream and downstream of those locations, (further filtering is described in Figure 3.5). We logged SC at a rate of 0.017 to 0.2 Hz (1 to 12 samples min^{-1}), and GPS coordinates at 6 Hz. We used the echo-sounder's event-

flagging mechanism to designate surface discharges into the river (lateral canals, effluent pipes) during the surveys.

To determine the appropriate scale for characterizing local salinity gradients, we used a moving linear regression analysis to estimate the slope of the SC trace data for segment sizes ranging from 200 m to the entire synoptic study section (38 km). We chose a 1 km segment size for further analysis since our lower SC sampling rate (0.017 Hz) averaged 12 observations per segment for flows up to 31.6 m^3 s^{-1}, a sufficient observation count to estimate slopes. Most surveys averaged higher sample counts per segment. For instance, combined high frequency sampling rates (0.2 Hz) with low flows yielded around 80 observations per km. Higher flows (> 84.8 m^3 s^{-1}) for the lower sampling rate had fewer observations per segment, but exhibited negligible overall SC gradients.

Three ungauged lateral surface water discharges (two canals and one treated wastewater effluent) existed within the study reach. Two typically caused minor perturbations in the survey results, but were overshadowed by the large number of surrounding sampling points. However, the final one (the Lower Stevinson Lateral at river km 8, just upstream of MST) caused large step increases in SC for most of the surveys and potentially signifies flow perturbations, causing us to eliminate this location and all lower sections of the LMR from the study (Figure 3.5). Other minor drains and outlets were seldom active during the sampling events and, when active, exerted negligible effects on the SC gradient.

3.3.3. GW-SW Salt Load Model

We used a simple mass balance to model flow and salt mixing in a river segment. The model assumes stable flow conditions for each sampling event. Neglecting surface discharges, and evaporation effects, which are small here relative to flows, the mass balance to account for flow increasing longitudinally via groundwater discharges in a river segment is as follows:

$$Q_d = Q_u + Q_g \tag{3.1}$$

where Q_d, Q_u and Q_g (m^3 s^{-1}) are the down-, upstream, and groundwater discharge for a river segment. Assuming the segment is well-mixed, we can estimate the salt loading for a segment as:

$$Q_g C_g = Q_d C_d - Q_u C_u \tag{3.2}$$

where C_d, C_u, and C_g (mg TDS L^{-1}) are the down-, upstream, and groundwater total dissolved solids concentrations in the segment (assuming $TDS = SC \cdot 0.65$) [39,40]. The term on the left side of Equation (3.2) can be treated as a lumped mass loading rate or, given knowledge of local groundwater salinity levels, can be used to estimate net local groundwater discharge rates (or vice versa) but does not differentiate patterns at the sub-segment scale [19,41].

We believe this model is appropriate for the Lower Merced River as it is a predominantly gaining river in its lower reaches [34] with elevated surrounding GW SC conditions. Assuming such conditions, longitudinal increases in SW SC are expected and the mixing model can be applied. While groundwater surface elevations suggest more

complex GW-SW interactions with potential gains on the north side and losses on the south side along the river reach (see Figure 3.1a), this model aggregates sub-segment spatial variation of GW-SW discharges to estimate bulk segment GW-SW discharge. The model, however, cannot identify losing segments (negative Q_g), which would indicate low SC inflow or potential in-stream processes [42]. Therefore, segment-estimated negative Q_g values were set to zero.

We expected the assumption of complete mixing to be valid for sufficiently long river segments. Vertical mixing is expected to occur over distances of roughly 50-100 times the river depth [43,44]. The average depth of the LMR ranged from about 0.5 to 3 m during the study period, and thus this model is expected to be relatively insensitive to vertical mixing limitations for river segments greater than 300 m in length. Transverse mixing is roughly two to three times slower than vertical mixing in the same river [45], suggesting that our 1000 m sampling segment size was adequate.

To characterize the salt-loading term (Q_gC_g) in a discretized manner, we developed a spatially distributed version of the above mixing model where C_g values were assigned as the observed SC from the interpolated SC field from Figure 1b (several methods tested, see Table S1). Using the independent estimates for C_g, we estimated Q_g by assigning the flow boundary conditions using CRS station data, and solving Equations (3.1) and (3.2). To assess the model performance, we compared cumulative groundwater discharge with differential gauging station estimates derived from daily mean station flow values, assuming a constant travel time estimate of 15 hours between CRS and MST stations for the varying flows. We necessarily limited the comparison to the two sampling events (3/23/12 and 3/31/10) for which the MST station was unaffected by the nearby lateral canal input.

3.4.   Results and Discussion

The high resolution synoptic surveys yielded 13 SC profiles for flows ranging from 1.3 to 31.6 $m^3 s^{-1}$ (Figure 3.6) with observed SC concentrations ranging from 24 to 197 μS cm^{-1}. Greater flows resulted in flat SC profiles due to dilution effects and were not considered further. To test the consistency of the surveying, we examined three SC profiles captured at similar flow rates (6.4-6.6 $m^3 s^{-1}$) in summer 2011 and spring 2012. The three profiles exhibited the same overall SC change (approximately 80 μS cm^{-1}) and slope (approximately 3 μS cm^{-1} km^{-1}). In addition, their starting and ending SC values agreed with upstream (CRS) and downstream (MST) monitoring data (not shown). This comparison demonstrated a degree of reproducibility of the method, except for local variations in the SC gradients which were evident in the profiles (Figure 3.6). It is worth noting that two unaccounted for spikes in SC (river km 34-35 and 27-28) withstood our filtering protocol for the 11/22/11 survey. We did not observe active surface drains in association with these spikes, and further investigation revealed that they may have been the result of disturbed sediments during unplanned stops in the survey.
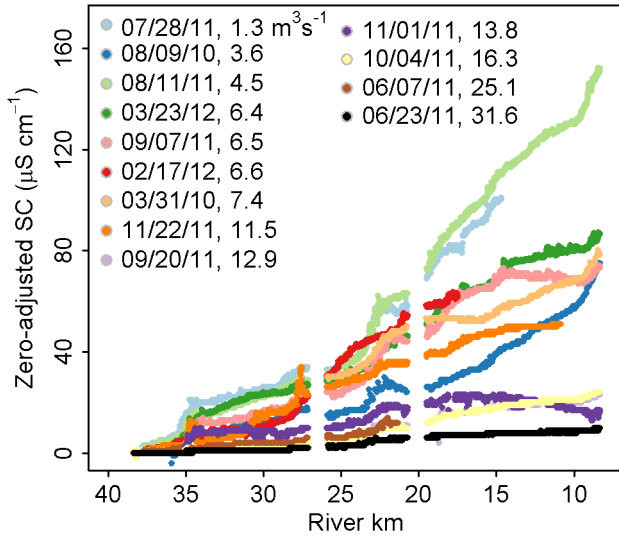
Figure 3.6. Thirteen synoptic survey results for the LMR showing zero-adjusted SC (change from initial SC measurement) over the roughly 38 km study reach for the dates and average flow rates shown. Data gaps denote filtered data at river km 20 and 26.5 (landing points for battery exchanges), and below river km 8, the approximate location of a large point source (drainage canal). The 3/31/10 survey started further downstream (river km 26), and the initial zero-adjusted SC value was estimated using the survey with the nearest flow (2/17/12).

The reach-averaged gradient in SC mainly decreased with increasing flow (Figure 3.6). However, a major exception was observed for one of the lower summer flows tested (3.6 m^3 s^{-1}, 8/9/10). While similar flows in the subsequent summer (1.3 and 4.5 m^3 s^{-1} 7/28/11 and 8/11/11) exhibited the largest reach-averaged SC gradients in this study, the 8/9/10 survey yielded a smaller SC gradient than other surveys completed at flows less than 13.8 m^3 s^{-1}. This finding suggested that additional factors could have affected the river SC gradient for the anomalous survey. The most likely cause of the lower SC gradient in summer 2010 (a dry water year) was the lower hydraulic gradients along the river relative to those of summer 2011 (a wet water year) (Figure 3.2). It is also worth noting that overbank flow occurred during the high flows of spring 2011. Thus, a more speculative explanation for the lower gradient in summer 2010 is that floodplain inundation and subsequent recession may have mobilized salts, rendering them more available to the river through recirculation or leaching in summer 2011.

Like the overall SC changes discussed above, most of the local (1 km segment) SC slopes decreased with increasing flow (left to right in Figure 3.7). For higher flows, local slope estimates and their spatial variation decreased, as dilution attenuated the transitions between river segments. In all cases, the local SC slopes varied along the length of the river reach, an observation we attribute to local groundwater discharge and salinity variation. The greatest slope changes occurred below about river km 26-28, which is near the area associated with the aforementioned regional groundwater mounding and prior investigations related to agricultural GW-SW discharges. It should be noted that the anomalously high negative SC slope for river km 34-35 in the 11/22/11 survey (red cell in Figure 3.7) is most likely the result of bias imparted by an unexplained SC spike occurring late in the segment. For the downstream spike of the same survey

38

(river km 26-27), additional SC observations within the segment were sufficient to overcome the spike (i.e., the resulting slope estimate was less biased).
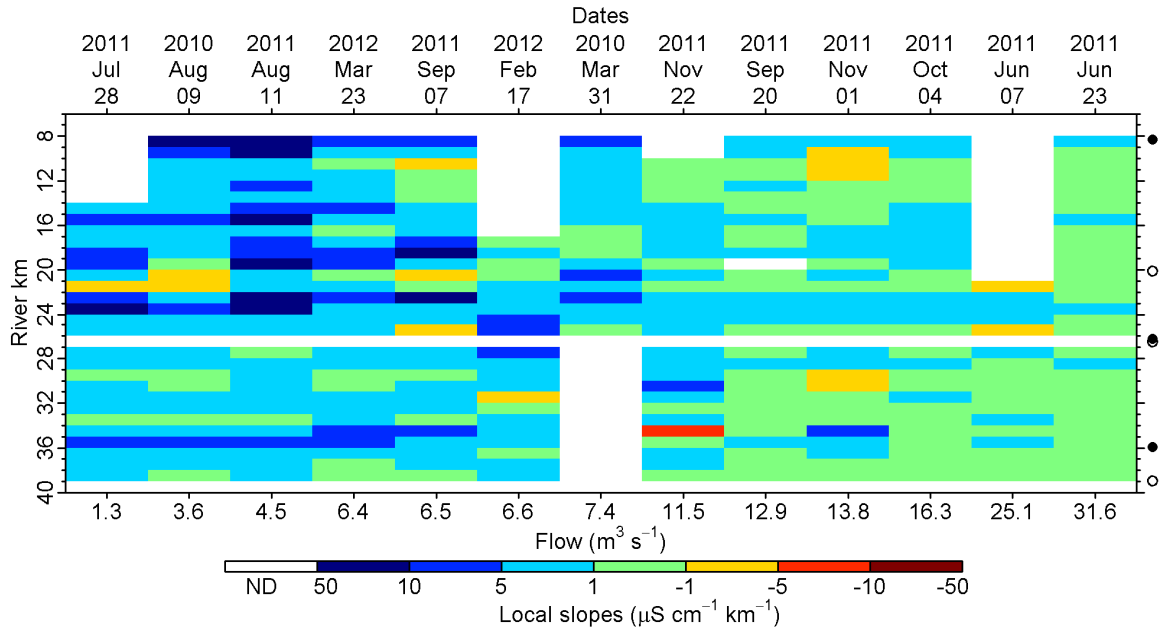
Figure 3.7. Summary of slope classifications based on linear regression of SC observations with distance within 1 km river segments for 13 synoptic surveys on the LMR. Positive/negative slope values indicate SC increasing/decreasing in the downstream direction. ND (blank areas) denotes segments for which data were filtered due to noisiness from stoppages for battery exchanges and partial surveys (surveys started/stopped late/early due to equipment problems). On the right axis, open circles denote battery exchange locations, and filled circles denote the location of SW lateral canals (only the last at river km 8 influenced SW SC).

The distributed GW discharge (Q_g) estimates derived from the model results are summarized in Figure 3.8 and depict variable gaining segments along the reach, which is in accord with regional hydrogeologic assessments [37]. Over the entire study reach, the estimated GW inflow generally decreased with higher flows but this trend was less consistent than the analogous trend of longitudinal SC slope changes discussed above. A plausible explanation can be attributed to local spatiotemporal variation in GW hydraulic gradients with river stage, potentially from local pumping and/or changing upstream flow conditions, affecting magnitude and flowline patterns.
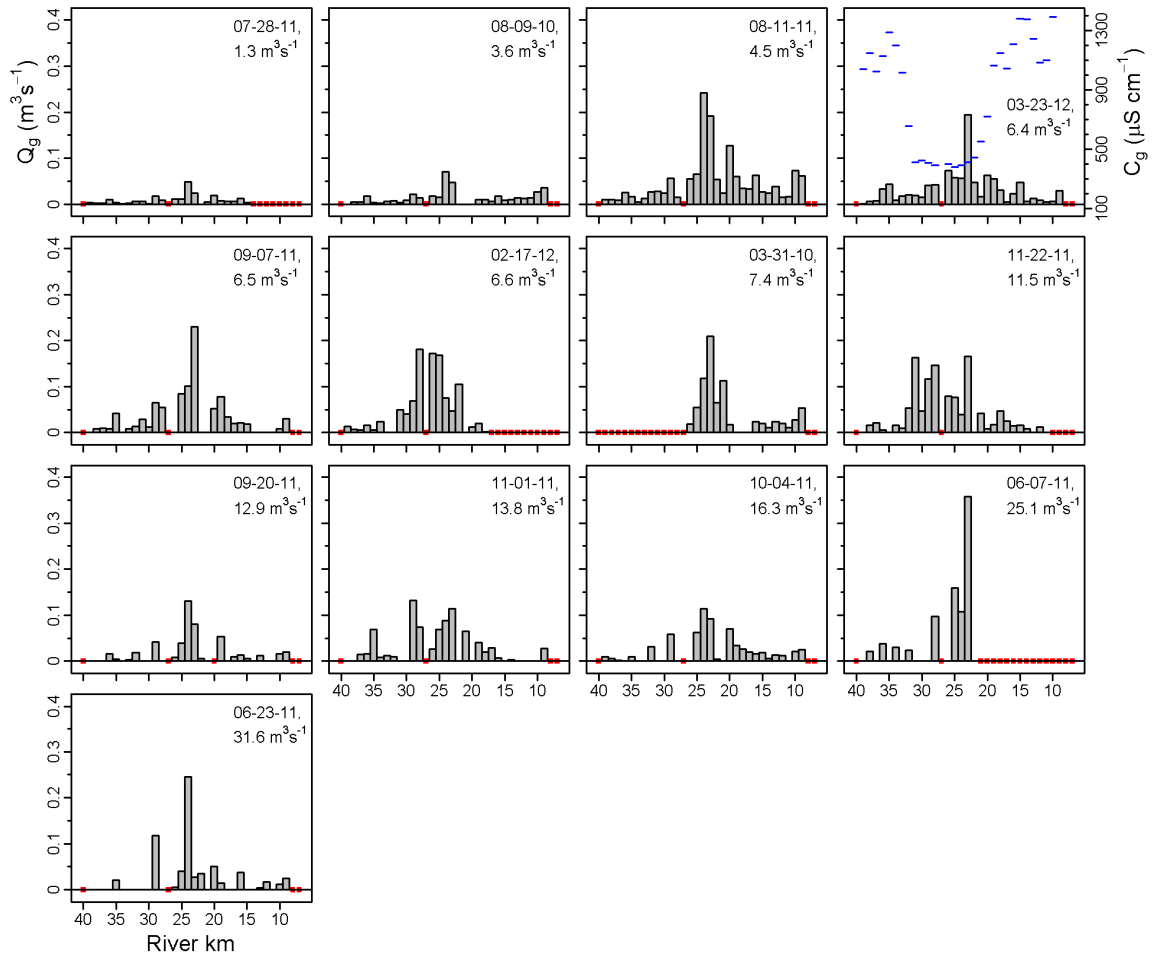
Figure 3.8. Model-based distributed Q_g estimates ordered by increasing flow. Red squares indicate sections of the river with no synoptic data to parameterize the model. The blue horizontal lines in the top right plot indicate the C_g (units on secondary axis) used to parameterize the model.

The two modeled cumulative Q_g estimates for surveys unbiased by the lateral canal (3/31/10 and 3/23/12) agreed reasonably well with estimates based on differential gauging (see all survey results in Figure 3.9, Figure 3.10, Table 3.1, and Table 3.2). The best match was for the 3/31/10 survey (modeled Q_g 0.79 m³ s⁻¹, differential Q_g 0.95 m³ s⁻¹). The fact that the starting point for the 3/31/10 survey was downstream of the typical location suggests slight underestimation of the model-based Q_g for this case. The match between model- and differential gauging-based Q_g values was not as good for the 3/23/12 survey (0.99 m³ s⁻¹ versus 0.34 m³ s⁻¹, respectively). The portion of flow attributed to estimated groundwater discharges is relatively small (< 15%; see Table 3.1). Therefore, the discrepancies in both cases could be due to errors in gauging station rating curves, minor transient flow behavior, and travel time uncertainties, making it difficult to conclusively assess Q_g by the differential gauging approach. In addition, the uncertainty in groundwater salinity levels (see Study Setting) is likely to have biased the model-based estimates. This point is illustrated by the different RMSE values achieved for the various groundwater salinity estimate methods (Table 3.2). In Figure 3.9, Figure 3.10, and Table

3.1, the lateral-biased results were included to provide greater context for the two unbiased results. In addition, because the lateral-bias occurs late in the survey, the underlying local Q_g estimates (discussed below) may still be reasonable despite the poor overall flow balance.
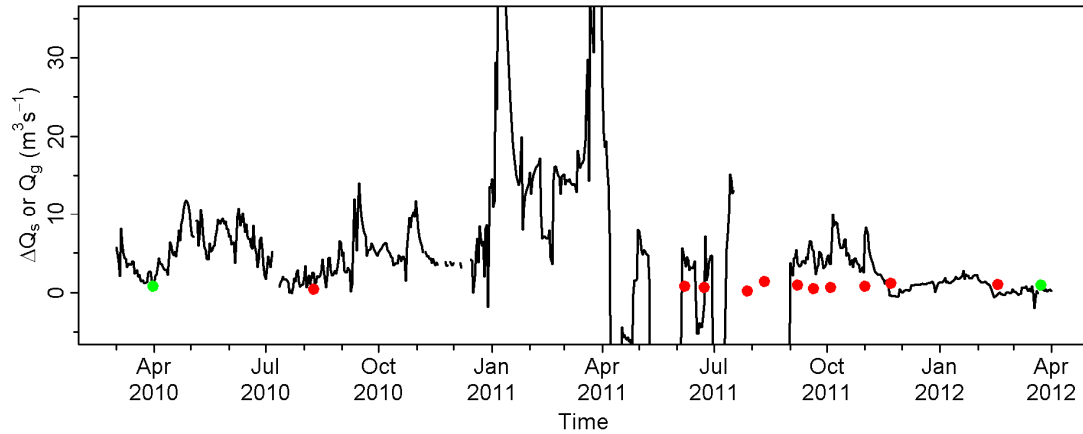
Figure 3.9. Comparison of differential gauging station estimates, ΔQ_s, (black line, based on average daily flows at CRS and MST stations) with model-estimated Q_g (green and red symbols). Red and green symbols are for surveys affected and unaffected by ungauged flow from the Lower Stevinson Lateral (approximate location river km 8). The travel time used to calculate the differential gauging estimates was 15 hours, based on hydrograph peak analysis between the two gauging stations. Large variations in differential gauging-based ΔQ_s estimates reflect sensitivity to flow changes with respect to travel time between the gauging stations.
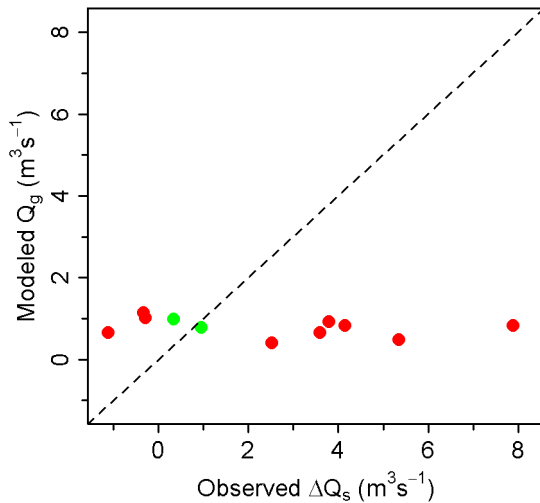
Figure 3.10. Comparison of modeled Q_g and daily differential flow gauging estimates, ΔQ_s, values (from Figure 3.9). The red symbols indicate surveys for which the Lower Stevinson Lateral had observable ungauged inflow to the Lower Merced River. Green symbols indicate surveys for which there were no observable SC influences from the same lateral.

41

Table 3.1. Comparison between modeled Q_g and observed differential gauging station values (ΔQ_s). Bold values are for surveys for which there were no observable SC influences from lateral canals (i.e., for bold cases, observed ΔQ_s is more representative of the observed Q_g).

Date	Daily CRS flow (m³ s⁻¹)	Modeled Q_g (m³ s⁻¹)	Daily observed ΔQ_s (m³ s⁻¹)	Modeled Q_g to daily MST flow (%)	Observed ΔQ_s to daily MST flow (%)
7/28/11[*]	1.33	0.21	ND	--	--
8/9/10	3.60	0.40	2.52	6.59	41.28
8/11/11	4.50	1.44	ND	--	--
3/23/12	**6.40**	**0.99**	**0.34**	**14.63**	**4.98**
9/7/11	6.54	0.93	3.79	8.99	36.69
2/17/12[*]	6.57	1.01	-0.29	16.10	4.65
3/31/10[*]	**7.39**	**0.79**	**0.95**	**9.44**	**11.38**
11/22/11	11.47	1.15	-0.33	10.29	3.00
9/20/11	12.88	0.48	5.35	2.62	29.38
11/1/11	13.79	0.82	7.89	3.81	36.67
10/4/11	16.25	0.65	3.59	3.27	18.09
6/7/11[*]	25.12	0.84	4.16	2.86	14.21
6/23/11	31.57	0.65	-1.12	2.16	3.71

ND = No data available for downstream gauging station (MST).

* = Incomplete survey runs.

Table 3.2. Root mean squared error (RMSE) between modeled and observed SW-GW discharge, Q_g, for two sampling dates (3/31/10 and 3/23/12) that were not affected by the Lower Stevinson Lateral (green symbols in Figures S4 and S5). Four spatial methods (nearest, average of 3 closest wells, inverse distance weighting of 3 closest wells, and applying interpolated GW SC surface) were used to assign SC to the distributed mixing model. The observed Q_g are daily estimates accounting for a constant 15 hour travel time.

Chosen GW SC, C_g, description	Q_g RMSE values for two sampling dates (m³ s⁻¹)
Nearest well	1.0823
Average of nearest 3 wells	0.8378
Inverse distance weighted of nearest 3 wells	0.8460
Interpolated SC surface	0.4738

In relative terms, the distributed GW discharge results indicate weak gains in the upper third, strong gains in the middle third, and weak to moderate gains in the lower

third. The consistently gaining middle zone's estimated discharges correspond with the regional groundwater mound and the presence of the underlying Corcoran clay unit (see Figure 3.1a and Figure 3.2), and with previous groundwater-surface water modeling results for a study within the zone [38]. More specifically, our modeled cumulative Q_g for river km 23-31 ranged from 0.10 to 0.75 m^3 s^{-1} with an average of 0.36 m^3 s^{-1}, which is comparable to a separate modeling study estimating 0.20 m^3 s^{-1} over the same reach [38].

Lastly, we estimated the distributed salt load along the LMR by taking the product of the model-based groundwater discharges (Q_g) and the associated local groundwater salinity concentration (C_g). The cumulative salt loading curves (Figure 3.11) exhibit similar behavior for most of the surveys, but do not correlate well with flow (for reasons similar to those expressed above in regard to the Q_g estimates). As with the GW discharge, most surveys result in only modest salt load estimates for the upper segments and relatively high salt load estimates beginning after river km 30. Downstream of river km 20, the estimated loading behavior varies (increases at an equal to or greater rate for 4 surveys, increases at lesser rate for five surveys, and levels off for 1 run). This variable behavior is likely related to the more variable groundwater conditions in the lowest elevation portion of the study reach (Figure 3.2). While there are relatively few observation wells in this zone, it is likely that the hydraulic gradient in this zone fluctuates in magnitude and direction in the lowlands between the two downstream regions. It is interesting to note that surveys closely following significant recession events (flows 6.5, 13.8, and 25.1 m^3 s^{-1}) exhibit similar behavior down to river km 23, pointing to the potential relationship between residual bank storage and the associated increase in near-river hydraulic gradient and salt loading.
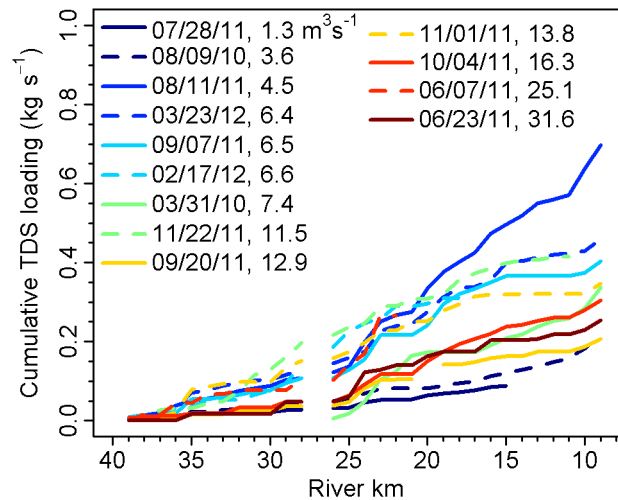
Figure 3.11. Cumulative salt or TDS loading (kg s^{-1}) for the 13 synoptic surveys, calculated from modeled local groundwater discharges (Q_g) and observed salinity levels (C_g). The 3/31/10 survey began at river km 26. The filtered values at river km 27-28 caused the line break. Filtered values did not cause a break around river km 20 because there were still enough observations in adjacent segments to build a regression.

3.4.1. Limitations

There are three main limitations to the outcomes reported in this work. First, and most importantly, the simplistic mixing model used here assumes stable flow conditions

and negligible ungauged lateral inflows and diversions. Post-survey analyses called both of these assumptions into question, in spite of our efforts to perform surveys under relatively stable conditions. Flow changes within our study reach required over 15 h to propagate through the reach. Such changes were evident from modest stage changes (but significant flow changes) during the course of several of our surveys. Ungauged lateral inputs were few and visibly small during our surveys except for the lower-most located just upstream of the MST gauging station. Given the relatively modest modeled groundwater gains for the study reach (< 15% of river flow), the ungauged lateral inputs were an important source of error to the differential gauge estimates for groundwater inputs. Regardless, based on the reasonable results developed from the two unaffected survey results and agreed with previous work [8,38], we believe that the spatial distribution reported here is accurately supported by the observed salinity distribution along the study reach.

A second limitation stems from the lack of higher granularity groundwater elevation and water quality data (Figure 3.1 and Figure 3.2). With respect to temporal groundwater data, only seasonal data were available and more for the north side of the LMR than the south side. Hence, we were forced to average data over long time spans in order to independently estimate the salt concentration contribution to the distributed loading model. Spatial coverage was also limited, and we were able to distinguish mainly the regional piezometric surface. We could not delineate local gradients due to the small number of wells near (~1 km or less) the river. While our results represent a good approximation of the distributed salt loads along the LMR, they would be enhanced by better groundwater data near the river.

Lastly, because we measured only SC, we were unable to distinguish between anthropogenic NPSP and natural origin(s) of the salinity. There are many potential anthropogenic salinity sources in the LMR region, including historical and current agricultural, food processing operations, dairies, and irrigation drains. There are also potential natural sources that include upwelling of deep saline groundwater [46]. As noted in the study setting, one segment within our study area (Figure 3.1) served for a NAWQA special study of agricultural chemicals and water quality [8,16,36]. The application here could be supplemented with more specific measurements, such as targeting specific ions or stable isotopes [47], to provide more information about the nature of the sources.

3.4.2. Implications

This work clearly delineates distributed salt loads on a km-scale resolution along a lowland river. Based on our analysis and interpretation, these loads are the result of groundwater discharges governed by the regional gradients and influenced by local variations in those gradients in and around the riparian zone. Understanding the connection between distributed GW discharges and the natural and anthropogenic activities causing them has major implications in terms of the sustainability of aquatic biodiversity and the growing human population depending upon river ecosystems. The spatial and temporal variation of distributed GW discharges along rivers is caused by processes spanning multiple scales. At regional to local scales, flow paths and residence time for water and nutrients are governed by hydrogeologic conditions that are often heavily influenced by human activities such as large-scale groundwater extraction (e.g.,

for municipalities and agriculture), irrigation, modified recharge potential (e.g., by land use change), and application of fertilizers, herbicides, and other chemicals [48–50]. Local hydraulic gradients and fluxes in turn, affect the state of the riparian zone at the hillslope scale depending on the morphology, evapotranspiration, and underlying sediment structure of that zone [36,51]. Similar to larger scale human activities, local groundwater extraction and irrigation events can change the magnitude and direction of local hydraulic gradients, and thus the connectivity between riparian groundwater and the hyporheic zone, and the stream. Lastly, the hyporheic zone-to-stream connection is balanced by the riparian zone groundwater conditions on one side, and the stream conditions (stage, velocity, and water quality) on the other. These stream conditions are dictated by natural phenomena (climate, hydrology, geomorphology) but can be dominated by human controls (e.g., dams, as in the present work). Such occurrences can strongly affect hyporheic zone chemistry and temperatures and consequently aquatic ecosystem health. For instance, reduced upwelling of warmer hyporheic flows during winter months may result in near-freezing conditions at spawning beds jeopardizing egg survival rates [52] and in lesser availability of nutrients necessary for rearing of post-emergent salmon [53]. A better understanding of this complex flow and reactive transport pathway and its connection to human activities will enable us to better inform stakeholders in the creation of resource management policies, particularly for groundwater extraction, agricultural practices, and buffer zone restoration and conservation.

A related but more specific area of environmental policy of relevance to this work is that associated with regulation of maximum allowable loads from a watershed (e.g., TMDLs). These loads are typically assigned on a watershed basis with knowledge of the main human activities therein. However, our work strongly suggests that a more aggressive approach for monitoring and mapping distributed contributions to the TMDL (or similar regulatory instrument) is plausible. Using the approach we have described, distributed load contributions could be assigned to land use practices more precisely than is currently done. Of course, there are limitations to the approach as it currently stands (see limitations section). However, as sensors for various water quality parameters of concern become more diverse, and local groundwater data (level and water quality) become more available and up-to-date, water quality managers and decision-makers should strongly consider adopting high resolution synoptic water quality surveys into their portfolio of tools. It is conceivable in the near term that such surveys could be carried out effectively (and more safely) with autonomous aquatic or aerial vehicles.

3.4.3. Summary and Conclusions

In this work, a high resolution, SW synoptic sampling system measuring a conservative tracer, SC, is used to estimate distributed GW-SW discharge. The SW concentration gradient coupled with available GW SC and upstream flow parameterize a steady-state, distributed mass balance model, similar to previous studies largely based on data from injected chemical and/or isotopic tracers. In our unique setting, elevated ambient GW SC concentrations and previous studies examining a preferential GW flowpath to the SW provide an opportunity to examine longitudinal GW-SW discharge behavior in a gaining river reach without adding a tracer. The model-estimated GW-SW discharge produced reasonable estimates for the whole reach (validated by differential gauging) and locally (validated by previous local estimates of the preferential GW-SW

discharge).   While clear SW SC dilution can be seen with increasing SW flows, any anticipated decrease in GW-SW discharge or TDS loading with larger SW flows are not as clearly seen.   These results highlight difficulties commonly found in hydrologic modeling, where sparse spatial and temporal sampling may miss complex characteristics affecting GW-SW exchange such as residual bank storage effects after SW flow reduction.   Selective deployment of GW sensing methods can better characterize these spatially or temporally varying phenomena on GW-SW exchange.   In spite of GW data limitations that were beyond the scope of this study, our synoptic approach clearly produced rapid, inexpensive multi-scale SW maps that can be used to delineate GW-SW discharges in terms of nonpoint source pollution.   The reported high resolutions data sets and their interpretation on the scale of this study (40 km) are the first of their kind in the literature.

3.5. References

[1] T. Pohlert, J.A. Huisman, L. Breuer, H.-G. Frede, Modelling of point and non-point source pollution of nitrate with SWAT in the river Dill, Germany, Adv. Geosci. 5 (2005) 7–12. doi:10.5194/adgeo-5-7-2005.

[2] G. Vazquez-Amabile, B.A. Engel, D.C. Flanagan, Modeling and risk analysis of nonpoint-source pollution caused by atrazine using SWAT, Transactions of the ASABE. 49 (2006) 667–678.

[3] R. Niraula, L. Kalin, P. Srivastava, C.J. Anderson, Identifying critical source areas of nonpoint source pollution with SWAT and GWLF, Ecological Modelling. 268 (2013) 123–133. doi:10.1016/j.ecolmodel.2013.08.007.

[4] P.J. Squillace, J.C. Scott, M.J. Moran, B.T. Nolan, D.W. Kolpin, VOCs, Pesticides, Nitrate, and Their Mixtures in Groundwater Used for Drinking Water in the United States, Environ. Sci. Technol. 36 (2002) 1923–1930. doi:10.1021/es015591n.

[5] M.L. van der Schans, T. Harter, A. Leijnse, M.C. Mathews, R.D. Meyer, Characterizing sources of nitrate leaching from an irrigated dairy farm in Merced County, California, Journal of Contaminant Hydrology. 110 (2009) 9–21. doi:10.1016/j.jconhyd.2009.06.002.

[6] K.R. Burow, B.T. Nolan, M.G. Rupert, N.M. Dubrovsky, Nitrate in Groundwater of the United States, 1991−2003, Environ. Sci. Technol. 44 (2010) 4988–4997. doi:10.1021/es100546y.

[7] A.E. Fryar, E.J. Wallin, D.L. Brown, Spatial and Temporal Variability in Seepage Between a Contaminated Aquifer and Tributaries to the Ohio River, Ground Water Monitoring & Remediation. 20 (2000) 129–146. doi:10.1111/j.1745-6592.2000.tb00279.x.

[8] H.I. Essaid, C.M. Zamora, K.A. McCarthy, J.R. Vogel, J.T. Wilson, Using heat to characterize streambed water flux variability in four stream reaches, J. Environ. Qual. 37 (2008) 1010–1023. doi:10.2134/jeq2006.0448.

[9] D.A. Stonestrom, J. Constantz, eds., Heat as a tool for studying the movement of ground water near streams, U.S. Dept. of the Interior, U.S. Geological Survey, 2003.

[10] E. Kalbus, F. Reinstorf, M. Schirmer, Measuring methods for groundwater - surface water interactions: a review, Hydrology and Earth System Sciences. 10 (2006) 873–887.

[11] C.A. Butler, T.C. Harmon, Groundwater-surface water discharges, in: J.H. Fernando (Ed.), Handbook of Environmental Fluid Dynamics, CRC Press, 2012: pp. 19–30.

[12] C.D. Kennedy, L.C. Murdoch, D.P. Genereux, D.R. Corbett, K. Stone, P. Pham, et al., Comparison of Darcian flux calculations and seepage meter measurements in a sandy streambed in North Carolina, United States, Water Resour. Res. 46 (2010) W09501. doi:10.1029/2009WR008342.

[13] B. Conant, Delineating and Quantifying Ground Water Discharge Zones Using Streambed Temperatures, Ground Water. 42 (2004) 243–257. doi:10.1111/j.1745-6584.2004.tb02671.x.

[14] C.E. Hatch, A.T. Fisher, J.S. Revenaugh, J. Constantz, C. Ruehl, Quantifying surface water–groundwater interactions using time series analysis of streambed thermal records: Method development, Water Resour. Res. 42 (2006) W10410. doi:10.1029/2005WR004787.

[15] J. Constantz, Heat as a tracer to determine streambed water exchanges, Water Resour. Res. 44 (2008) W00D10. doi:10.1029/2008WR006996.

[16] L.J. Puckett, C. Zamora, H. Essaid, J.T. Wilson, H.M. Johnson, M.J. Brayton, et al., Transport and fate of nitrate at the ground-water/surface-water interface, J. Environ. Qual. 37 (2008) 1034–1050. doi:10.2134/jeq2006.0550.

[17] C. Schmidt, A. Musolff, N. Trauth, M. Vieweg, J.H. Fleckenstein, Transient analysis of fluctuations of electrical conductivity as tracer in the stream bed, Hydrol. Earth Syst. Sci. 16 (2012) 3689–3697. doi:10.5194/hess-16-3689-2012.

[18] D.P. Genereux, S. Leahy, H. Mitasova, C.D. Kennedy, D.R. Corbett, Spatial and temporal variability of streambed hydraulic conductivity in West Bear Creek, North Carolina, USA, Journal of Hydrology. 358 (2008) 332–353. doi:10.1016/j.jhydrol.2008.06.017.

[19] R.A. Payn, M.N. Gooseff, B.L. McGlynn, K.E. Bencala, S.M. Wondzell, Channel water balance and exchange with subsurface flow along a mountain headwater stream in Montana, United States, Water Resour. Res. 45 (2009) W11427. doi:10.1029/2008WR007644.

[20] M.A. Briggs, L.K. Lautz, J.M. McKenzie, A comparison of fibre-optic distributed temperature sensing to traditional methods of evaluating groundwater inflow to streams, Hydrol. Process. 26 (2012) 1277–1290. doi:10.1002/hyp.8200.

[21] J. Selker, N. van de Giesen, M. Westhoff, W. Luxemburg, M.B. Parlange, Fiber optics opens window on stream dynamics, Geophys. Res. Lett. 33 (2006) L24401. doi:10.1029/2006GL027979.

[22] C.S. Lowry, J.F. Walker, R.J. Hunt, M.P. Anderson, Identifying spatial variability of groundwater discharge in a wetland stream using a distributed temperature sensor, Water Resour. Res. 43 (2007) W10408. doi:10.1029/2007WR006145.

[23] S.W. Tyler, J.S. Selker, M.B. Hausner, C.E. Hatch, T. Torgersen, C.E. Thodal, et al., Environmental temperature sensing using Raman spectra DTS fiber-optic methods, Water Resour. Res. 45 (2009) W00D23. doi:10.1029/2008WR007052.

[24] C.E. Torgersen, R.N. Faux, B.A. McIntosh, N.J. Poage, D.J. Norton, Airborne thermal remote sensing for water temperature assessment in rivers and streams, Remote Sensing of Environment. 76 (2001) 386–398. doi:10.1016/S0034-4257(01)00186-9.

[25] S.P. Loheide, S.M. Gorelick, Quantifying Stream−Aquifer Interactions through the Analysis of Remotely Sensed Thermographic Profiles and In Situ Temperature Histories, Environ. Sci. Technol. 40 (2006) 3336–3341. doi:10.1021/es0522074.

[26] R.S. Deitchman, S.P. Loheide, Ground-based thermal imaging of groundwater flow processes at the seepage face, Geophys. Res. Lett. 36 (2009) L14401. doi:10.1029/2009GL038103.

[27] G.M. Sivirichi, S.S. Kaushal, P.M. Mayer, C. Welty, K.T. Belt, T.A. Newcomer, et al., Longitudinal variability in streamwater chemistry and carbon and nitrogen fluxes in restored and degraded urban stream networks, J Environ Monit. 13 (2011) 288–303. doi:10.1039/c0em00055h.

[28] S. Jasechko, J.J. Gibson, S. Jean Birks, Y. Yi, Quantifying saline groundwater seepage to surface waters in the Athabasca oil sands region, Applied Geochemistry. 27 (2012) 2068–2076. doi:10.1016/j.apgeochem.2012.06.007.

[29] A.H. Haria, P. Shand, C. Soulsby, S. Noorduijn, Spatial delineation of groundwater–surface water interactions through intensive in-stream profiling, Hydrol. Process. 27 (2013) 628–634. doi:10.1002/hyp.9551.

[30] A. David, M.-G. Tournoud, J.-L. Perrin, D. Rosain, C. Rodier, C. Salles, et al., Spatial and temporal trends in water quality in a Mediterranean temporary river impacted by sewage effluents, Environ Monit Assess. 185 (2012) 2517–2534. doi:10.1007/s10661-012-2728-4.

[31] United States Geological Survey (USGS) California Geology, (n.d.). http://mrdata.usgs.gov/sgmc/ca.html.

[32] California Deparment of Water Resources (CA DWR) Contour Data Report, (n.d.). http://www.water.ca.gov/waterdatalibrary/groundwater/contour/.

[33] State Water Resources Control Board (CA SWRCB) Groundwater Ambient Monitoring and Assessment, (n.d.). http://geotracker.waterboards.ca.gov/gama/.

[34] K.R. Burow, J.L. Shelton, J.A. Hevesi, G.S. Weissmann, Hydrogeologic Characterization of the Modesto Area, San Joaquin Valley, California, 2004.

[35] R.G. Larkin, J.M. Sharp, On the relationship between river-basin geomorphology, aquifer hydraulics, and ground-water flow direction in alluvial aquifers, Geological Society of America Bulletin. 104 (1992) 1608–1620. doi:10.1130/0016-7606(1992)104<1608:OTRBRB>2.3.CO;2.

[36] J.L. Domagalski, S.P. Phillips, E.R. Bayless, C. Zamora, C. Kendall, R.A.W. Jr, et al., Influences of the unsaturated, saturated, and riparian zones on the transport of nitrate near the Merced River, California, USA, Hydrogeol J. 16 (2008) 675–690. doi:10.1007/s10040-007-0266-x.

[37] C.C. Faunt, Groundwater Availability of the Central Valley Aquifer, California, U.S. Geological Survey, 2009. http://pubs.usgs.gov/pp/1766/.

[38] S.P. Phillips, C.T. Green, K.R. Burow, J.L. Shelton, D.L. Rewis, Simulation of Multiscale Ground-Water Flow in Part of the Northeastern San Joaquin Valley, California, U.S. Geological Survey, 2007. http://pubs.usgs.gov/sir/2007/5009/.

[39] J.D. Hem, Study and Interpretation of the Chemical Characteristics of Natural Water, 3rd ed., U.S. Geological Survey, 1985. http://pubs.usgs.gov/wsp/wsp2254/.

[40] J.W. Lloyd, J.A. Heathcote, Hydrochemical parameter measurement and sample collection, in: Natural Inorganic Hydrochemistry in Relation to Groundwater: An Introduction, Clarendon Press, Oxford, 1985: pp. 56–90.

[41] T.P. Covino, B.L. McGlynn, Stream gains and losses across a mountain-to-valley transition: Impacts on watershed hydrology and stream water chemistry, Water Resour. Res. 43 (2007) W10431. doi:10.1029/2006WR005544.

[42] M. Hayashi, T. Vogt, L. Mächler, M. Schirmer, Diurnal fluctuations of electrical conductivity in a pre-alpine river: Effects of photosynthesis and groundwater exchange, Journal of Hydrology. 450–451 (2012) 93–104. doi:10.1016/j.jhydrol.2012.05.020.

[43] N. Yotsukura, W.W. Sayre, Transverse mixing in natural channels, Water Resour. Res. 12 (1976) 695–704. doi:10.1029/WR012i004p00695.

[44] H.B. Fischer, E.J. List, R.C. Koh, J. Imberger, N.H. Brooks, Mixing in Rivers, in: Mixing in Inland and Coastal Waters, Academic Press, Orlando, Florida, 1979: pp. 104–147.

[45] J.C. Rutherford, Transverse Mixing, in: River Mixing, John Wiley and Sons Ltd, West Sussex, England, 1994: pp. 95–173.

[46] M.K. Landon, K. Belitz, B.C. Jurgens, J.T. Kulongoski, T.D. Johnson, Status and understanding of groundwater quality in the Central–Eastside San Joaquin Basin, 2006: GAMA Priority Basin Project, U.S. Geological Survey, 2009.

[47] S.S. Kaushal, P.M. Groffman, L.E. Band, E.M. Elliott, C.A. Shields, C. Kendall, Tracking Nonpoint Source Nitrogen Pollution in Human-Impacted Watersheds, Environ. Sci. Technol. 45 (2011) 8225–8232. doi:10.1021/es200779e.

[48] T.E. Jordan, D.L. Correll, D.E. Weller, Relating nutrient discharges from watersheds to land use and streamflow variability, Water Resour. Res. 33 (1997) 2579–2590. doi:10.1029/97WR02005.

[49] S. Krause, A. Bronstert, E. Zehe, Groundwater–surface water interactions in a North German lowland floodplain – Implications for the river discharge dynamics and riparian water balance, Journal of Hydrology. 347 (2007) 404–417. doi:10.1016/j.jhydrol.2007.09.028.

[50] A.J. Ranalli, D.L. Macalady, The importance of the riparian zone and in-stream processes in nitrate attenuation in undisturbed and agricultural watersheds – A review of the scientific literature, Journal of Hydrology. 389 (2010) 406–415. doi:10.1016/j.jhydrol.2010.05.045.

[51] K.G. Jencso, B.L. McGlynn, M.N. Gooseff, K.E. Bencala, S.M. Wondzell, Hillslope hydrologic connectivity controls riparian groundwater turnover: Implications of catchment structure for riparian buffering and stream water sources, Water Resour. Res. 46 (2010) W10524. doi:10.1029/2009WR008818.

[52] R. Casas-Mulet, K. Alfredsen, Å. Brabrand, S.J. Saltveit, Survival of eggs of Atlantic salmon (Salmo salar) in a drawdown zone of a regulated river influenced by groundwater, Hydrobiologia. 743 (2014) 269–284. doi:10.1007/s10750-014-2043-x.

[53] A.J. Boulton, T. Datry, T. Kasahara, M. Mutz, J.A. Stanford, Ecology and management of the hyporheic zone: stream–groundwater interactions of running waters and their floodplains, Journal of the North American Benthological Society. 29 (2010) 26–40. doi:10.1899/08-017.1.

4. Synoptic multi-tracer sampling for groundwater-surface water nitrate loading and dynamics along a lowland river

4.1. Abstract

Elevated nitrate concentrations in water supplies are a concern for human health and aquatic ecosystems. Nitrate transport in the watershed is difficult to track due to challenges in characterizing denitrification processes spatially. In this work, we analyze ambient specific conductance (SC) and nitrate (NO_3^-) as tracers using high-resolution longitudinal synoptic in-situ sensing along the lower Merced River (38 river km) in central California. With available surrounding GW SC, we first calibrate a distributed GW-surface water (SW) discharge model for a conservative solute using 13 synoptic sampling events at daily flows ranging from 1.3 to 31.6 m^3s^{-1}. We then applied the GW-SW distributed discharge estimates to a similar distributed nitrate loading model, adding a first-order decay term representing shallow aquifer denitrification. We assumed the denitrification term to be inversely proportional to estimated local GW-SW discharge and adjusted the decay rate and representative volume to best-fit observed SW nitrate data. When wells reporting less than the detection limits (typically around 0.5 mg L^{-1} NO_3-N) were censored from further analysis the best-fit model results were in good agreement with the observed river distribution across the synoptic surveys (RMSE = 0.06-0.98 mg L^{-1}). The reach-estimated dimensionless denitrification term varied from 0 to 0.432, which is lower than previous local results for a segment of the study reach (0.92) and regional results (0.17-1.06). This work provides proof-of-concept for a relatively low cost approach characterizing nitrate nonpoint source pollution and groundwater denitrification patterns at the watershed scale for a consistently gaining river reach.

4.2. Introduction

Worldwide terrestrial ecosystems have steadily seen increases in nitrogen loading corresponding with increasing human fertilizer use, confined animal feed operations (CAFOs), and NO_x emissions [1]. Nitrate (NO_3^-) is a labile species that is commonly transferred from soils to groundwater (GW) and surface water (SW), and can accumulate to potentially toxic levels in rural drinking water wells [2]. Elevated nitrate levels are also linked to eutrophication of freshwater ecosystems which can result in harmful algal blooms and hypoxia [3–5]. While natural attenuation of nitrogen species occurs through biological nitrification-denitrification processes, limits on removal efficiency have spurred research focused on (1) best management practices for fertilizer application and other nitrogen loading on the environment [6,7], and (2) the transport and fate of nitrogen in the environment. Such practices and reactive transport pathways are dependent on site-specific watershed conditions that take into account denitrification processes in multiple aquatic environments such as shallow aquifer and riverine environments [8–12]. In the agriculturally dominated regions of California, changes in crop type and practices and production increases have resulted in non-uniform application and subsequent leaching from nitrogen sources to the GW that is of growing concern [13]. For this work, we specifically examine longitudinal nitrate loading and potential denitrification from the shallow aquifer to the lower Merced River (LMR) system located in the Central Valley, CA.

Understanding nitrogen cycling along rivers and shallow aquifers continues to be challenging, although we know that both hydrologic units have large potential for denitrification [1]. Within the subsurface, biogeochemical conditions affecting redox conditions and subsequent denitrification can vary locally with reactivity of heterogeneous sediments, which can be difficult to characterize at the watershed scale [11,14,15]. Additional transport processes such as convection, dispersion, sorption, and associated travel times within the GW or SW complicate accurate descriptions of reactive nitrogen transport [11,16,17]. Interstitial river SW flow within sediments at GW-SW interfaces creates a complicated mixing zone between potential GW and SW nitrate sources, commonly known as the hyporheic zone (HZ). Nitrogen transformations (nitrification and denitrification) within the HZ depend on residence time and oxygen depletion where denitrification is likely to occur along oxygen-depleted deeper substrates or shallow microzones of low oxygen [17–20]. Additionally, high suspended sediment concentrations within the SW water column has been shown to cause increased denitrification where potential low-oxygen microsites exist within or around sediment particles [21]. For SW systems, the varying diurnal and seasonal light conditions which drive photosynthetic oxygen production is considered inversely related with denitrification activity [22,23]. These complications make local field estimates of denitrification difficult to scale spatially through the watershed.

To address such complexity within river network systems, transport models for river networks and watershed scales have ranged from statistical relationships [16,24] to more deterministic multi-parameter models combining flow, transport, and chemical kinetics [25]. The statistical models often depend on SW river travel time and volumetric flow variables, but have been adjusted to account for both point and nonpoint source contributions to the SW system [26]. These models have been applied to regional characterizations for constituent loading and discretizing the models to subdomains produced better model estimates with the tradeoff of increased coefficient uncertainties [27,28]. In contrast, process-based or deterministic watershed transport models are typically first calibrated for flow then chemical kinetics. Such models may require exhaustive calibration exercises targeting numerous spatially distributed parameters associated with flow, subsurface material properties, and chemical kinetics. In practice, the magnitude of this calibration problem may limit the extent and spatial resolution at which these models can reasonably be applied [11,29,30]. Less complex models, such as mass balance or geographical information systems (GIS)-based models, simplify processes by incorporating assumptions and associated analytic solutions, attempting to address processes at larger spatial scales than the more complex models [9,31].

Assessing nitrogen cycling, including within denitrification component, within environmental systems encompasses multiple methods focusing on mass balance of chemical species (e.g. N_2, NO_3, etc.) and isotopic composition along reactive transport pathways. Observations and accompanying models for nitrogen removal are often described using simplified (e.g., first order) kinetics. This approach lumps a large range of potential pathways that are associated with geochemical properties of the system (e.g. mineralogy, redox potential, pH, temperature, etc.), which are challenging to estimate over large spatial scales [15,32]. Determining the denitrification rate, which can vary over orders of magnitude within GW flowpaths, requires an age or travel time of the

water using other isotopic or neutral chemical tracers. Additional measurements often include environmental redox conditions noted above that affect rate behavior. An overview of the measurement methods and considerations is provided by Groffman et al. [33]. Many of the measurements require sample collection and subsequent laboratory analyses, which are costly, particularly for isotopic analyses. Recent advances in the development of in situ spectrophotometers allow high temporal resolution studies analyzing diurnal fluctuations on some nitrogen species, like nitrate [23]. Increasingly, these sensors are transported with mobile vehicles creating high spatial resolution maps and detecting unseen variability [34], likely due to the localized nature of nitrogen cycling [35].

In this work, we take advantage of the recent developments in UV sensing technology to examine longitudinal nitrate loading to the lower 38-km reach of a lowland river surrounded by predominantly agricultural land use. We incorporate mobile delivery of an in-situ UV-visible (UV-Vis) spectrometer and water quality sonde to measure nitrate and specific conductance (SC) respectively, at high frequency. The synoptic data sets and analytical framework provide a rapid and practical approach for measuring longitudinal geochemical behavior. We attribute SW nitrate concentration gradients to distributed GW-SW discharge and potential denitrification capacity along the GW flowpath to the river, within the hyporheic zone, or within the water column. To our knowledge, such aggregation of high-resolution and analysis has not been conducted and provides a unique spatially distributed perspective of potential nitrogen transformations along an agriculturally impacted watershed system.

4.3. Methods

We characterized nitrate loading into the Lower Merced River by combining available GW SC and NO_3^- data from wells and corresponding high spatial resolution SW data from the in situ sensor. The sampling strategy is similar to Chapters 2 and 3 with additional focus on nitrate sensing and analysis, as the data originated from the same synoptic sampling runs. These GW and SW SC data parameterize a steady-state, distributed mixing model for nonpoint source loading, validated with differential gauging station discharge and previous modeling studies [36]. We build off this model using considerations (e.g., well depth, well sampling date difference) detailed within Chapter 2. In this chapter, we apply an additional first-order denitrification term affecting the well NO_3 data representing the lumped nitrate reduction occurring between the GW well, within aquifer sediments, through the HZ, and within the river SW where our in situ measurements are made. We relate the GW-SW volumetric discharge to the travel time needed for estimating actual denitrification. River measurements for this study were completed from 2010-2012, over a range of flows (1.3-31.6 m^3s^{-1}) around a wet water year (WY2011).

4.3.1. Measuring Nitrate

The two river constituents of interest to this study are SC and nitrate. Measuring specific conductance (SC) is a relatively standard method of measuring total dissolved solids within the aquatic environment and was described in further detail in Chapter 2.

To measure nitrate, common methods include wet chemistry analysis, ion selective electrodes, and emerging spectrophotometers focusing on the ultraviolet (UV)

part of the spectrum with particular focus on the range of wavelengths 190-370 nm [37]. For high resolution surface water studies, wet chemistry analysis becomes impractical as multiple field samples are required, prone to irregular sampling storage techniques per sample, and cost per sample. Ion selective electrodes, while generally less expensive, can be prone to interferences from other ions and sensitive to drift [37]. Spectrophotometers are initially expensive but reliability for in situ sensing shows promise though there are potential optical interferences.

In this work, we use a spectrophotometer (s::can spectro::lyser, Vienna, Austria) measuring the UV-visible (UV-Vis) spectrum (200-750 nm) and with an optical path length of 35 mm. The spectrophotometer uses a Xenon source lamp emitting dual beams, a measurement and reference beam, to account for potential lamp output variations. At the end of both beam paths, a photodiode array collects the attenuated or absorbed spectrum at a resolution of 2.5 nm wavelength intervals. The measurement beam path is attenuated by constituents within the water sample and lamp variations are corrected with the reference beam. The resulting absorbance at specific wavelengths for a particular species can then be linearly related to concentration as stated by Lambert-Beer's law [37,38]. The optical path length for the measurement beam can vary for spectrophotometers. For our device, the longer path length is suitable for freshwater applications as shorter path lengths are more common for waters with high turbidity which attenuates the beam and a major source of interference [37]. While local calibrations have been used to improve general sensor calibration [39], we relied on the manufacturer-offered global freshwater calibration and spot samples were verified with ion chromatography (C. Butler, personal communication, May 18, 2015).

4.3.2. Nitrate Groundwater and Surface Water Setting

The SC conditions and hydrogeology for the region were described in detail in Chapters 2 and 3. We briefly describe the site hydrology in the context of GW to SW discharge. We then examine the hydrogeological conditions and their potential effects on nitrate GW well concentrations from the nearby aquifer and hyporheic zone. Additional SW nitrate considerations for potential inputs (e.g. atmospheric, etc.) and transformations are also discussed.

This study collected data along a consistently gaining stretch of the LMR located in Central Valley, CA. The LMR is an impounded tributary for the San Joaquin River (SJR), which provides 13% of the inflow into the Sacramento-San Joaquin Delta and San Francisco Bay [40]. The confluence of the LMR with the SJR identifies river km 0 and increases upstream the Merced River. Along this study reach, the last 38 river km stretch, a localized GW flowpath to the river (~ river km 23-31) with elevated GW-SW discharge, as noted in Chapter 3, has been a site for numerous GW-SW interaction studies [36,41,42]. The site provides a unique setting for assessing connectivity with agricultural land use, the dominant land coverage for the region and considered as a nonpoint source contributor to the SW. Surrounding GW well data are available online through the Groundwater Ambient Monitoring and Assessment (GAMA) program and maintained by the California State Water Resources Control Board [43]. For SW conditions, the California Department of Water Resources (DWR) has two SW gauging stations along our study reach. The upstream station is located at river km 46 near

Cressey (station id: CRS), and the downstream station is located at river km 8 near Stevinson (MST). A noticeable SW input is located at river km 8 just upstream of MST.

In GW systems, nitrate reduction is governed by residence time of the water and redox conditions governing nitrogen transformations. For this study, higher regional denitrification potential represented by anoxic (or reduced) well conditions was noticeable along the valley trough, coinciding with the SJR, and to a lesser extent along the tributary corridors, including the LMR. Otherwise, regional anoxic well conditions were small in proportion (9.5% of the total regional wells) suggesting low denitrification potential in the wells more than 1 km from the rivers [15]. A local study along the LMR supported higher denitrification potential closer to rivers and within the HZ, affecting waters with simulated GW residence times of up to 30 years. The older GW was simulated to maintain legacy or natural nitrate levels in low amounts [44]. For transport restricted to the subsurface at the same site along the LMR, including effects of mixing and dispersion on model-estimated denitrification rates differed by over an order of magnitude compared to observed rates [11]. The combination of low regional denitrification potential in wells with increased fertilizer use and subsequent leaching to the aquifer likely caused increasing trends for GW well nitrate concentrations, with noticeable concentration differences between shallow and deep wells [45]. A recent view of an interpolated NO_3 concentration surface for the shallow aquifer is shown in Figure 4.1.
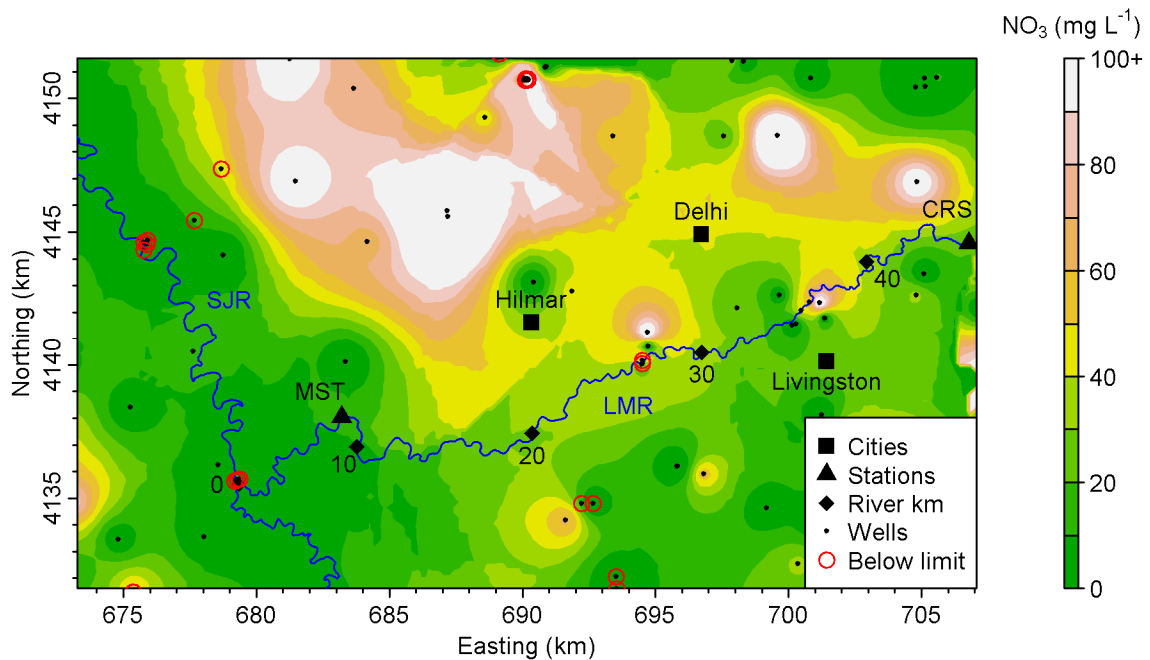
Figure 4.1. Interpolated regional GW NO_3 concentrations made by ArcGIS default IDW settings and plotted in R. The interpolation was based on shallow (< 85 m) and recent (1980 to present) well data from GAMA [43] and the US Geological Survey National Water Information System (USGS-NWIS) [46] and removed points below the highest method detection limit ($NO_3 \leq 2.2$ mg L^{-1}; i.e. all well locations in the figure without the red circle).

For the LMR, potential nitrate input pathways other than GW include atmospheric nitrogen deposition, given the relatively poor air quality of the region, and instream

biological processes. The rate of total nitrogen atmospheric deposition to the SJR Basin estimated from a measurement station in Davis, CA ranged from 0.41 to 1.24 g m^{-2} yr^{-1}. Recent study data showed inter-annual variability from 1985-2004, but unclear trends [47]. Spatially, the contribution of atmospheric nitrogen addition relative to fertilizer and manure application is small for the lowland portion of the SJR (and contributions for the LMR are likely similar) [40]. Generally, however, the effect atmospheric nitrogen on downstream nitrate remains uncertain likely due to in-stream processes [48]. In-stream biological processes include denitrification, nitrification, and assimilation, but were largely found to have small effects on NO_3 variability in the SJR [23]. Like atmospheric deposition, influences from such biological activities were small relative to point (e.g., canals) sources and GW contributions [23]. In our study, we examine the longitudinal NO_3 loading from GW to the SW of the LMR and reduction capacity. We ignore the potential atmospheric source of nitrogen, arguing that the surface area of the stream is relatively small, and that direct runoff from the watershed is minimal on the LMR.

4.3.3. Synoptic Sampling Strategy

The sampling strategy is similar to Chapters 2 and 3 (NO_3 and SC data collected concurrently) and is briefly reviewed here emphasizing the nitrate measurements. We continuously logged water quality data using in situ sensors, a multi-parameter sonde (Hydrolab MS5) for SC, temperature, and dissolved oxygen (DO) at rates ranging from 5 s to one minute for different surveys. We also logged nitrate concentrations using the submersible UV-Vis spectrophotometer (s::can spectro::lyser) every minute. Both were housed in perforated polyvinyl chloride (PVC) tubes for protection. The sensors were suspended from the sides of a motor-propelled tandem kayak so that the sensors were immersed. The in situ sensor data were localized with a high frequency (6 samples per s) GPS echo sounder from the Valeport (Midas Surveyor Echo Sounder). We transported the sensor suite along the LMR thalweg (river km 2-38) completing the synoptic surveys within 5-7 hrs, including 2 intermediate stops (river km 20 and 26.5) for battery swaps powering the kayak motor. These stops were filtered from further analysis due to sand disturbance influences on SC and NO_3 measurements. Since the focus of this study is for nonpoint source loading (GW to SW discharge), we also filtered data downstream of river km 8, where the Lower Stevinson Lateral had noticeable SW SC effects. For nitrate filtering alone, we removed zero readings for concentration from the spectrophotometer. We conducted the surveys 17 times from 2010-2012 to examine longitudinal gradients identified with our in situ sensors, where the water year for 2011 (WY2011) was wetter than 2010 and 2012. As reported in Chapters 2 and 3, 13 of the 17 surveys showed noticeable gradients for lower flow regimes (CRS daily flows ranging from 1.3 to 31.6 m^3 s^{-1}). Greater flows resulted in overly diluted conditions to use in the analysis. We used the same 13 surveys for further models and analysis in this chapter.

4.3.4. Model and Analysis

Given available GW well SC and NO_3 data and our corresponding in situ synoptic surveys, we developed exploratory steady state mixing models to first estimate distributed GW-SW discharge using SC (assumed to be conservative) and applied the distributed discharge to a NO_3 (assumed to be non-conservative) loading and mixing model accounting for potential nitrate reduction. Chapters 2 and 3 covered the GW-SW

discharge model with SC at a 1 km resolution and are briefly described here in the context of the NO$_3$ reactive transport model.

Initially, we applied the distributed GW-SW discharge model, as described in Equation (2.3), and found the lowest RMSE between the modeled and observed cumulative GW-SW discharge estimates. We used the parameterization schemes described in Chapter 2 (see Table 2.1) to Scenario 2 (describing well data from 1980 to present and shallow well screen depths), which better describes GW sources reaching the LMR in this study. We chose 1980 as a date boundary where confidence intervals of nitrate concentrations presented in a previous regional study did not show consistent upward trend despite continuing median concentration increases [45]. The nitrate concentration increase in the two surrounding counties (Merced and Stanislaus) was plotted in Figure 4.2 for conformational purposes. The observed cumulative GW-SW discharge was estimated from differential flow between the two nearby gauging stations along the LMR, CRS and MST, assuming 15-hr travel time (as described in Chapter 3). The parameterization scheme producing the best agreement (RMSE) between modeled and observed cumulative GW-SW discharge was used in subsequent reactive transport modeling for well parameterization consistency.
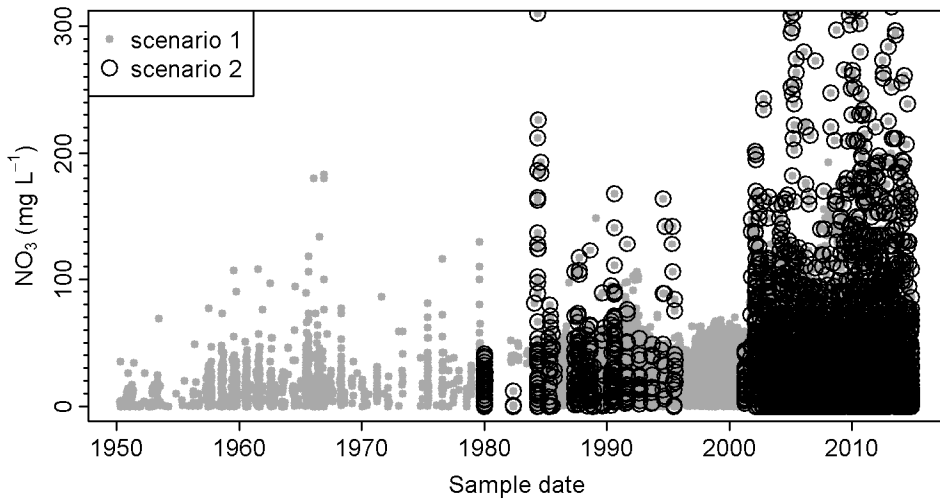
Figure 4.2. Well GW NO$_3$ values under 300 mg L^{-1} plotted for Merced and Stanislaus counties. The two scenarios, defined from Table 2.1, are presented. The data show noticeable upward trend with time under either scenario. The well data were aggregated from GAMA [43] and USGS-NWIS [46].

We next used the distributed GW-SW discharge estimates, Q_g, to define a nitrate reduction term, the first order decay rate often used in denitrification models [32], expressed as:

$$C_{gn} = C_{gn0}\exp(-kt) \qquad (4.1)$$

where C_{gn} is the GW NO$_3$ concentration at the foot of the flowpath as GW discharges and expressed in mg L^{-1}, C_{gn0} is the initial NO$_3$ concentration at the head of the flowpath to the river (defined in our study by the GW parameterization methods utilizing available well nitrate concentration data), k is the first order decay coefficient [T^{-1}], and t is the

time over which that denitrification occurs, i.e., the travel time in the GW flowpath. We substituted the following unitless decay term, kt, into Equation (4.1):

$$kt = \frac{kV\phi}{Q_g} \tag{4.2}$$

where V is the hypothetical volume the water travels through (from well to river) and ϕ is the sediment porosity for which the value of 0.38 was used from a previous GW modeling study [11]. Similar terms regarding GW flows and velocities were used in other transport studies for the region [9].

Our mixing model for the river examines the GW-SW discharge at the GW-SW interface specifically. From Chapter 2 (Equation 2.2) and Equations (4.1) and (4.2), this bcomes:

$$Q_d C_{dn} = Q_u C_{un} + Q_{gn} C_{gn0} \exp\left(-\frac{kV\phi}{Q_{gn}}\right) \tag{4.3}$$

where Q_d is model-estimated downstream flow from the SC mixing model, Q_u is the upstream flow where the initial cell is estimated from the upstream gauging station (CRS), C_{un} is upstream NO_3 concentration where the initial value is the first measured value, and Q_{gn} is a length-scaled GW-SW discharge. Because the estimated 1-km distributed GW-SW discharge (Q_g) was assumed to be uniform per km cell (see Equation (2.3)) the resulting rescaled distributed GW-SW discharge (Q_{gn}) was evaluated by multiplying Q_g with the distance between consecutive measurements and dividing by 1 km. The model expressed in Equation (4.3) was evaluated at every observed location from the synoptic sampling runs, where only the first upstream cell uses observed values (first C_{un} value).

The main fitting parameter for this model was the lumped parameter, kV, which we constrained between 0 to 0.01 m^3 s^{-1}. We tested kV in discrete increments (0.0001 m^3 s^{-1}) from 0 to 0.001 m^3 s^{-1} and larger increments (0.0005 m^3 s^{-1}) from 0.001 to 0.01 m^3 s^{-1}. The resulting model-estimated nitrate concentrations, C_{dn}, were then compared with observed. We evaluated the best fit for individual synoptic sampling model runs using RMSE between model (C_{dn}) and observed SW nitrate. The model denitrification outcomes (best fitting kt values) were then compared with those from previous work focusing on GW nitrate reactive transport modeling (0.92 assuming 20 yr travel time [11]) and with a regional statistical model examining total nitrogen loss in multiple streams and rivers (0.17-1.06 assuming 15 hr travel time for the LMR [40]). To examine loading loss, we subtracted the last term on the right of Equation (4.3) from loading assuming no loss ($Q_{gn}C_{gn0}$) and divided the difference by the no-loss loading term to create the fractional loss expression:

$$1 - \exp\left(-\frac{kV\phi}{Q_{gn}}\right). \tag{4.4}$$

This term was evaluated at the whole reach scale to estimate kt and at 1-km resolution.

Although we believe the modeling results here provide a reasonable approximation of a complex, spatially distributed environmental system, it is important to recognize the model simplicity and potential limitations. The sources of upstream flow

(Q_u) were assumed to be steady per synoptic sample run and GW conditions (GW surface elevation and GW SC and NO_3 concentrations) were assumed to be steady for all the synoptic sampling events. The model is limited because of the focus on GW-SW discharge and does not capture reaches showing simultaneous gains or losses (e.g., hyporheic exchanges or local hydraulic gradients), also described in Chapter 3. For nitrate kinetics, the model would not be able to differentiate biogeochemical processes occurring within HZ from surrounding aquifer processes further from the LMR. More complex models of the GW-SW would have to be undertaken. For example, the effect of hydrodynamic dispersion was not included as the model does not describe transport within the subsurface explicitly. While advection and dispersion mechanisms would be relatively straightforward to incorporate, parameterizing such a model in the spatially distributed manner that this problem calls for would be challenging and would add substantially to the uncertainty of the results.

A key model consideration was treatment of well NO_3 concentrations, particularly relative to the highest method detection limit (MDL). For samples collected over time, methods of nitrate measurement have varied within the time with different detection limits. Including low concentrations for time trend or frequency analysis has been subject to research in itself [49]. For our exploratory purposes, we examined both including and disregarding the values below the highest method detection limit (2.2 mg L^{-1} of NO_3 or 0.5 mg L^{-1} NO_3-N, nitrate as nitrogen) for initial analysis. Shallow wells with nitrate concentrations below the highest method detection limit (MDL) can be seen circled in red in Figure 4.1. We anticipated that including low concentrations would lead to model under-predicting loading, while excluding the low concentrations would lead to model over-prediction if there is nitrate reduction occurring.

4.4. Results and Discussion

Results from the sensitivity analysis pertaining to parameter assignment approaches are summarized in Table 4.1. We wanted the parameterization scheme exhibiting the lowest RMSE between modeled and observed cumulative GW-SW discharge for Senario 2 (lin, avg3, t_avg). This scenario more accurately described GW nitrate conditions and sources for our study [45]. For this scheme, the lowest RMSE for Scenario 2 (0.61 m^3 s^{-1}) was appreciable, nearly equal to the observed Q_g (0.64 m^3 s^{-1}, averaged from 2010-3-31 and 2012-3-23 events seen in Table 3.1), but reasonable given rating curve accuracy. Differences in RMSE were small between the SW piecewise linear regression and GW temporal methods. Noticeable differences between GW spatial methods are focused on well data availability for Scenario 2 (shallow screen depth and more recent well samples), and associated downscaling with the remaining wells. For further analysis, we will focus on the parameterization scheme (lin, avg3, t_avg) for wells sampled from 1980 on and with shallow well screen-depths (Scenario 2).

Table 4.1. RMSE between modeled and observed cumulative GW-SW discharge for 2 different synoptic sampling runs (0.95 m^3 s^{-1} on 2010-3-31 and 0.34 m^3 s^{-1} on 2012-3-23 and found in Table 3.1). The RMSE is ordered by lowest value for Scenario 2 (1980 on and wells shallower than 85 m). The abbreviation scheme for the parameterization methods are listed in Table 2.1 and briefly described in parentheses.

SW piecewise linear regression methods	GW spatial methods	GW temporal methods	Scenario 2 RMSE (m^3 s^{-1})
lin (least square regression)	avg3 (average of closest 3 wells)	t_avg (averaged over scenario)	0.610
sen (Sen's slope)	avg3	t_avg	0.613
seg (R-pkg segmented)	avg3	t_avg	0.624
lin	avg3	t_clo (average within synoptic period or closest date)	0.625
sen	avg3	t_clo	0.628
seg	avg3	t_clo	0.638
sen	sp_clo (closest single well)	t_avg	1.097
lin	sp_clo	t_avg	1.136
seg	sp_clo	t_avg	1.195
sen	sp_clo	t_clo	1.242
lin	sp_clo	t_clo	1.292
seg	sp_clo	t_clo	1.351
seg	idw12 (inverse distance weight of 12 closest wells)	-	2.017
sen	idw12	-	2.081
lin	idw12	-	2.190

A major data preprocessing question before applying the reactive transport model was whether to include NO_3 concentration values below the highest method detection limit (MDL) for estimating C_{gn0} (i.e., the analytical method detection limit). Figure 4.3 shows C_{gn0} when including values below the MDL (grey dots) and for excluding (black line) using the same parameterization scheme as the GW-SW discharge model for consistency. We see clear C_{gn0} differences from river km 17-27 due to wells reporting below the MDL south of the LMR (around river km 20) and near the LMR (around river km 28) seen in Figure 4.1. Due to previous studies finding low regional denitrification [15,45], we feel these wells can be safely excluded as either isolated well locations with

favorable denitrification conditions [15] or as HZ wells exhibiting the nitrate reduction we are attempting to capture in our model. The resulting case is equivalent to excluding wells reporting nitrate concentrations below the MDL, seen in black in Figure 4.3, and will be used for further model analysis.
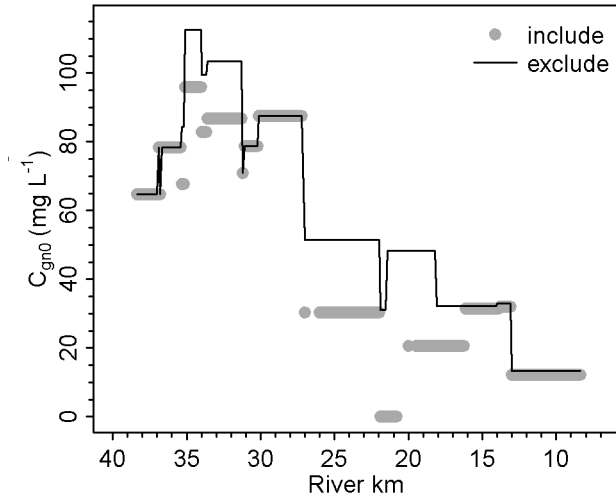
Figure 4.3. Distributed nitrate concentrations, C_{gn0}, used in the model expressed in Equation (4.3) based on the average of the 3 closest wells GW NO_3 parameterization scheme. The grey dots indicate inclusion of well readings below the highest detection limit (2.2 mg L^{-1} NO_3 or 0.5 mg L^{-1} NO_3-N). The solid black line excludes those low well NO_3 concentration readings. The well data were aggregated from GAMA [43] and USGS-NWIS [46].

With the estimated distributed GW-SW discharge rescaled for the reactive transport model as Q_{gn} and the appropriate C_{gn0} parameterization, we estimated the NO_3 concentrations in the LMR, C_{dn}, from Equation (4.4) assuming no nitrate reduction ($kt = 0$ or $kV = 0$ m^3 s^{-1}). The ratios between the modeled and observed along the whole study reach for all flows are plotted in Figure 4.4. Overall, the model tends to overestimate the observed concentrations (ratios > 1) indicating potential nitrate reduction is occurring along the reach and at multiple flow regimes. The high flow regime, $Q_u > 14$ m^3 s^{-1} denoted in the lightest shade of grey, seems to be the most consistent ratios but also the flow regime showing the least potential nitrate reduction [40]. Other flow regimes (< 7 and 7-14 m^3 s^{-1}) show wider ratio variance and often had larger modeled to observed ratios than the high flow regime, suggesting higher nitrate reduction is occurring. Spatially, the model shows higher ratios upstream (river km > 27) indicative of the C_{gn0} parameterization seen in Figure 4.3.
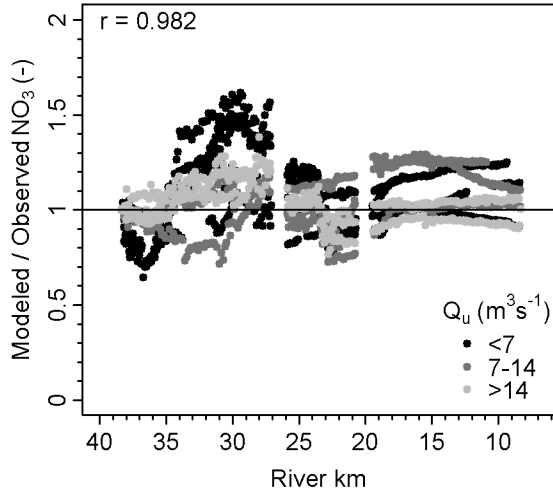
Figure 4.4. Longitudinal ratios of modeled to observed LMR NO$_3$ concentrations for all synoptic sampling runs with no nitrate reduction ($kt = 0$). The model results are for the C_{gn} concentrations defined by the black line in Figure 4.3. The model does show good correlation (Pearson's r) suggesting the estimated GW-SW discharge derived from SC loading are likely correlated. Further delineation between synoptic events by upstream flow regimes (Q_u) is depicted by dot shades.

To account for potential nitrate reduction, we varied kV for all synoptic runs to minimize RMSE between modeled and observed NO$_3$ concentrations in the LMR. The results of this analysis are shown in Figure 4.5, where the best fits are denoted as the green lines, and the observed data are shown as black dots. Generally, as surface flows increased, RMSE values decreased and are more clearly shown in Figure 4.6. The decrease is likely due to the influence of SW dilution dominating potential local deviations. Excluding synoptic sampling events showing no nitrate reduction as the best fit, the mid-range flow regime ranging from 7-14 m^3 s^{-1} showed higher rates (0.229-0.432) of nitrate reduction defined by the unitless decay term, kt. This term result is noticeably larger than the high flower regime (> 14 m^3 s^{-1}) exhibiting kt values 0.053-0.068. The low regime (< 7 m^3 s^{-1}) showed less nitrate reduction (kt) but showed larger degree of variability (0.037-0.164) than the high flow regime. While these results generally underestimate previous studies for the decay term (kt) [11,40], these results do support previous work which found less nitrogen loss for flows for the high flow regime ($kt = 0.17$ assuming a 15 hr travel time) than lesser flows ($kt = 1.06$).
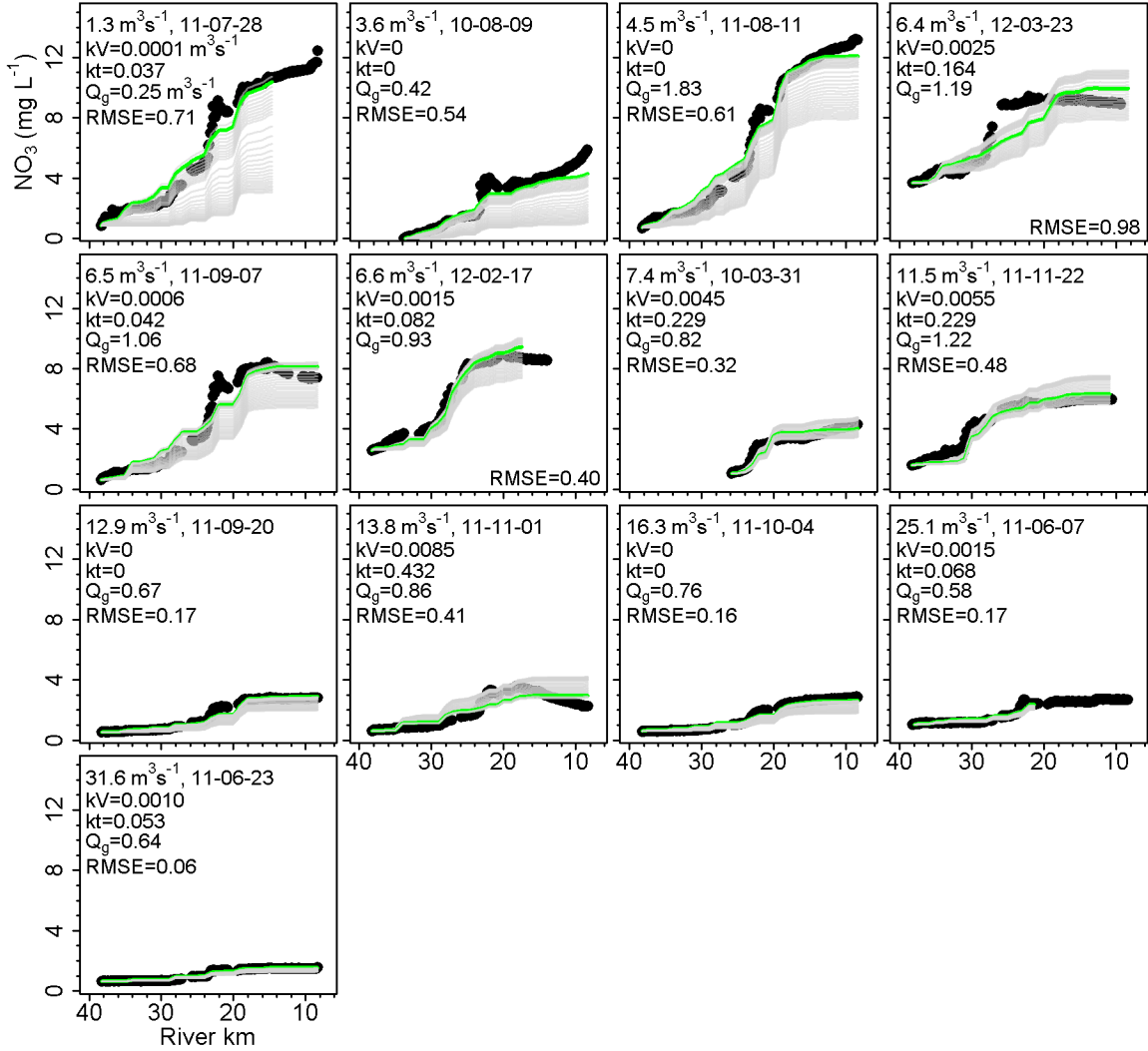
Figure 4.5. Individual plots per sampling event of modeled (lines) versus observed (black dots) NO$_3$ concentrations considering potential nitrate reduction ($kV \neq 0$ m^3 s^{-1}). The lowest RMSE between modeled and observed is shown in green while the sensitivity range for kV (0-0.01 m^3 s^{-1}) is shown in transparent grey. The lowest RMSE (mg L^{-1}), associated kV values and reach kt values, and cumulative reach GW-SW discharge (Q_g) are presented in the top right of each plot below the daily upstream flow (with which the plots are ordered) and date. The presented results are for the GW well NO$_3$ parameterization (C_{gn}) scheme that excluded well NO$_3$ concentrations below the highest detection limit (< 2.2 mg L^{-1} NO$_3$).

Localized longitudinal deviations from the modeled best fit and observed LMR nitrate concentrations are described for the constrained range of denitrification rates (kV) and are also seen in Figure 4.5. The localized deviations potentially biased the best fit model estimate of the reach estimated denitrification term (kt) to underestimate actual nitrate reduction. A noticeable deviation or "spike" that occurs consistently across different flows occurs around river km 20-24, where the observed concentrations exhibit an increasing gradient upstream and then consistently decreases near river km 20. This spiking in observed longitudinal gradient is seen across multiple upstream daily flows (< 6.5 m^3 s^{-1}) as well as in some higher flow regimes. To compensate for occasions when

63

this observed spike is large, the best fit model tends to overestimate upstream (~river kms 24-36) concentrations and clearly seen for synoptic runs occurring on 2011/7/28, 2011/8/11, and 2011/9/7. The cause of the spiking behavior is unknown. It could stem from an unidentified point source or from preferential groundwater flows with elevated nitrated concentrations. However, the consistent decrease in the gradient suggests the presence of a relatively low nitrate input downstream of the elevated nitrate input. Further field investigations would be required to identify the true source.
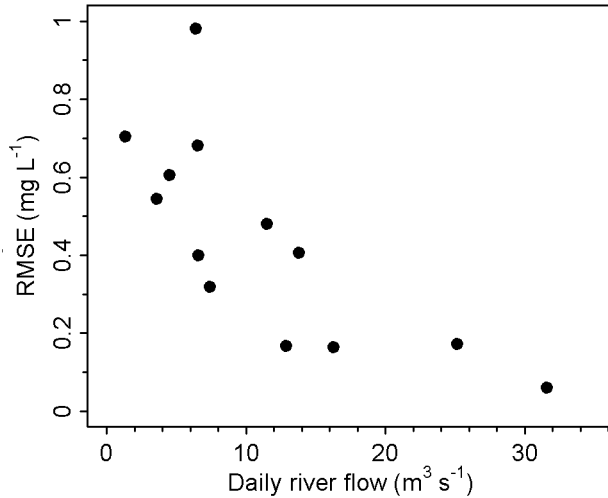
Figure 4.6. Plot showing RMSE between the modeled and observed nitrate concentrations per sampling event at given daily upstream river flows reported at CRS (downloaded from California Data Exchange Center [50]).

Interestingly, downstream LMR nitrate concentration behavior (river km < 20) exhibits a range of different responses, decreasing, increasing, and relatively stable, which do not show clear seasonal or flow-related patterns. When SC data are available (Figure 3.6), the concavity of the nitrate curves also generally mimics SC behavior with the exception of the 2012/3/23 run where SC concentrations increase but NO_3 levels decrease. The decreases in downstream concentrations occur during the time period following the last noticeable upstream pulse (around early September of 2011 and seen in Figure 3.4), indicating potential residual bank storage of low nitrate concentration from upstream releases from the previous months and year, and eventual reconnection with the SW. It is worth noting, however, that some runs after this pulse did show stable or slight increases in NO_3 concentration (2011/11/22, 2011/9/20, and 2011/10/4).

The plots in Figure 4.7 describe the distributed NO_3 GW loading to the SW (grey bars) and associated fraction loss (blue dashes). These parameters are evaluated at a 1-km resolution, where the mass loading term is expressed as the last term on the right in Equation (4.3), and the fraction loss is expressed in Equation (4.4). The view of distributed NO_3 loading generally tracks well with the distributed GW-SW discharge (Q_g) in Figure 2.7 or 3.8. Exaggerated loading spikes upstream (river km > 33-36) correspond with lesser spikes of GW-SW discharge coupled with elevated GW nitrate concentrations (Figure 4.3). Higher nitrate loading from ~river kms 20-30 support elevated GW-SW discharge findings discussed in previous chapters and studies [36]. Over the same region (river km 20-30), the fractional loss tends to be smaller for other longitudinal locations

within the respective survey events, showing the effects of the higher groundwater discharge on the exponential term expressed in Equation (4.4). Conversely, low GW-SW discharge (and low loading on the river segment), but non-zero, greatly decreases the exponential term in Equation (4.4) causing high fractional loss. Areas of no GW-SW discharge, we set to zero fractional loss.
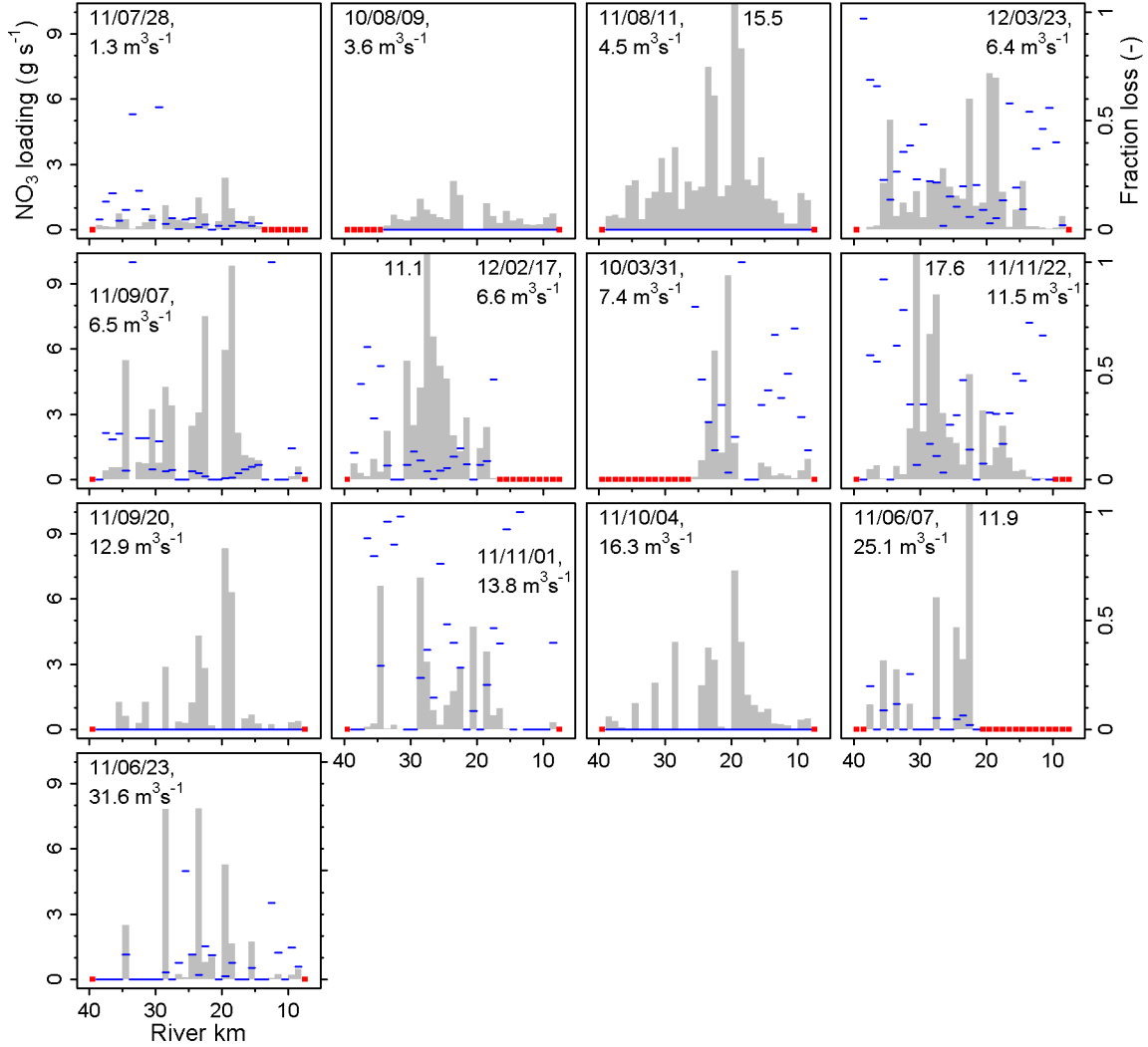
Figure 4.7. View of distributed NO₃ loading per km (grey bars) and fraction loss of NO3 estimated from the first order decay term (blue dashes and from Equation (4.4)) for best fit model results shown with green line in Figure 4.5. Loading above the axis limit (10 g s⁻¹) has the loading rate labeled next to the bar. Red squares indicate parts of the reach without any available data (filtered or boundaries of analysis). Areas of no GW-SW discharge, we set the fraction loss to zero.

4.4.1. Additional Considerations

The results presented here have several limitations. First, our analysis aimed at estimating nitrate removal rates assumes that all denitrification occurs along the groundwater pathway. Our in situ nitrate sensing approach aggregates all types of nitrate removal dynamics from the groundwater well to the river, including the water column

nitrogen processes between measurement points. We decided that aquifer denitrification near the river-aquifer interface was the likely cause of nitrate mass-balance deficits based on results from previous studies. These studies have shown that, within the regional groundwater, the anaerobic conditions (favorable for denitrification) were found to be more prevalent closer to the river corridors [15]. Previous local denitrification modeling studies along a GW flowpath to the LMR further support this assumption [11]. Regarding potential nitrate removal within the river water column itself, biological processes (i.e., assimilation, nitrification, and denitrification) within the SW column downstream within the San Joaquin River exhibited low to negligible effects on diurnal nitrate concentration variability [23].

Another limitation specific to our model calibration of nitrate removal rates is the characterization of local travel times within the unitless denitrification term in Equation (4.2). In this study, complexities governing travel time within the subsurface (i.e., sediment heterogeneity, spatially varying GW surface elevations) and within the interstitial exchange at the GW-SW interface (i.e., channel morphology) are either aggregated within our method's discharge estimates (Q_{gn}) uniform hydrogeologic characterization (porous media porosity), or adjusted for in our calibration term lumping denitrification rate with drainage volume, kV. Previous studies have characterized travel time distributions at the local hyporheic exchange scale using injected tracers [17], using groundwater transport model parameter sensitivity analysis (e.g., hydraulic conductivities, dispersion coefficients) at the groundwater flowpath scale [9,11], and for in-stream (SW) flows in relation to stream nutrient spiraling [8,40]. Estimates of regional of nitrogen removal [40] scaled to LMR travel time and the local denitrification along GW flowpath [11] had higher estimates for the unitless denitrification term that our studies across different flow regimes (see kt values in Figure 4.5).

The final (and major) limitation is associated with the sparsity of groundwater wells in relation to the discretized 1-km longitudinal model. Due to regional nitrate concentration trends and depth differentiation [45], we chose recent sampled well nitrate (1980 to present) and shallow well screens (less than 85 m). The resulting sparse well distribution (see Figure 4.1) led to differences in well assignment performance for GW-SW discharge using specific conductance as a conservative tracer (see Table 4.1). Figure 4.3 shows longitudinal segments of constant nitrate concentrations indicating the application of common wells for multiple consecutive discretization boundary conditions (C_{gn0} assignments). The potential to use subsurface geochemical relationships between nitrate concentrations and specific conductance was explored but did not show a sufficiently strong correlation, as seen in Figure 4.8b.

The results presented for denitrification were reasonable based on prior findings in the region. This finding suggests that the novel synoptic sensing approach proposed in this work has the potential to change the way rivers and land use changes are monitored and interpreted. However, the multiple limitations discussed in this section point to the need for more work on the method and supporting data sets. For instance, the results could be greatly improved with additional groundwater data along the river reach but outside the hyporheic zone. Such data collection would more likely be performed by the relevant county and state water agencies. Improvements in the understanding of the mechanisms and rates of nitrate removal could also greatly improve the outcomes of this

work and the potential of the synoptic sampling approach. Such improvements would require intensive tracer studies and isotopic investigations more likely to be performed by researchers and/or USGS personnel.
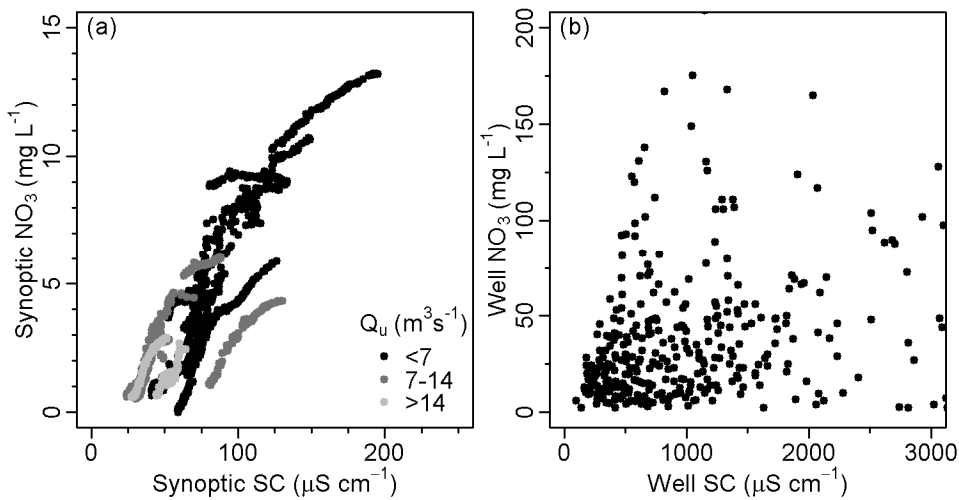
Figure 4.8. Scatter of observed and available NO$_3$ to SC concentrations for both synoptic SW (a) and GW wells (b) respectively. A stronger correlation is visible in the synoptic SW data. The synoptic asynchronous data were paired by closest points with max distance difference of 15 m. The well data were paired by same well name, well county, and sample date.

4.4.2. Summary and Conclusions

In this work, a multi-parameter SW data collection system and analytic framework linking GW-SW discharge with denitrification in a spatially explicit manner have been demonstrated. The distributed mass balance model describing GW-SW interactions, using ambient tracers as boundary conditions, extends from previous methods using injected chemical and/or isotopic tracers. Our prior estimates of GW-SW discharge (Chapter 3) were used as boundary conditions for our river mixing model. However, in this chapter, a reaction term was introduced to account for potential denitrification. Optimizing the model for these denitrification rates, we obtained rate values consistent with those from more localized investigations on the same river, validating our approach. As with the salinity issues (Chapter 3), sparsity of GW nitrate data was also the main factor limiting our interpretation of the results for nitrate. Nonetheless, the nitrate mapping from this work points to clear connections between land-use and SW quality on a realistic scale that has not been studied to date.

References

[1] S. Seitzinger, J.A. Harrison, J.K. Böhlke, A.F. Bouwman, R. Lowrance, B. Peterson, et al., Denitrification across landscapes and waterscapes: a synthesis, Ecological Applications. 16 (2006) 2064–2090. doi:10.1890/1051-0761(2006)016[2064:DALAWA]2.0.CO;2.

[2] R.F. Spalding, M.E. Exner, Occurrence of nitrate in groundwater—a review, Journal of Environmental Quality. 22 (1993) 392–402.

[3] Caraco, J.J. Cole, Human impact on nitrate export: an analysis using major world rivers, Ambio. 28 (1999) 167–170.

[4] R.W. Howarth, R. Marino, Nitrogen as the limiting nutrient for eutrophication in coastal marine ecosystems: Evolving views over three decades, Limnol. Oceanogr. 51 (2006) 364–376. doi:10.4319/lo.2006.51.1_part_2.0364.

[5] K.R. Burow, B.T. Nolan, M.G. Rupert, N.M. Dubrovsky, Nitrate in Groundwater of the United States, 1991−2003, Environ. Sci. Technol. 44 (2010) 4988–4997. doi:10.1021/es100546y.

[6] H.J. Di, K.C. Cameron, Nitrate leaching in temperate agroecosystems: sources, factors and mitigating strategies, Nutrient Cycling in Agroecosystems. 64 (2002) 237–256. doi:10.1023/A:1021471531188.

[7] F. Laurent, D. Ruelland, Assessing impacts of alternative land use and agricultural practices on nitrate pollution at the catchment scale, Journal of Hydrology. 409 (2011) 440–450. doi:10.1016/j.jhydrol.2011.08.041.

[8] P.J. Mulholland, A.M. Helton, G.C. Poole, R.O. Hall, S.K. Hamilton, B.J. Peterson, et al., Stream denitrification across biomes and its response to anthropogenic nitrate loading, Nature. 452 (2008) 202–205. doi:10.1038/nature06686.

[9] L. Wang, M. Ye, J.F. Rios, R. Fernandes, P.Z. Lee, R.W. Hicks, Estimation of nitrate load from septic systems to surface water bodies using an ArcGIS-based software, Environ Earth Sci. 70 (2013) 1911–1926. doi:10.1007/s12665-013-2283-5.

[10] J.J. Beaulieu, J.L. Tank, S.K. Hamilton, W.M. Wollheim, R.O. Hall, P.J. Mulholland, et al., Nitrous oxide emission from denitrification in stream and river networks, PNAS. 108 (2011) 214–219. doi:10.1073/pnas.1011464108.

[11] C.T. Green, J.K. Böhlke, B.A. Bekins, S.P. Phillips, Mixing effects on apparent reaction rates and isotope fractionation during denitrification in a heterogeneous aquifer, Water Resour. Res. 46 (2010) W08525. doi:10.1029/2009WR008903.

[12] J.K. Böhlke, R.C. Antweiler, J.W. Harvey, A.E. Laursen, L.K. Smith, R.L. Smith, et al., Multi-scale measurements and modeling of denitrification in streams with varying flow and nitrate concentration in the upper Mississippi River basin, USA, Biogeochemistry. 93 (2009) 117–141. doi:10.1007/s10533-008-9282-8.

[13] T.S. Rosenstock, D. Liptzin, K. Dzurella, A. Fryjoff-Hung, A. Hollander, V. Jensen, et al., Agriculture's Contribution to Nitrate Contamination of Californian Groundwater (1945–2005), Journal of Environment Quality. 43 (2014) 895. doi:10.2134/jeq2013.10.0411.

[14] A.J. Tesoriero, H. Liebscher, S.E. Cox, Mechanism and rate of denitrification in an agricultural watershed: Electron and mass balance along groundwater flow paths, Water Resour. Res. 36 (2000) 1545–1559. doi:10.1029/2000WR900035.

[15] M.K. Landon, C.T. Green, K. Belitz, M.J. Singleton, B.K. Esser, Relations of hydrogeologic factors, groundwater reduction-oxidation conditions, and temporal and spatial distributions of nitrate, Central-Eastside San Joaquin Valley, California, USA, Hydrogeol J. 19 (2011) 1203–1224. doi:10.1007/s10040-011-0750-1.

[16] S.P. Seitzinger, R.V. Styles, E.W. Boyer, R.B. Alexander, G. Billen, R.W. Howarth, et al., Nitrogen retention in rivers: model development and application to watersheds in the northeastern U.S.A., Biogeochemistry. 57-58 (2002) 199–237. doi:10.1023/A:1015745629794.

[17] J.P. Zarnetske, R. Haggerty, S.M. Wondzell, M.A. Baker, Dynamics of nitrate production and removal as a function of residence time in the hyporheic zone, J. Geophys. Res. 116 (2011) G01025. doi:10.1029/2010JG001356.

[18] J.W. Harvey, J.K. Böhlke, M.A. Voytek, D. Scott, C.R. Tobias, Hyporheic zone denitrification: Controls on effective reaction depth and contribution to whole-stream mass balance, Water Resour. Res. 49 (2013) 6298–6316. doi:10.1002/wrcr.20492.

[19] M.A. Briggs, F.D. Day-Lewis, J.P. Zarnetske, J.W. Harvey, A physical explanation for the development of redox microzones in hyporheic flow, Geophys. Res. Lett. (2015) 2015GL064200. doi:10.1002/2015GL064200.

[20] J.P. Zarnetske, R. Haggerty, S.M. Wondzell, V.A. Bokil, R. González-Pinzón, Coupled transport and reaction kinetics control the nitrate source-sink function of hyporheic zones, Water Resour. Res. 48 (2012) W11508. doi:10.1029/2012WR011894.

[21] T. Liu, X. Xia, S. Liu, X. Mou, Y. Qiu, Acceleration of Denitrification in Turbid Rivers Due to Denitrification Occurring on Suspended Sediment in Oxic Waters, Environ. Sci. Technol. 47 (2013) 4053–4061. doi:10.1021/es304504m.

[22] P.B. Christensen, L.P. Nielsen, J. Sørensen, N.P. Revsbech, Denitrification in nitrate-rich streams: Diurnal and seasonal variation related to benthic oxygen metabolism, Limnology and Oceanography. 35 (1990) 640–651.

[23] B.A. Pellerin, B.D. Downing, C. Kendall, R.A. Dahlgren, T.E.C. Kraus, J. Saraceno, et al., Assessing the sources and magnitude of diurnal nitrate variability in the San Joaquin River (California) with an in situ optical nitrate sensor and dual nitrate isotopes, Freshwater Biology. 54 (2009) 376–387. doi:10.1111/j.1365-2427.2008.02111.x.

[24] R.A. Smith, G.E. Schwarz, R.B. Alexander, Regional interpretation of water-quality monitoring data, Water Resour. Res. 33 (1997) 2781–2798. doi:10.1029/97WR02171.

[25] M.N. Almasri, J.J. Kaluarachchi, Assessment and management of long-term nitrate pollution of ground water in agriculture-dominated watersheds, Journal of Hydrology. 295 (2004) 225–245. doi:10.1016/j.jhydrol.2004.03.013.

[26] G.E. Schwarz, A.B. Hoos, R.B. Alexander, R.A. Smith, The SPARROW Surface Water-Quality Model- Theory, Application and User Documentation, 2006. http://pubs.usgs.gov/tm/2006/tm6b3/.

[27] S.P. Seitzinger, R.V. Styles, E.W. Boyer, R.B. Alexander, G. Billen, R.W. Howarth, et al., Nitrogen retention in rivers: model development and application to

watersheds in the northeastern U.S.A., Biogeochemistry. 57-58 (2002) 199–237. doi:10.1023/A:1015745629794.

[28] R. Dupas, F. Curie, C. Gascuel-Odoux, F. Moatar, M. Delmas, V. Parnaudeau, et al., Assessing N emissions in surface water at the national level: Comparison of country-wide vs. regionalized models, Science of The Total Environment. 443 (2013) 152–162. doi:10.1016/j.scitotenv.2012.10.011.

[29] A. Saleh, B. Du, Evaluation of SWAT and HSPF within BASINS Program for the Upper North Bosque River Watershed in Central Texas, Transactions of the ASAE. 47 (2004) 1039–1049. doi:10.13031/2013.16577.

[30] F. Maggi, C. Gu, W.J. Riley, G.M. Hornberger, R.T. Venterea, T. Xu, et al., A mechanistic treatment of the dominant soil nitrogen cycling processes: Model development, testing, and application, J. Geophys. Res. 113 (2008) G02016. doi:10.1029/2007JG000578.

[31] J.E. McCray, M. Geza, K.E. Murray, E.P. Poeter, D. Morgan, Modeling Onsite Wastewater Systems at the Watershed Scale: A User's Guide, (2009). http://www.iwaponline.com/wio/2009/09/wio200909WF04DEC6.htm.

[32] M. Heinen, Simplified denitrification models: Overview and properties, Geoderma. 133 (2006) 444–463. doi:10.1016/j.geoderma.2005.06.010.

[33] P.M. Groffman, M.A. Altabet, J.K. Böhlke, K. Butterbach-Bahl, M.B. David, M.K. Firestone, et al., Methods for measuring denitrification: diverse approaches to a difficult problem, Ecological Applications. 16 (2006) 2091–2122. doi:10.1890/1051-0761(2006)016[2091:MFMDDA]2.0.CO;2.

[34] J.T. Crawford, L.C. Loken, N.J. Casson, C. Smith, A.G. Stone, L.A. Winslow, High-Speed Limnology: Using Advanced Sensors to Investigate Spatial Variability in Biogeochemistry and Hydrology, Environ. Sci. Technol. 49 (2015) 442–450. doi:10.1021/es504773x.

[35] P.M. Groffman, K. Butterbach-Bahl, R.W. Fulweiler, A.J. Gold, J.L. Morse, E.K. Stander, et al., Challenges to incorporating spatially and temporally explicit phenomena (hotspots and hot moments) in denitrification models, Biogeochemistry. 93 (2009) 49–77. doi:10.1007/s10533-008-9277-5.

[36] S.P. Phillips, C.T. Green, K.R. Burow, J.L. Shelton, D.L. Rewis, Simulation of Multiscale Ground-Water Flow in Part of the Northeastern San Joaquin Valley, California, U.S. Geological Survey, 2007. http://pubs.usgs.gov/sir/2007/5009/.

[37] B.A. Pellerin, B.A. Bergamaschi, J.F. Saraceno, J.D. Garrett, L.D. Olsen, Optical techniques for the determination of nitrate in environmental waters: Guidelines for instrument selection, operation, deployment, maintenance, quality assurance, and data reporting, U.S. Geological Survey, 2013. http://pubs.usgs.gov/tm/01/d5/.

[38] G. Langergraber, N. Fleischmann, F. Hofstädter, A multivariate calibration procedure for UV/VIS spectrometric quantification of organic matter and nitrate in wastewater., Water Sci Technol. 47 (2002) 63–71.

[39] T.T. Snazelle, Results from laboratory and field testing of nitrate measuring spectrophotometers, U.S. Geological Survey, 2015. http://pubs.usgs.gov/of/2015/1065/.

[40] D. Saleh, J. Domagalski, SPARROW Modeling of Nitrogen Sources and Transport in Rivers and Streams of California and Adjacent States, U.S., J Am Water Resour Assoc. (2015). doi:10.1111/1752-1688.12325.

[41] C. Zamora, Estimating Water Fluxes Across the Sediment-Water Interface in the Lower Merced River, California, United States Geological Survey, 2007. http://pubs.usgs.gov/sir/2007/5216/.

[42] H.I. Essaid, C.M. Zamora, K.A. McCarthy, J.R. Vogel, J.T. Wilson, Using heat to characterize streambed water flux variability in four stream reaches, J. Environ. Qual. 37 (2008) 1010–1023. doi:10.2134/jeq2006.0448.

[43] State Water Resources Control Board (CA SWRCB) Groundwater Ambient Monitoring and Assessment, (n.d.). http://geotracker.waterboards.ca.gov/gama/.

[44] J.L. Domagalski, S.P. Phillips, E.R. Bayless, C. Zamora, C. Kendall, R.A.W. Jr, et al., Influences of the unsaturated, saturated, and riparian zones on the transport of nitrate near the Merced River, California, USA, Hydrogeol J. 16 (2008) 675–690. doi:10.1007/s10040-007-0266-x.

[45] K.R. Burow, B.C. Jurgens, K. Belitz, N.M. Dubrovsky, Assessment of regional change in nitrate concentrations in groundwater in the Central Valley, California, USA, 1950s–2000s, Environ Earth Sci. 69 (2012) 2609–2621. doi:10.1007/s12665-012-2082-4.

[46] US Geological Survey (USGS)- National Water Information System: Web Interface, (n.d.). http://waterdata.usgs.gov/nwis.

[47] C.R. Kratzer, R.H. Kent, D.K. Seleh, D.L. Knifong, P.D. Dileanis, J.L. Orlando, Trends in nutrient concentrations, loads, and yields in streams in the Sacramento, San Joaquin, and Santa Ana Basins, California, 1975-2004, U.S. Geological Survey, 2011. http://pubs.er.usgs.gov/publication/sir20105228.

[48] M.A. Mast, D.W. Clow, J.S. Baron, G.A. Wetherbee, Links between N Deposition and Nitrate Export from a High-Elevation Watershed in the Colorado Front Range, Environ. Sci. Technol. 48 (2014) 14258–14265. doi:10.1021/es502461k.

[49] D.R. Helsel, Less than obvious - statistical treatment of data below the detection limit, Environ. Sci. Technol. 24 (1990) 1766–1774. doi:10.1021/es00082a001.

[50] California Deparment of Water Resources (CA DWR) California Data Exchange Center, (n.d.). http://cdec.water.ca.gov/.

5. Conclusions

5.1. Main Outcomes

This dissertation focuses on advancing our understanding of groundwater (GW)-surface water (SW) discharges and nonpoint source pollution in lowland, agriculturally dominated rivers. It presents a novel high resolution SW data collection and analysis approach with multiple ambient tracers using distributed GW-SW mixing models. The approach is demonstrated on the Lower Merced River (LMR) in Central California, and carried out over a wide range of flow and stage conditions. The main outcomes and findings stemming from this work are as follows:

i) Development of a high resolution synoptic sampling method for assessing nonpoint source pollution discharges for salinity, nitrate and, by extension, other constituents measurable by continuous sensing

ii) Creation and validation of an analytical tool for translating nonpoint source discharges into GW discharges using regional GW quality data

iii) Extension of these analytical tools to reactive pollutants like nitrate in form of a novel technique for assessing distributed denitrification patterns at the watershed scale

iv) Elucidation of the GW-SW interactions along the Lower Merced River in terms of connections between land management activities and underlying hydrogeology (e.g., Corcoran Clay unit)

We exploited in situ sensing technology to create high resolution longitudinal description of SW tracers and applied a simple mixing model to describe GW-SW discharge, given available GW tracer data for the conservative tracer SC. A major challenge to apply the mixing model was to resolve spatial and temporal resolution differences between the dense synoptic SW data and sparser GW well data (Chapter 2). We presented methods to account for both SW and GW systems, examining different piecewise linear regressions to upscale SW data and simple spatial downscaling methods involving single or multiple nearby wells. We also considered the appropriate source of GW that would reach the SW (i.e., shallow GW above the confining layer and age). In our study, applying the more realistic source effectively excluded well data inhibiting downscaling substantially and improved the model outcomes. While previous studies have largely examined spatial differences alone and GW interpolations independently, there appears to be no comparable work rescaling regional GW data to a higher resolution, distributed GW-SW mixing model.

We further validated our results, assuming only nonpoint source pollution (distributed small sources), through favorable comparisons with nearby gauging station data and previous modeling studies for a sub-reach located within our larger study reach (Chapter 3). This enabled us to discuss effects of environmental conditions (such as upstream flow and bank storage of recession events) on distributed (1-km) GW-SW discharge estimates. While the SW experienced the anticipated dilution with increased upstream flow, GW-SW discharge was varied inconsistently with flow, both over the whole reach and locally. This would suggest that sediment heterogeneity, varying GW hydraulic gradients, and unaccounted for GW pumping near the LMR may be additional

drivers for GW-SW discharge. Higher temporal resolution GW surface elevation data would be required to explore these possibilities.

The validation of synoptic sampling for describing GW-SW discharge and potential localization of higher zones of GW-SW discharge should be of interest to aquatic ecologists where GW-SW exchange is of particular interest in affecting temperature and oxygen conditions and for transport of other constituents that are of interest downstream to regulators.

Finally, we applied the results from the distributed GW-SW flow model to a non-conservative, NPSP loading model for NO_3, commonly a byproduct of agricultural practices, using a similar mixing model. We added a first order decay term to describe potential nitrate losses in the GW, hyporheic zone (HZ), and in-stream processes (Chapter 4). We incorporated the distributed discharge in estimating the unitless decay term, and calibrated our model by varying a coupled variable defining the unmeasured decay rate and the volume the GW flows through. The major physical consideration was treatment of low concentration well (below the highest detection limit), indicative of a potential hotspot for denitrification, and we decided to exclude low concentrations from our analyses. Building from this consideration, we estimated local NO_3 reduction effects, scaled by the distributed discharge term. The reach nitrate reduction, expressed by the unitless decay term, underestimated previous studies, with the caveat that our estimation was at different scales than those studies, but saw similar unitless decay term behavior across different flow regimes with a previous regional study. The model allows for local variable estimates for the nitrate reduction term due to its dependence on the distributed GW-SW discharge, and would require further field evaluations to verify potential nitrate processes and their relationship to GW-SW discharge.

5.2. Practical Implications

This work provides estimates of distributed GW-SW discharge, constituent loading, and potential capacity of the GW-SW system to affect reactive species (nitrate) at multiple scales. For water quality purposes, the methods presented can estimate reach loads for conservative and reactive constituents that are of concern to environmental policy-makers and regulated by maximum loads for watershed basins. As analytical and in situ sensor technology improves, the same methodology can be used to analyze multiple constituents of interest. For assessing sustainability of aquatic ecosystems, characterizing GW-SW connection is important across scales, particularly in human-impacted watersheds. Human impact on GW supplies and associated transport varies across scale from large-scale activities, like groundwater extraction, irrigation, and land use change, to similar activities occurring at smaller scales. These activities can also vary by season and SW availability, often determined by dam storage capacity and preceding precipitation conditions. Hence, a relatively efficient approach for linking human behavior (land use activity) to nonpoint source pollution would be valuable to regulatory agencies and environmental policy-makers as they strive to create more sustainable practices.

5.3. Future Recommendations

In order to enhance and extend the impact of this work, field campaigns aimed at verification of local GW discharges and chemical fluxes should be undertaken. With

riparian corridor access and installation of multiple monitoring piezometers, the collected GW and SW tracer data (e.g., chemical constituent, temperature, or isotope) and water surface elevations would enable the better estimation of local GW velocities (and related discharges), residence times, and chemical kinetics. The methods and analysis we presented would also be enhanced with the additional in-field GW data collection. For instance, spatial and temporal interpolation of GW characteristics could be better verified with higher resolution data. Additionally questions focused on residual bank storage from SW flow pulses could also be better addressed with higher temporal resolution GW surface elevation data (hours-days).

The simulation model parameterization could be improved with field tests (e.g., pumping tests in available wells) to help characterize nearby aquifer characteristics (e.g., hydraulic conductivities) and better defining potential areas of preferential flows. Additional bathymetric mapping at appropriate river stage conditions would also map bed topography affecting HZ mixing, residence times, and associated chemical kinetics. The resulting physical models with better locally characterized shallow aquifer characteristics and HZ processes would also be able to estimate and potentially verify the distributed GW-SW discharges and chemical fluxes we present in this work.